Twisted bilayer graphene. III. Interacting Hamiltonian and exact symmetries

B. Andrei Bernevig,[1,*] Zhi-Da Song,[1] Nicolas Regnault,[1,2] and Biao Lian[1,†]
[1]*Department of Physics, Princeton University, Princeton, New Jersey 08544, USA*
[2]*Laboratoire de Physique de l'Ecole normale superieure, ENS, Université PSL, CNRS, Sorbonne Université, Université Paris-Diderot, Sorbonne Paris Cité, Paris, France*

(Received 28 October 2020; accepted 16 April 2021; published 11 May 2021)

We derive the explicit Hamiltonian of twisted bilayer graphene (TBG) with Coulomb interaction projected into the flat bands and study the symmetries of the Hamiltonian. First, we show that all projected TBG Hamiltonians can be written as positive semidefinite Hamiltonians, an example of which was found in work by Kang and Vafek [Phys. Rev. Lett. **122**, 246401 (2019)]. We then prove that the interacting TBG Hamiltonian exhibits an exact U(4) symmetry in the exactly flat band (nonchiral-flat) limit. We further define, besides a first chiral limit where the AA stacking hopping is zero, a second chiral limit where the AB/BA stacking hopping is zero. In the first chiral-flat limit (or second chiral-flat limit) with exactly flat bands, the TBG is enhanced to have an exact U(4)×U(4) symmetry, whose generators are different between the two chiral limits. While in the first chiral limit and in the nonchiral case these symmetries have been found in work by Bultinck *et al.* [Phys. Rev. X **10**, 031034 (2020)], for the eight lowest bands, we here prove that they are valid for projection into *any* $8n_{\max}$ particle-hole symmetric TBG bands, with $n_{\max} > 1$ being the practical case for small twist angles $<1^\circ$. Furthermore, in the first or second chiral-nonflat limit without flat bands, an exact U(4) symmetry still remains. We also elucidate the link between the U(4) symmetry presented here and the similar but different U(4) of Kang and Vafek [Phys. Rev. Lett. **122**, 246401 (2019)]. Furthermore, we show that our projected Hamiltonian can be viewed as the normal-ordered Coulomb interaction plus a Hartree-Fock term from passive bands, and exhibits a *many-body* particle-hole symmetry which renders the physics symmetric around charge neutrality. We also provide an efficient parametrization of the interacting Hamiltonian. The existence of two chiral limits with an enlarged symmetry suggests a possible duality of the model yet undiscovered.

DOI: 10.1103/PhysRevB.103.205413

I. INTRODUCTION

Twisted bilayer graphene (TBG) near the magic angle $\theta \approx 1.1^\circ$ hosts flat electron bands and exhibits remarkable interacting phases including correlated insulators, Chern insulators, and superconductors [1–111]. Both transport [2–17] and scanning tunneling microscope [18–25] experiments show the correlated insulators and Chern insulators originate from strong many-body interactions. Extensive theoretical studies have been devoted to understanding the electron interactions in TBG [51–104]. Kang and Vafek [71] proposed that, by projecting in a non-maximally-symmetric Wannier basis, a non-negative interaction Hamiltonian can be obtained, whose ground state at $\nu = \pm 2$ electrons per unit cell (with respect to charge neutrality) is an exactly solvable insulator with some mild approximation. A U(4) symmetry was also identified for the TBG interaction [71–73] (both Refs. [71,72] identified a U(4), which we show here to be similar but different), which was shown to enlarge into a U(4)×U(4) symmetry in the chiral limit $w_0 = 0$ [72]. However, these symmetries were proposed only for the eight lowest bands (two bands per valley-spin) around the charge neutrality point, which applies for the first magic angle, while the TBG theoretically and experimentally exhibits, for example, 32 low-energy "active" bands (eight bands per valley-spin) around charge neutrality at lower angles $\theta = 0.45^\circ$ [28].

In this paper, we derive the explicit TBG Hamiltonian Coulomb Hamiltonian projected within any number of $8n_{\max}$ ($2n_{\max}$ per spin per valley, $n_{\max} \geqslant 1$) particle-hole symmetric low-lying moiré bands. For the first magic angle, the number of bands where the projection makes sense is eight (two per spin-valley) moiré bands in momentum space; for smaller angles, the number increases. We show the exact projected Coulomb interaction Hamiltonian can *always* be written into a Kang-Vafek type [71] non-negative form, which we hereby call positive semidefinite Hamiltonian (PSDH). The projected Hamiltonian we derived can be understood as the normal-ordered Coulomb interaction in the active bands plus a Hartree-Fock potential from the passive bands. Furthermore, the projected Hamiltonian has a many-body particle-hole symmetry, which ensures that all the physics are particle-hole symmetric about charge neutrality, in agreement with the overall picture of the experimental observations. We then study the TBG symmetries in the flat band limit. We prove the existence of not one but two (first and second) chiral limits defined by zero hopping at either AA or AB/BA stackings. We prove that the projected TBG Hamiltonian in the nonchiral-flat limit has an exact U(4) symmetry, which breaks to a U(2) × U(2) when kinetic energy is added (nonchiral-nonflat case). This symmetry is enhanced into an exact U(4)×U(4)

*bernevig@princeton.edu
†biao@princeton.edu

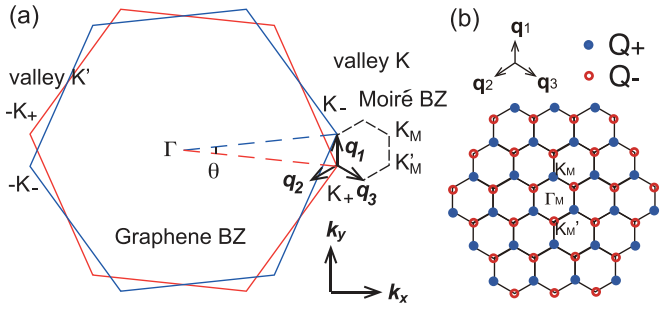

FIG. 1. Illustration of the relation between the graphene BZs of two layers and the moiré BZ (MBZ). Blue solid and red empty circles represent $\mathcal{Q}_+$ and $\mathcal{Q}_-$, respectively.

symmetry in either the first chiral-flat limit or the second chiral-flat limit. The U(4)×U(4) symmetry for the first chiral limit, and for projection into two low-lying active bands was obtained in Ref. [72], but we here extend it to any number of projected bands as well as to a second chiral limit. In the first chiral-nonflat limit or the second chiral-nonflat limit, a kinetic term is also considered, and the bands are not flat; however, we show that an exact U(4) symmetry still remains. All these symmetries, in all limits, are shown to be not only valid for the eight active bands at the first magic angle [72] but also for the projected Hamiltonian within any number of particle-hole symmetric bands. This is relevant at smaller twist angles: In Ref. [28], it was experimentally and theoretically found that 32 bands (eight bands per valley/spin) contribute to the low-energy physics. Besides, for Hamiltonian projected in the lowest eight bands (two bands per spin per valley), we reveal that the Hamiltonian in the first or second chiral limit can be enhanced into a stabilizer code Hamiltonian under certain assumptions. Furthermore, we elucidate the similarities and differences between the U(4) symmetry of Kang and Vafek [71] and the U(4) in the current paper. The explicit form and symmetries of Hamiltonian here greatly simplify the study of TBG many-body states, as we will discuss in Refs. [109] and [110].

II. BISTRITZER-MACDONALD MODEL AND COULOMB INTERACTION

We first present a short overview of the Bistritzer-MacDonald (BM) model [1] to define our notations. The reader might refer to Refs. [107,108] for a in-depth discussion. For convenience, we also provide a detailed summary in Appendix A. To begin, we assume $c^\dagger_{\mathbf{p},\alpha,s,l}$ denotes the creation operator of the spin $s=\uparrow,\downarrow$ electron at momentum $\mathbf{p}$ in the graphene sublattice $\alpha = A, B$ and layer $l = \pm$ (denoting top and bottom) of TBG, where $\mathbf{p}$ is measured from the Γ point of the graphene Brillouin zone (BZ) of layer l. The low-energy physics of TBG is concentrated at the two graphene valleys K, K' (which we denote as valleys $\eta = \pm$) at momenta $\mathbf{p} = \pm\mathbf{K}_\ell$ in layer ℓ, respectively [1]. We further define $\mathbf{q}_j = C_{3z}^{j-1}(\mathbf{K}_- - \mathbf{K}_+)$ $(j = 1, 2, 3)$, where C_{3z} is the three-fold rotation about z axis [see Fig. 1(a)]. The kinetic Hamiltonian of TBG is then given by the continuum model [1,108] as

$$\hat{H}_0 = \sum_{\mathbf{k}\in\mathrm{MBZ}} \sum_{\eta\alpha\beta s} \sum_{\mathbf{Q}\mathbf{Q}'} \left[h^{(\eta)}_{\mathbf{Q},\mathbf{Q}'}(\mathbf{k})\right]_{\alpha\beta} c^\dagger_{\mathbf{k},\mathbf{Q},\eta,\alpha,s} c_{\mathbf{k},\mathbf{Q}',\eta,\beta,s}, \quad (1)$$

where $\eta = \pm$ and $s = \uparrow, \downarrow$ are the valley and spin indices, and the momentum $\mathbf{k}$ is measured from the center (Γ_M point) of the moiré BZ (MBZ). The momenta $\mathbf{Q}, \mathbf{Q}' \in \{\mathcal{Q}_+, \mathcal{Q}_-\}$ is shown in Fig. 1(b), where we have defined $\mathcal{Q}_\pm = \mathcal{Q}_0 \pm \mathbf{q}_1$, and $\mathcal{Q}_0$ is the moiré reciprocal lattice generated by reciprocal vectors $\mathbf{b}_{Mj} = \mathbf{q}_3 - \mathbf{q}_j$ $(j = 1, 2)$. The electron basis $c^\dagger_{\mathbf{k},\mathbf{Q},\eta,\alpha,s}$ is defined as $c^\dagger_{\eta\mathbf{K}_{\eta\cdot l}+\mathbf{k}-\mathbf{Q},\alpha,s,\eta\cdot l}$ if $\mathbf{Q} \in \mathcal{Q}_l$. The detailed kinetic term $h^{(\eta)}_{\mathbf{Q},\mathbf{Q}'}(\mathbf{k})$ at valley $\eta = \pm$ is given in Appendix A. In particular, there are two parameters w_0 and w_1 in the single-particle Hamiltonian $h^{(\eta)}_{\mathbf{Q},\mathbf{Q}'}(\mathbf{k})$ which correspond to the interlayer hoppings at AA and AB/BA stacking centers, respectively [see Eq. (A7)]:

$$\begin{aligned} w_0 &\geqslant 0: \quad \text{AA hopping}, \\ w_1 &\geqslant 0: \quad \text{AB/BA hopping}. \end{aligned} \quad (2)$$

Generically, $w_0 < w_1$ due to the lattice relaxation and corrugation [108,112–115].

The Coulomb interaction term in TBG takes the form (for details, see Appendix C 1)

$$\hat{H}_I = \frac{1}{2\Omega_{\mathrm{tot}}} \sum_{\mathbf{G}\in\mathcal{Q}_0} \sum_{\mathbf{q}\in\mathrm{MBZ}} V(\mathbf{q}+\mathbf{G}) \delta\rho_{-\mathbf{q}-\mathbf{G}} \delta\rho_{\mathbf{q}+\mathbf{G}}, \quad (3)$$

where

$$\delta\rho_{\mathbf{q}+\mathbf{G}} = \sum_{\eta,\alpha,s,\mathbf{k},\mathbf{Q}\in\mathcal{Q}_\pm} \left(c^\dagger_{\mathbf{k}+\mathbf{q},\mathbf{Q}-\mathbf{G},\eta,\alpha,s} c_{\mathbf{k},\mathbf{Q},\eta,\alpha,s} - \frac{1}{2}\delta_{\mathbf{q},\mathbf{0}}\delta_{\mathbf{G},\mathbf{0}} \right) \quad (4)$$

is the total electron density at momentum $\mathbf{q}+\mathbf{G}$ relative to the charge neutral point (CNP) of the uncoupled twisted bilayer graphene without interlayer couplings (which has a density $\langle c^\dagger_{\mathbf{k}+\mathbf{q},\mathbf{Q}-\mathbf{G},\eta,\alpha,s} c_{\mathbf{k},\mathbf{Q},\eta,\alpha,s}\rangle = \frac{1}{2}\delta_{\mathbf{q},\mathbf{0}}\delta_{\mathbf{G},\mathbf{0}}$), and Ω_{tot} is the total area of TBG. The interaction coefficient

$$V(\mathbf{q}) = \pi\xi^2 U_\xi \frac{\tanh(\xi|\mathbf{q}|/2)}{\xi|\mathbf{q}|/2} \quad (5)$$

is the Fourier transform of the Coulomb potential with dielectric constant ϵ screened by top and bottom gates at distance ξ away, where $U_\xi = e^2/\epsilon\xi$ (see Appendix C). Typical TBG experiments have a screening length $\xi \approx 10$ nm [7,8] and dielectric constant $\epsilon \sim 6$ as estimated from the hBN substrates. This yields $U_\xi \approx 24$ meV.

Due to the absence of spin-orbit coupling, the total Hamiltonian

$$\hat{H} = \hat{H}_0 + \hat{H}_I \quad (6)$$

of TBG has the spinless symmetries

$$[C_{3z}, \hat{H}] = [C_{2z}, \hat{H}] = [T, \hat{H}] = 0\,, \quad (7)$$

where C_{3z} is the threefold z-axis rotation symmetry satisfying $C_{3z} c^\dagger_{\mathbf{k},\mathbf{Q},\eta,\alpha,s} C_{3z}^{-1} = (e^{i\eta 2\pi\sigma_z/3})_{\beta\alpha} c^\dagger_{C_{3z}\mathbf{k},C_{3z}\mathbf{Q},\eta,\beta,s}$, C_{2z} is the twofold z-axis rotation symmetry satisfying $C_{2z} c^\dagger_{\mathbf{k},\mathbf{Q},\eta,\alpha,s} C_{2z}^{-1} = (\sigma_x)_{\beta\alpha} c^\dagger_{-\mathbf{k},-\mathbf{Q},-\eta,\beta,s}$, and T is the antiunitary time-reversal symmetry satisfying $TiT^{-1} = -i$ and $T c^\dagger_{\mathbf{k},\mathbf{Q},\eta,\alpha,s} T^{-1} = c^\dagger_{-\mathbf{k},-\mathbf{Q},-\eta,\alpha,s}$. Besides, each graphene

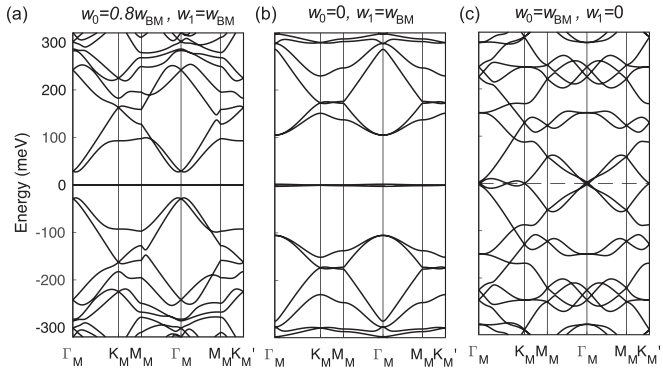

FIG. 2. The single-valley TBG band structure at $\theta = 1.05^\circ$ (with exact ph symmetry P) for (a) the nonchiral-nonflat limit with $w_0 = 0.8w_{\rm BM}$ and $w_1 = w_{\rm BM}$, (b) the first chiral limit with $w_0 = 0$ and $w_1 = w_{\rm BM}$, and (c) the second chiral limit $w_0 = w_{\rm BM}$ and $w_1 = 0$, where $w_{\rm BM} = 110$ meV is the hopping in the original Bistritzer-MacDonald TBG model [1]. In particular, in the second chiral limit, the band structure is a perfect metal where all bands are connected (proof given in Ref. [108]).

valley exhibits a charge U(1) symmetry and a spin rotational SU(2) symmetry, leading to a global U(2)×U(2) symmetry of two valleys (see Appendix A 3).

There also exists a unitary single-particle particle-hole (ph) transformation P [43,108], which anticommutes with $\hat{H}_0$ in Eq. (1) (see Appendix A 3) and commutes with $\hat{H}_I$ in Eq. (3):

$$\{P, \hat{H}_0\} = 0, \quad [P, \hat{H}_I] = 0, \tag{8}$$

where P is defined by $Pc^\dagger_{\mathbf{k},\mathbf{Q},\eta,\alpha,s}P^{-1} = \zeta_{\mathbf{Q}} c^\dagger_{-\mathbf{k},-\mathbf{Q},\eta,\alpha,s}$, with $\zeta_{\mathbf{Q}} = \pm 1$ for $\mathbf{Q} \in \mathcal{Q}_\pm$. In particular, $[P, \hat{H}_I] = 0$ can be seen by noting that $\delta\rho_{\mathbf{q}+\mathbf{G}}$ in Eq. (3) satisfies $P\delta\rho_{\mathbf{q}+\mathbf{G}}P^{-1} = \delta\rho_{-\mathbf{q}-\mathbf{G}}$. We note that an antiunitary ph transformation $\mathcal{P} = PC_{2z}T$ can also be defined, which is adopted in some literature [72,108].

III. PROJECTED HAMILTONIAN

We denote the eigenstates and eigenvectors of $h^{(\eta)}_{\mathbf{Q},\mathbf{Q}'}(\mathbf{k})$ in Eq. (1) as $\epsilon_{n,\eta}(\mathbf{k})$ and $u_{\mathbf{Q}\alpha n\eta}(\mathbf{k})$ (which are spin independent), where the integer $n \neq 0$ is the band index so defined that $n > 0$ ($n < 0$) labels the $|n|$th conduction (valence) band of valley η.

Near the first magic angle $\theta \approx 1.1^\circ$, the lowest conduction and valence bands ($n = \pm 1$) of two spins and two valleys of TBG form eight extremely flat bands which are energetically isolated from the higher bands [Fig. 2(a)]. Therefore, it is appropriate to project the Hamiltonian into the eight flat bands for low-energy physics at the first magic angle. At higher magic angles, the number of low-energy bands increase; for instance, around the second magic angle $\theta \approx 0.5^\circ$ [1], the lowest conduction and valence bands form 32 (eight per spin or valley, $|n| \leqslant 4$) low-energy bands [28]. In this case, the projection of Hamiltonian into more ph symmetric bands is needed for studying low-energy physics. Therefore, to keep our discussions generic, we consider the projection into a set of $8n_{\rm max}$ number of ph symmetric low-energy bands $|n| \leqslant n_{\rm max}$ with any $n_{\rm max} \geqslant 1$. As we will show, since the symmetries C_{2z}, T, P which we will study are closed within each pair of bands $\pm n$, it is sufficient to focus on the two-dimensional band space of each pair of bands $\pm n$ when examining the symmetries of the projected Hamiltonian.

The projection of the kinetic Hamiltonian $\hat{H}_0$ in the set of bands $|n| \leqslant n_{\rm max}$ is thus (which we denote by H_0 without hat)

$$H_0 = \sum_{|n|\leqslant n_{\rm max}} \sum_{\mathbf{k}\eta s} \epsilon_{n,\eta}(\mathbf{k}) c^\dagger_{\mathbf{k},n,\eta,s} c_{\mathbf{k},n,\eta,s}, \tag{9}$$

where $c^\dagger_{\mathbf{k},n,\eta,s} = \sum_{\mathbf{Q},\alpha} u_{\mathbf{Q}\alpha n\eta}(\mathbf{k}) c^\dagger_{\mathbf{k},\mathbf{Q},\eta,\alpha,s}$ gives the band basis of electrons and $\pm n_{\rm max}$ are the highest and lowest bands we project into. Meanwhile, the projection of Coulomb interaction $\hat{H}_I$ in the flat bands can be written as (denoted by H_I without hat; see Appendix C 2)

$$H_I = \frac{1}{2\Omega_{\rm tot}} \sum_{\mathbf{q}\in \rm MBZ} \sum_{\mathbf{G}\in\mathcal{Q}_0} O_{-\mathbf{q},-\mathbf{G}} O_{\mathbf{q},\mathbf{G}}, \tag{10}$$

where

$$O_{\mathbf{q},\mathbf{G}} = \sum_{\mathbf{k}\eta s} \sum_{|m|,|n|\leqslant n_{\rm max}} \sqrt{V(\mathbf{q}+\mathbf{G})} M^{(\eta)}_{m,n}(\mathbf{k}, \mathbf{q}+\mathbf{G}) \times \left(\rho^\eta_{\mathbf{k},\mathbf{q},m,n,s} - \frac{1}{2}\delta_{\mathbf{q},\mathbf{0}}\delta_{m,n}\right). \tag{11}$$

Here we have defined the coefficient called the *form factors (overlaps)*:

$$M^{(\eta)}_{m,n}(\mathbf{k}, \mathbf{q}+\mathbf{G}) = \sum_{\alpha,\mathbf{Q}\in\mathcal{Q}_\pm} u^*_{\mathbf{Q}-\mathbf{G},\alpha m\eta}(\mathbf{k}+\mathbf{q}) u_{\mathbf{Q},\alpha n\eta}(\mathbf{k}), \tag{12}$$

and $\rho^\eta_{\mathbf{k},\mathbf{q},m,n,s} = c^\dagger_{\mathbf{k}+\mathbf{q},m,\eta,s} c_{\mathbf{k},n,\eta,s}$ is the density operator. The form factors (overlaps) $M^{(\eta)}_{m,n}(\mathbf{k}, \mathbf{q}+\mathbf{G})$ were shown to exhibit properties such as exponential decay in the magnitude of $\mathbf{G}$ in Ref. [107]. As such, only $|\mathbf{G}| = 0$ and $|\mathbf{G}| = |\mathbf{b}_{M_1}|$ momentum vectors will contribute to $O_{\mathbf{q},\mathbf{G}}$, with all other $\mathbf{G}$ leading to exponentially smaller form factors (overlaps). We now note that $O_{-\mathbf{q},-\mathbf{G}} = O^\dagger_{\mathbf{q},\mathbf{G}}$, such that $O_{-\mathbf{q},-\mathbf{G}} O_{\mathbf{q},\mathbf{G}}$ is a positive semidefinite operator for any $\mathbf{q}$, $\mathbf{G}$. Thus, the interaction Hamiltonian H_I, being a sum of positive semidefinite operators, is also positive semidefinite. We call such Hamiltonians positive semidefinite Hamiltonians (PSDH).

Below, we investigate the symmetries of the projected Hamiltonian $H = H_0 + H_I$ in various different limits. Without loss of generality, we will consider the subspace of a particular pair of ph symmetric bands $n = \pm n_{\rm B}$ with $1 \leqslant n_{\rm B} \leqslant n_{\rm max}$, since all the single-particle symmetries we will be discussing are closed within the band pair $n = \pm n_{\rm B}$.

Hereafter, we shall use ζ^a, τ^a, s^a to denote the identity matrix ($a = 0$) and Pauli matrices ($a = x, y, z$) in the energy band $n = \pm n_{\rm B}$, valley $\eta = \pm$, and spin $s = \uparrow, \downarrow$ bases, respectively. In particular, when $n_{\rm B} = 1$, our discussion applies to the projected Hamiltonian in the lowest eight flat bands near the first magic angle.

IV. SYMMETRIES IN THE GENERIC NONCHIRAL-NONFLAT CASE

The projected Hamiltonian $H = H_0 + H_I$ preserves all the discrete TBG symmetries C_{3z}, C_{2z}, T (see Appendix C). Moreover, the projected Hamiltonian respects the global U(2)×U(2) spin-charge rotational symmetry of two valleys, which has eight group generators

$S^{ab} = \sum_{\mathbf{k}} (s^{ab})_{m,\eta,s;n,\eta',s'} c^\dagger_{\mathbf{k},m,\eta,s} c_{\mathbf{k},n,\eta',s'}$ ($a = 0, z$ and $b = 0, x, y, z$; repeated indices are summed automatically hereafter). Within each band pair $n = \pm n_{\mathrm{B}}$, the matrices s^{ab} are given by

$$s^{0b} = \zeta^0 \tau^0 s^b, \quad s^{zb} = \zeta^0 \tau^z s^b, \quad (b = 0, x, y, z). \tag{13}$$

We note that s^{ab} has no nonzero matrix elements between different pairs of ph symmetric bands $n_{\mathrm{B}} \neq n'_{\mathrm{B}}$. Also, note that the operators S^{ab} preserve the electron momentum $\mathbf{k}$.

Another $\mathbf{k}$-preserving transformation is given by the combined unitary operator $C_{2z}P$ (P is the ph transformation), which acts as

$$(C_{2z}P) c^\dagger_{\mathbf{k},\mathbf{Q},\eta,\alpha,s} (C_{2z}P)^{-1} = \zeta_{\mathbf{Q}} (\sigma_x)_{\beta\alpha} c^\dagger_{\mathbf{k},\mathbf{Q},-\eta,\beta,s}, \tag{14}$$

and thus satisfies $(C_{2z}P)^2 = 1$. Since $(C_{2z}P) H_0 (C_{2z}P)^{-1} = -H_0$, the single-particle band energies satisfy $\epsilon_{n,\eta}(\mathbf{k}) = -\epsilon_{-n,-\eta}(\mathbf{k})$, and the eigenstate wave functions satisfy $\zeta_{\mathbf{Q}} (\sigma_x)_{\beta\alpha} u_{\mathbf{Q},\alpha,n,\eta}(\mathbf{k}) = [B^{C_{2z}P}(\mathbf{k})]_{-n,-\eta;n\eta} u_{\mathbf{Q},\beta,-n,-\eta}(\mathbf{k})$, where $B^{C_{2z}P}(\mathbf{k})$ is the unitary sewing matrix of $C_{2z}P$. This implies

$$(C_{2z}P) c^\dagger_{\mathbf{k},n,\eta,s} (C_{2z}P)^{-1} = [B^{C_{2z}P}(\mathbf{k})]_{-n,-\eta;n\eta} c^\dagger_{\mathbf{k},-n,-\eta,s}. \tag{15}$$

Using the explicit form of $B^{C_{2z}P}(\mathbf{k})$, one can prove that $[C_{2z}P, O_{\mathbf{q},\mathbf{G}}] = 0$ (see Appendix D 2), and thus

$$\{C_{2z}P, H_0\} = 0, \quad [C_{2z}P, H_I] = 0. \tag{16}$$

Therefore, $C_{2z}P$ is a commuting symmetry of H_I but not H_0.

Furthermore, there is a many-body charge conjugation symmetry $\mathcal{P}_c$ defined by $C_{2z}PT$ followed by the interchange of annihilation and creation operators, namely, $\mathcal{P}_c c^\dagger_{\mathbf{k},n,\eta,s} \mathcal{P}_c^{-1} = (C_{2z}PT) c_{\mathbf{k},n,\eta,s} (C_{2z}PT)^{-1}$ (see Appendix C 4). By showing that $\mathcal{P}_c O_{\mathbf{q},\mathbf{G}} \mathcal{P}_c^{-1} = -O_{\mathbf{q},\mathbf{G}}$, one can prove that the projected Hamiltonian within bands $|n| \leqslant n_{\max}$ satisfies [see Eq. (C33) in Appendix C 4]

$$\mathcal{P}_c (H_0 + H_I) \mathcal{P}_c^{-1} = H_0 + H_I. \tag{17}$$

In particular, $\mathcal{P}_c$ maps a many-body state from filling ν to $-\nu$, where ν is the number of electrons per moiré unit cell relative to the CNP. Therefore, $\mathcal{P}_c$ ensures that the eigenstates of the projected Hamiltonian $H = H_0 + H_I$ is ph symmetric about $\nu = 0$, in agreement with the (big picture) experimental observations.

We note that H_I in Eq. (10) is not normal ordered. We can rewrite $H_I =: H_I : + \Delta H_I + E_I$, where $: H_I :$ is the normal ordered four-fermion interaction, ΔH_I is a quadratic fermion term, and E_I is a constant. One can then show that $\Delta H_I = \frac{1}{2}(H_{\mathrm{HF}}^{\nu=-4n_{\max}} - H_{\mathrm{HF}}^{\nu=4n_{\max}})$, where H_{HF}^{ν} is the Hartree-Fock potential in the projected bands contributed by all the occupied bands below filling ν (see Appendix C 5) and the factor of 4 comes from two spins and two valleys. Note that H_{HF}^{ν} sums over all the bands below filling ν, instead of only the projected active bands (see derivation in Appendix C 5). Therefore, ΔH_I can be understood as the mean-field Hartree-Fock potential from the remote bands projected away symmetrized about the CNP. We note that $: H_I :$ alone does not have the $\mathcal{P}_c$ symmetry, and thus ΔH_I is indispensable as an effective background Hartree-Fock potential.

V. U(4) SYMMETRY IN THE NONCHIRAL-FLAT LIMIT

In the limit of exactly flat $|n| \leqslant n_{\max}$ bands, we have $H_0 = 0$, so the projected Hamiltonian is simply $H = H_I$. By Eq. (16), $C_{2z}P$ becomes a symmetry of H. Note that $C_{2z}P$ preserves the electron momentum $\mathbf{k}$ and thus is a local unitary symmetry. Accordingly, the $C_{2z}P$ symmetry and the spin-charge U(2)×U(2) symmetry together generate a global U(4) symmetry of the Hamiltonian $H = H_I$. To see this, we define an operator

$$S^{y0} = \sum_{\mathbf{k},s} \sum_{nn'\eta\eta'} [B^{C_{2z}P}(\mathbf{k})]_{n\eta,n'\eta'} c^\dagger_{\mathbf{k},n,\eta,s} c_{\mathbf{k},n',\eta',s} \tag{18}$$

with sewing matrix $B^{C_{2z}P}(\mathbf{k})$ of $C_{2z}P$. It can be proved that $[S^{y0}, H_I] = 0$ (see Appendix D 2). Note that S^{y0} is identical to $C_{2z}P$ when acting on single-electron states. For many-body states, one can show that $C_{2z}P = e^{i\pi S^{y0}/2}$ (up to a phase factor). With the eight generators S^{0b}, S^{zb} of U(2)×U(2) ($b = 0, x, y, z$), we can define another 8 operators $S^{xb} = -\frac{i}{2}[S^{y0}, S^{zb}]$ and $S^{yb} = \frac{i}{2}[S^{x0}, S^{zb}]$. The 16 operators S^{ab} then satisfy the Lie algebra of U(4):

$$[S^{ab}, S^{cd}] = \sum_{ef} f_{ef}^{ab,cd} S^{ef}, \quad (a, b = 0, x, y, z), \tag{19}$$

where $f_{ef}^{ab,cd}$ are U(4) group structure constants defined by $[\tau^a s^b, \tau^c s^d] = \sum_{ef} f_{ef}^{ab,cd} \tau^e s^f$.

It is useful to fix the gauge of wave functions to obtain an explicit form of S^{ab}. We do this by requiring

$$(C_{2z}T) c^\dagger_{\mathbf{k},n,\eta,s} (C_{2z}T)^{-1} = c^\dagger_{\mathbf{k},n,\eta,s}, \tag{20}$$

which imposes $(\sigma_x)_{\alpha\beta} u_{\mathbf{Q},\beta,n,\eta}(\mathbf{k}) = u^*_{\mathbf{Q},\alpha,n,\eta}(\mathbf{k})$. $(\sigma_x)_{\alpha\beta} u_{\mathbf{Q},\beta,n,\eta}(\mathbf{k}) = u^*_{\mathbf{Q},\alpha,n,\eta}(\mathbf{k}) = u_{-\mathbf{Q},\alpha,n,-\eta}(-\mathbf{k})$. A consistent $\mathbf{k}$-independent gauge for $C_{2z}P$ is then

$$(C_{2z}P) c^\dagger_{\mathbf{k},n,\eta,s} (C_{2z}P)^{-1} = -\mathrm{sgn}(n) \eta c^\dagger_{\mathbf{k},-n,-\eta,s}. \tag{21}$$

In addition, we require a $\mathbf{k}$-space continuous gauge [which is crucial for the useful bases Eqs. (26) and (28)] defined below to have well-defined Berry curvature (see Sec. B 3):

$$\lim_{\mathbf{q}\to\mathbf{0}} |u^\dagger_{n,\eta}(\mathbf{k}+\mathbf{q}) u_{n,\eta}(\mathbf{k}) - u^\dagger_{-n,\eta}(\mathbf{k}+\mathbf{q}) u_{-n,\eta}(\mathbf{k})| = 0. \tag{22}$$

Under this gauge, we can rewrite the 16 U(4) generators as $S^{ab} = \sum_{\mathbf{k}} (s^{ab})_{m,\eta,s;n,\eta',s'} c^\dagger_{\mathbf{k},m,\eta,s} c_{\mathbf{k},n,\eta',s'}$ ($a, b = 0, x, y, z$), where the matrices s^{ab} within each ph pair of bands $n = \pm n_{\mathrm{B}}$ read

$$s^{ab} = \{\zeta^0 \tau^0 s^b,\ \zeta^y \tau^x s^b,\ \zeta^y \tau^y s^b,\ \zeta^0 \tau^z s^b\}. \tag{23}$$

We note that s^{ab} has no nonzero matrix elements between different pairs of ph symmetric bands $n_{\mathrm{B}} \neq n'_{\mathrm{B}}$. Meanwhile, the form factors (overlaps) $M^{(\eta)}_{m,n}(\mathbf{k}, \mathbf{q}+\mathbf{G}) = [M(\mathbf{k}, \mathbf{q}+\mathbf{G})]_{m\eta,n\eta}$ are gauge fixed into the following matrix form in the band and valley basis (Appendix C 3):

$$M(\mathbf{k}, \mathbf{q}+\mathbf{G}) = \sum_{j=0}^{3} M_j \alpha_j(\mathbf{k}, \mathbf{q}+\mathbf{G}), \tag{24}$$

where $\alpha_j(\mathbf{k}, \mathbf{q}+\mathbf{G})$ are *real* $n_{\max} \times n_{\max}$ matrices, and we have defined $M_0 = \zeta^0 \tau^0$, $M_1 = \zeta^x \tau^z$, $M_2 = i\zeta^y \tau^0$, and $M_3 = \zeta^z \tau^z$ in the space of each pair of band basis $n = \pm n_{\mathrm{B}}$ ($1 \leqslant$

$n_B \leqslant n_{max}$), all of which are real matrices. Here $M_j \alpha_j$ means the Kronecker direct product of matrices M_j and α_j.

We note that we could further fix the gauges of the $\mathbf{k}$ nonpreserving symmetries C_{2z}, T, and P in a $\mathbf{k}$-independent way consistent with Eqs. (20)–(22) [see Appendix B 2 and Eq. (B18)]. Under a further gauge fixing $C_{2z} c^\dagger_{\mathbf{k},n,\eta,s} C_{2z}^{-1} = c^\dagger_{-\mathbf{k},n,-\eta,s}$, one can show that the functions $\alpha_j(\mathbf{k}, \mathbf{q}+\mathbf{G})$ $(0 \leqslant j \leqslant 4)$ satisfy the conditions in Eqs. (C24) and (C25). In particular, these conditions require

$$\alpha_0(\mathbf{k}, \mathbf{G}) = \alpha_0^T(-\mathbf{k}, \mathbf{G}),$$
$$\alpha_j(\mathbf{k}, \mathbf{G}) = -\alpha_j^T(-\mathbf{k}, \mathbf{G}), \quad (j = 1, 2, 3), \tag{25}$$

at $\mathbf{q} = \mathbf{0}$ (see Appendix C 3).

With the gauge fixing of Eqs. (20)–(22), we can define a new basis within the pair of bands $n = \pm n_B$ as

$$d^{(n_B)\dagger}_{\mathbf{k},e_Y,\eta,s} = \frac{c^\dagger_{\mathbf{k},n_B,\eta,s} + i e_Y c^\dagger_{\mathbf{k},-n_B,\eta,s}}{\sqrt{2}}, \quad (e_Y = \pm 1), \tag{26}$$

which we show in Appendix B 3 have well-defined Berry curvatures. The reason for the notation $e_Y = \pm 1$ is because this basis is the eigenbasis of the Pauli matrix ζ_y with eigenvalue e_Y in the two-dimensional energy band basis of $n = \pm n_B$. We shall call the basis (26) the *irrep basis*, for the reason below.

At each $\mathbf{k}$ and Chern number e_Y, as shown in Appendix D 2 b, the four irrep basis creation operators $d^{(n_B)\dagger}_{\mathbf{k},e_Y,\eta,s}$ of valleys $\eta = \pm$ and spins $s = \uparrow, \downarrow$ form the basis of a fundamental U(4) irreducible representation (irrep), where the generators S^{ab} have 4×4 representation matrices

$$s^{ab}(e_Y) = \{\tau^0 s^b,\ e_Y \tau^x s^b,\ e_Y \tau^y s^b,\ \tau^z s^b\}. \tag{27}$$

This can be seen by observing that $d^{(n_B)\dagger}_{\mathbf{k},e_Y,\eta,s}$ diagonalizes the matrix ζ^y in Eq. (23) with the eigenvalue being e_Y. Note that the two irreps $s^{ab}(e_Y)$ with $e_Y = \pm 1$ differ by a unitary transformation τ^z, namely, a π valley rotation about z axis. Despite this difference by a unitary transformation, the two irreps $s^{ab}(e_Y)$ are both the fundamental irrep of U(4). In Young-tableaux accepted notations, we shall denote the fundamental irrep of U(4) as $[1]_4$ and the trivial identity irrep of U(4) as $[0]_4$ (see Appendix D 1, and see Ref. [109] for a detailed explanation of the Young tableaux notations). An electron with a fixed $e_Y = \pm 1$ and $\mathbf{k}$ thus occupies a U(4) irrep $[1]_4$.

For $n_B = 1$, namely, for the lowest conduction and valence bands $n = \pm 1$, we denote the basis in Eq. (26) in simplified notations without upper index as

$$d^\dagger_{\mathbf{k},e_Y,\eta,s} = \frac{c^\dagger_{\mathbf{k},+1,\eta,s} + i e_Y c^\dagger_{\mathbf{k},-1,\eta,s}}{\sqrt{2}}, \quad (e_Y = \pm 1), \tag{28}$$

which will be extensively used for solving the projected Hamiltonian within the lowest eight flat bands in Refs. [109–111]. As proved in Ref. [108] (see also similar discussions in Refs. [72,74]) and briefly reviewed in Appendix B 3, if a pair of energy bands $n = \pm n_B$ are disconnected with other bands, the irrep band we defined in Eq. (26) will carry a Chern number $e_Y e_{2,n_B}$, where e_{2,n_B} is the Wilson loop winding number of the two bands $n = \pm n_B$. Due to the nontrivial topological winding number $e_{2,1} = 1$ in the $n = \pm 1$ bands [43–47,76,116,117], the irrep basis $d^\dagger_{\mathbf{k},e_Y,\eta,s}$ in Eq. (28) of all $\mathbf{k}$ for each fixed e_Y, η, s form the basis of a Chern band of Chern number $e_Y = \pm 1$ (see proof in details in Ref. [108] and also a brief review in Appendix B 3), provided the $n = \pm 1$ energy bands are gapped from the higher bands (which is true near the first magic angle). For this reason, we shall call $d^\dagger_{\mathbf{k},e_Y,\eta,s}$ (within the $n = \pm 1$ energy band space) the *Chern band electron basis*, or simply the *Chern basis*. We note that our Chern basis in Eq. (28) is (adiabatically) equivalent to the Chern bands defined in Refs. [72,74].

If the $|n| \leqslant n_{max}$ bands are gapped from higher bands but are connected among themselves, we would expect the net Chern number of the n_{max} irrep basis $d^{(n_B)\dagger}_{\mathbf{k},e_Y,\eta,s}$ $(1 \leqslant n_B \leqslant n_{max})$ to be equal to e_Y (see Appendix B 3).

VI. U(4)×U(4) SYMMETRY IN THE (FIRST) CHIRAL-FLAT LIMIT

The symmetry of flat-band TBG is enhanced when $w_0 = 0 < w_1$ in Eq. (2), which is known as the *chiral limit* [37]. In this paper, we shall also call it the *first chiral limit*, to distinguish with the second chiral limit defined below in Sec. VIII. In this first chiral limit, there is a unitary chiral transformation C acting as $C c^\dagger_{\mathbf{k},\mathbf{Q},\eta,\alpha,s} C^{-1} = (\sigma_z)_{\beta\alpha} c^\dagger_{\mathbf{k},\mathbf{Q},\eta,\beta,s}$, which satisfies $C \hat{H}_0 C^{-1} = -\hat{H}_0$ and $C^2 = 1$. Therefore, the energy band eigenstates satisfy $\epsilon_{n,\eta}(\mathbf{k}) = -\epsilon_{-n,\eta}(\mathbf{k})$ and $(\sigma_z)_{\beta\alpha} u_{\mathbf{Q},\alpha,n,\eta}(\mathbf{k}) = [B^C(\mathbf{k})]_{-n,\eta;n\eta} u_{\mathbf{Q},\beta,-n,\eta}(\mathbf{k})$, where $B^C(\mathbf{k})$ is the unitary sewing matrix of C. This implies $C c^\dagger_{\mathbf{k},n,\eta,s} C^{-1} = [B^C(\mathbf{k})]_{-n,\eta;n\eta} c^\dagger_{\mathbf{k},-n,\eta,s}$.

When projected into the flat bands $|n| \leqslant n_{max}$, by Eq. (11), one can prove that $[C, O_{\mathbf{q},\mathbf{G}}] = 0$, and thus

$$\{C, H_0\} = 0, \quad [C, H_I] = 0. \tag{29}$$

Therefore, in the first chiral-flat limit where $H_0 = 0$ and thus $H = H_I$, the chiral transformation C becomes a symmetry. Note that C preserves the electron momentum $\mathbf{k}$ and thus is a local unitary symmetry.

We can then define a Hermitian operator

$$S'^{z0} = \sum_{\mathbf{k},s} \sum_{nn'\eta\eta'} [B^C(\mathbf{k})]_{n\eta,n'\eta'} c^\dagger_{\mathbf{k},n,\eta,s} c_{\mathbf{k},n',\eta',s}, \tag{30}$$

which commutes with H_I. Note that S'^{z0} is identical to C when acting on single-electron states. For many-body states, one can verify that $C = e^{i\pi S'^{z0}/2}$ (up to a phase factor). Its commutations with the 16 U(4) generators S^{ab} in Eq. (19) yield another 16 new operators S'^{ab}, and one can prove that S^{ab} and S'^{ab} form the 32 generators of a U(4)×U(4) group (Appendix D 3). This can be seen explicitly under the gauge fixing of Eqs. (20) and (21), for which the only $\mathbf{k}$-independent gauge choice (up to a global sign) for C is $C c^\dagger_{\mathbf{k},n,\eta,s} C^{-1} = i\mathrm{sgn}(n)\eta c^\dagger_{\mathbf{k},-n,\eta,s}$ (Appendix D 3). We note that this gauge choice is also consistent with the $\mathbf{k}$-independent gauge fixings of C_{2z}, T and P in Eq. (B18). The 16 new generators can then be expressed as $S'^{ab} = \sum_{\mathbf{k}} (s'^{ab})_{m,\eta,s;n,\eta',s'} c^\dagger_{\mathbf{k},m,\eta,s} c_{\mathbf{k},n,\eta',s'}$ $(a, b = 0, x, y, z)$, where s'^{ab} within each pair of bands $n = \pm n_B$ are given by

$$s'^{ab} = \{\zeta^y \tau^0 s^b,\ \zeta^0 \tau^x s^b,\ \zeta^0 \tau^y s^b,\ \zeta^y \tau^z s^b\}. \tag{31}$$

We note that s'^{ab} has no nonzero matrix elements between different pairs of ph symmetric bands $n_B \neq n'_B$. We can

further linear combine S^{ab} and S'^{ab} into operators $S^{ab}_{\pm} = \sum_{\mathbf{k}} (s^{ab}_{\pm})_{m,\eta,s;n,\eta',s'} c^{\dagger}_{\mathbf{k},m,\eta,s} c_{\mathbf{k},n,\eta',s'}$ $(a, b = 0, x, y, z)$, where

$$s^{ab}_{\pm} = (\zeta^0 \pm \zeta^y)\tau^a s^b/2. \tag{32}$$

One can then verify that

$$\left[S^{ab}_{e_Y}, S^{cd}_{e'_Y}\right] = \delta_{e_Y,e'_Y} \sum_{ef} f^{ab,cd}_{ef} S^{ef}_{e_Y}, \quad (e_Y = \pm 1), \tag{33}$$

where $f^{ab,cd}_{ef}$ are the U(4) structure constants in Eq. (19). Therefore, each set of $S^{ab}_{e_Y}$ $(e_Y = \pm 1)$ generates a U(4) group, leading to a total U(4)×U(4) symmetry. We note that the nonchiral-flat U(4) in Eq. (23) is *not* one of the two U(4)s with fixed e_Y here, although it is a subgroup of the first chiral-flat U(4)×U(4) here.

The 4 irrep band (Chern band if $n_{\mathrm{B}} = 1$) basis creation operators $d^{(n_{\mathrm{B}})\dagger}_{\mathbf{k},e_Y,\eta,s}$ (of valley-spin flavors $\eta = \pm, s = \uparrow, \downarrow$) at a fixed $\mathbf{k}$ and e_Y in Eq. (26) occupy a fundamental irrep of the U(4) generated by $S^{ab}_{e_Y}$ and a trivial identity irrep of the U(4) generated by $S^{ab}_{-e_Y}$ $(e_Y = \pm 1)$. The corresponding representation matrices of $S^{ab}_{\pm}$ are

$$s^{ab}_{\pm} = (1 \pm e_Y)\tau^a s^b/2, \tag{34}$$

which can be derived by replacing matrix ζ^0 (ζ^y) by its eigenvalue 1 (e_Y) in the irrep band basis $d^{(n_{\mathrm{B}})\dagger}_{\mathbf{k},e_Y,\eta,s}$. If we use $([\lambda_1]_4, [\lambda_2]_4)$ to represent a U(4)×U(4) irrep which is the tensor product of an irrep $[\lambda_1]_4$ of the first U(4) and an irrep $[\lambda_2]_4$ of the second U(4), we see that the irrep basis $d^{(n_{\mathrm{B}})\dagger}_{\mathbf{k},+1,\eta,s}$ at a fixed $\mathbf{k}$ occupies an irrep $([1]_4, [0]_4)$, while the irrep basis $d^{(n_{\mathrm{B}})\dagger}_{\mathbf{k},-1,\eta,s}$ at a fixed $\mathbf{k}$ occupies an irrep $([0]_4, [1]_4)$.

Furthermore, in Appendix D 3 we proved that [see Eq. (D30)] the C symmetry restricts

$$\alpha_1(\mathbf{k}, \mathbf{q} + \mathbf{G}) = \alpha_3(\mathbf{k}, \mathbf{q} + \mathbf{G}) = 0 \tag{35}$$

in Eq. (24). This makes $O_{\mathbf{q},\mathbf{G}}$ in Eq. (11) diagonal in index e_Y in the basis $d^{(n_{\mathrm{B}})\dagger}_{\mathbf{k},e_Y,\eta,s}$ [see Eq. (D45)], and thus the number of electrons in the $n_{\max}$ irrep bands (particularly, Chern band if $n_{\max} = 1$) with a fixed e_Y is conserved.

VII. U(4) SYMMETRY IN THE (FIRST) CHIRAL-NONFLAT LIMIT

We now turn to the first chiral-nonflat case which is in the first chiral limit $w_0 = 0$ [thus Eq. (29) holds], but does not have exactly flat bands ($H_0 \neq 0$). Since the chiral symmetry implies $\epsilon_{n,\eta}(\mathbf{k}) = -\epsilon_{-n,\eta}(\mathbf{k})$, the projected kinematic term in Eq. (9) within each pair of bands $n = \pm n_{\mathrm{B}}$ can be rewritten as

$$H_0^{(n_{\mathrm{B}})} = \sum_{\mathbf{k}} \epsilon_{+n_{\mathrm{B}},\eta}(\mathbf{k})(\zeta^z\tau^0 s^0)_{m,\eta,s;n,\eta',s'} c^{\dagger}_{\mathbf{k},m,\eta,s} c_{\mathbf{k},n,\eta',s'}. \tag{36}$$

As a result, H_0 only commutes with 16 out of the 32 U(4)×U(4) generators S^{ab} and S'^{ab} in Eqs. (23) and (31). We denote these 16 generators commuting with H_0 as $\tilde{S}^{ab} = \sum_{\mathbf{k}} (\tilde{s}^{ab})_{m,\eta,s;n,\eta',s'} c^{\dagger}_{\mathbf{k},m,\eta,s} c_{\mathbf{k},n,\eta',s'}$, where $\tilde{s}^{ab}$ within each pair of bands $n = \pm n_{\mathrm{B}}$ read

$$\tilde{s}^{ab} = \zeta^0 \tau^a s^b, \quad (a, b = 0, x, y, z). \tag{37}$$

They form the 16 generators of a U(4) group. In particular, the representation matrix $\tilde{s}^{x0}$ of generator $\tilde{S}^{x0}$ at each $\mathbf{k}$ is given by the sewing matrix of $iCC_{2z}P$, and thus $\tilde{S}^{x0}$ is identical to $iCC_{2z}P$ when acting on single-electron states. For many-body states, one has $iCC_{2z}P = e^{i\pi \tilde{S}^{x0}/2}$ (up to a phase factor). Therefore, in the first chiral-nonflat limit with $H_0 \neq 0$, there is a global U(4) symmetry generated by $\tilde{S}^{ab}$, which is reduced from the U(4)×U(4) symmetry of the first chiral-flat limit. We note that this first chiral-nonflat U(4) here (Eq. (37)) *is different* from the nonchiral-flat U(4) (Eq. (23)).

Since $\tilde{S}^{ab}$ is proportional to ζ^0 in the band basis, the energy band creation operators $c^{\dagger}_{\mathbf{k},n,\eta,s}$ in each band n at a fixed $\mathbf{k}$ occupy a fundamental irrep $[1]_4$ of the first chiral-nonflat U(4) group. Equivalently, the irrep band (Chern band if $n_{\mathrm{B}} = 1$) creation operators $d^{(n_{\mathrm{B}})\dagger}_{\mathbf{k},e_Y,\eta,s}$ for fixed e_Y, n_{B}, and $\mathbf{k}$ also occupy a fundamental U(4) irrep $[1]_4$. For the irrep of either $c^{\dagger}_{\mathbf{k},n,\eta,s}$ or $d^{(n_{\mathrm{B}})\dagger}_{\mathbf{k},e_Y,\eta,s}$, the representation matrices of $\tilde{S}^{ab}$ are given by

$$\tilde{s}^{ab}(n) = \tilde{s}^{ab}(e_Y) = \tau^a s^b \quad (a, b = 0, x, y, z). \tag{38}$$

Note that the representation matrices $\tilde{s}^{ab}(n)$ [or $\tilde{s}^{ab}(e_Y)$] are independent of n (or e_Y). This is in contrast to the nonchiral-flat limit, where the representation matrices of S^{ab} for $e_Y = \pm 1$ differ by a unitary transformation τ_z [although $e_Y = \pm 1$ therein still give the same fundamental nonchiral-flat U(4) irrep; see Eq. (27)].

VIII. U(4)×U(4) SYMMETRY IN THE SECOND CHIRAL-FLAT LIMIT

We find that there exists a *second chiral limit* $w_1 = 0 < w_0$ where the continuous symmetry of TBG is largely enhanced, similar to the situation in the first chiral limit discussed in Secs. VI and VII. Although this limit is far from the experimental reality of the TBG samples, its existence suggests the possibility of a possible hidden duality in the BM model and its interactions. For $w_1 = 0 < w_0$, we can define a second chiral transformation C' satisfying $C'^2 = 1$ and $C'\hat{H}_0 C'^{-1} = -\hat{H}_0$, which acts as $C' c^{\dagger}_{\mathbf{k},\mathbf{Q},\eta,\alpha,s} C'^{-1} = (\sigma_z)_{\beta\alpha}\zeta_{\mathbf{Q}} c^{\dagger}_{\mathbf{k},\mathbf{Q},\eta,\beta,s}$ with $\zeta_{\mathbf{Q}} = \pm 1$ for $\mathbf{Q} \in \mathcal{Q}_{\pm}$. This new chiral symmetry has *unusual* commutation relations with the twofold rotation C_{2z}, time-reversal T, and the unitary particle-hole symmetry P (see Appendix D 5 a and Ref. [108] for details). It also satisfies (see Appendix D 5)

$$\{C', H_0\} = 0, \quad [C', H_I] = 0, \tag{39}$$

similar to the first chiral symmetry C [Eq. (29)]. Note that the second chiral symmetry C' preserves electron momentum $\mathbf{k}$. In the *second chiral-flat limit* with $w_1 = 0$ and $H_0 = 0$, similar to the first chiral-flat limit, we can define a symmetry

$$S''^{z0} = \sum_{\mathbf{k},s} \sum_{nn'\eta\eta'} [B^{C'}(\mathbf{k})]_{n\eta,n'\eta'} c^{\dagger}_{\mathbf{k},n,\eta,s} c_{\mathbf{k},n',\eta',s}, \tag{40}$$

where $B^{C'}(\mathbf{k})$ is the sewing matrix of C'. Together with S^{ab} in Eq. (19), it generates a U(4)×U(4) group with 32 generators $S'^{ab}_{\pm}$ (see Appendix D 5). Under the gauge fixings of Eqs. (20) and (21), and a further gauge fixing for C' as $C' c^{\dagger}_{\mathbf{k},n,\eta,s} C'^{-1} = i\mathrm{sgn}(n)\eta c^{\dagger}_{\mathbf{k},-n,\eta,s}$ [which is consistent with the continuous condition (22); see Appendix D 5 b], we find $S'^{ab}_{\pm} = \sum_{\mathbf{k}} (s'^{ab}_{\pm})_{m,\eta,s;n,\eta',s'} c^{\dagger}_{\mathbf{k},m,\eta,s} c_{\mathbf{k},n,\eta',s'}$, where $s'^{ab}_{\pm}$

within each pair of bands $n = \pm n_B$ read

$$s'^{ab}_{\pm} = (\zeta^0 \pm \zeta^y)\tau^a s^b/2. \tag{41}$$

Again, we note that $s'^{ab}_{\pm}$ has no nonzero matrix elements between different pairs of ph symmetric bands $n_B \neq n'_B$.

It is worthwhile to mention that, due to the unusual commutation relations of C' with C_{2z}, T, and P which flip $\mathbf{k}$, one cannot further fix the sewing matrices of C_{2z}, T, and P into a $\mathbf{k}$-independent form as in Eq. (B18). Instead, the sewing matrices of these $\mathbf{k}$ flipping symmetries have to be $\mathbf{k}$-dependent, for instance, given by Eq. (D65) in Appendix D 5 b. This is closely related to the topologically protected double degeneracies at C_{2z}-invariant points of the MBZ, as proved in Ref. [108].

In this second chiral-flat limit, the four irrep band basis creation operators $d^{(n_B)\dagger}_{\mathbf{k},e_Y,\eta,s}$ ($\eta = \pm, s = \uparrow, \downarrow$) at a fixed $\mathbf{k}$ and e_Y in Eq. (26) occupy a fundamental irrep of the U(4) generated by $S'^{ab}_{e_Y}$ and a trivial identity irrep of the U(4) generated by $S'^{ab}_{-e_Y}$ ($e_Y = \pm 1$). The corresponding representation matrices of $S'^{ab}_{\pm}$ are

$$s'^{ab}_{\pm} = (1 \pm e_Y)\tau^a s^b/2, \tag{42}$$

which can be see by substituting matrix ζ^0 (ζ^y) by its eigenvalue 1 (e_Y) in the irrep band basis $d^{(n_B)\dagger}_{\mathbf{k},e_Y,\eta,s}$. Therefore, the irrep basis $d^{(n_B)\dagger}_{\mathbf{k},+1,\eta,s}$ at a fixed $\mathbf{k}$ occupies an irrep $([1]_4, [0]_4)$ of the second chiral-flat U(4)×U(4), while the irrep basis $d^{(n_B)\dagger}_{\mathbf{k},-1,\eta,s}$ at a fixed $\mathbf{k}$ occupies an irrep $([0]_4, [1]_4)$.

Furthermore, in Appendix D 5 we proved that [see Eq. (D66)] the C' symmetry restricts

$$\alpha_1(\mathbf{k}, \mathbf{q}+\mathbf{G}) = \alpha_3(\mathbf{k}, \mathbf{q}+\mathbf{G}) = 0 \tag{43}$$

in Eq. (24).

However, with $w_1 = 0 < w_0$, there is barely an angle where a set of low-energy bands become flat, and it is proved in Ref. [108] that all the energy bands are topologically connected into a perfect metal (see Fig. 2(c), Appendix D 5, and Refs. [108,118]). This makes the second chiral-flat limit less related to experimental realities, although it can possibly be achieved by artificial patterning of the moiré lattice to enhance AA hopping. Besides, we note that for the lowest ph band pair of $n_B = 1$, the "Chern band basis" $d^{\dagger}_{\mathbf{k},e_Y,\eta,s}$ in Eq. (28) no longer has a well-defined Chern number, since the $n = \pm 1$ bands are connected with all the higher bands.

We also note that although the representation matrices in the two chiral limits in Eqs. (32) and (41) are the same, their physical operations are different, since they are generated by the sewing matrices of the first chiral symmetry C and the second chiral symmetry C', respectively.

IX. U(4) SYMMETRY IN THE SECOND CHIRAL-NONFLAT LIMIT

With the TBG bands in the second chiral limit poorly flat, the *second chiral-nonflat limit* where $w_1 = 0 < w_0$ and $H_0 \neq 0$ gives a more physical limit, which may be realized by artificial patterning of moiré lattices. In this limit, similar to the first chiral-nonflat limit, we can prove that (see Appendix D 6) a U(4) symmetry remains, which is generated by the remaining $iC'C_{2z}P$ symmetry. The 16 U(4) generators are a subset of the generators $S'^{ab}_{\pm}$ in the second chiral-flat limit [Eq. (41)], which we denote by $\widetilde{S}'^{ab} = \sum_{\mathbf{k}} (\tilde{s}'^{ab})_{m,\eta,s;n,\eta',s'} c^{\dagger}_{\mathbf{k},m,\eta,s} c_{\mathbf{k},n,\eta',s'}$, where $\tilde{s}'^{ab}$ within each pair of bands $n = \pm n_B$ is given by

$$\tilde{s}'^{ab} = \zeta^0 \tau^a s^b. \tag{44}$$

This simply gives the spin-valley rotations without affecting the space of energy band indices n. Accordingly, either the energy band basis $c^{\dagger}_{\mathbf{k},n,\eta,s}$ or the irrep band basis $d^{(n_B)\dagger}_{\mathbf{k},e_Y,\eta,s}$ at a fixed $\mathbf{k}$ and n or e_Y occupy a fundamental U(4) irrep, with the representation matrices of $\widetilde{S}'^{ab}$ given by

$$\tilde{s}'^{ab}(n) = \tilde{s}'^{ab}(e_Y) = \tau^a s^b \quad (a, b = 0, x, y, z). \tag{45}$$

TABLE I. Symmetries in different limits. The last column shows the contributing ph and chiral symmetries.

TBG limit	H_0	w_0	w_1	Symmetry	ph/chiral
Nonchiral-nonflat	$\neq 0$	>0	>0	U(2)×U(2)	
Nonchiral-flat	$=0$	>0	>0	U(4)	$C_{2z}P$
(1st) chiral-flat	$=0$	$=0$	>0	U(4)×U(4)	$C_{2z}P$, C
(1st) chiral-nonflat	$\neq 0$	$=0$	>0	U(4)	$iCC_{2z}P$
2nd chiral-flat	$=0$	>0	$=0$	U(4)×U(4)	$C_{2z}P$, C'
2nd chiral-nonflat	$\neq 0$	>0	$=0$	U(4)	$iC'C_{2z}P$

X. THE STABILIZER CODE LIMIT

Generically, the projected interaction Hamiltonian H_I in Eq. (10) cannot be analytically diagonalized, since generically $[O_{\mathbf{q},\mathbf{G}}, O_{\mathbf{q}',\mathbf{G}'}] \neq 0$ for $\mathbf{q} \neq \mathbf{q}'$ or $\mathbf{G} \neq \mathbf{G}'$ [see Eq. (C16)], and thus the terms $O_{-\mathbf{q},-\mathbf{G}} O_{\mathbf{q},\mathbf{G}}$ in H_I are noncommuting.

However, in the case we are only projecting into the lowest eight bands with $n = \pm 1$ (namely, $n_{\max} = 1$), there is limit which we call the *stabilizer code limit*, where the Hamiltonian becomes similar to (but not strictly identical to; see Appendix E) a stabilizer code Hamiltonian with all of its terms mutually commuting. The stabilizer code limit is defined in either the first chiral-flat limit (with first chiral symmetry C) or the second chiral-flat limit (with second chiral symmetry C'), where Eq. (35) or (43) is satisfied, and the condition is that the form factors $M(\mathbf{k}, \mathbf{q}+\mathbf{G})$ in Eq. (24) are $\mathbf{k}$ independent for any $\mathbf{q}, \mathbf{G}$. In this limit, as we proved in Appendix E, one would have $[O_{\mathbf{q},\mathbf{G}}, O_{\mathbf{q}',\mathbf{G}'}] = 0$. Thus, all the terms $O_{-\mathbf{q},-\mathbf{G}} O_{\mathbf{q},\mathbf{G}}$ in the Hamiltonian $H = H_I$ in Eq. (10) will be commuting:

$$[O_{-\mathbf{q},-\mathbf{G}} O_{\mathbf{q},\mathbf{G}}, O_{-\mathbf{q}',-\mathbf{G}'} O_{\mathbf{q}',\mathbf{G}'}] = 0. \tag{46}$$

This stabilizer code-like Hamiltonian has all of its many-body eigenstates exactly solvable, which will be solved in a separate paper [109].

XI. DISCUSSION

We have demonstrated that for the projected Hamiltonian with Coulomb interaction in the lowest $8n_{\max}$ ($2n_{\max}$ per spin-valley) bands of any $n_{\max} \geqslant 1$, there exists various different limits where global U(4) or U(4)×U(4) symmetries emerge. For $n_{\max}$, there exists a stabilizer code limit for the Hamiltonian in either the first or the second chiral flat limit, where all the terms in the Hamiltonian are mutually commuting. Our conclusions are summarized in Table I and Fig. 3. Near

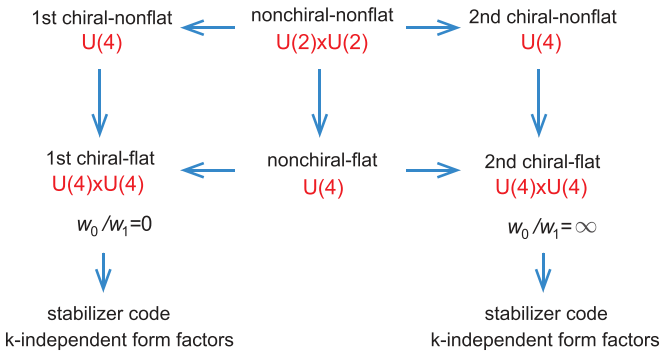

FIG. 3. The relations between the symmetries of projected Hamiltonian within any set of ph symmetric bands of full spin-valley flavors in various limits. The arrows point along the directions along which the symmetry groups are enhanced into a larger one.

the first magic angle, the low-energy physics is expected to be governed by the projected Hamiltonian with $n_{\max} = 1$. A projected Hamiltonian within higher number of bands could be a good approximation at higher magic angles, where more than two bands per spin-valley can become flat.

The U(4) symmetry in the nonchiral-flat limit in Eq. (23) and U(4)×U(4) symmetry in the first chiral-flat limit in Eq. (32) that we prove here agree with those discussed in Ref. [72] for the lowest eight flat bands near the first magic angle. We note that, however, we show the symmetries are generic for the projection into any number of ph symmetric bands with full spin-valley degrees of freedom. Besides, we have identified a second chiral limit, which also enjoys a U(4)×U(4) symmetry in a second chiral-flat limit. We have also derived the explicit irrep band basis of the symmetries in all the different limits. Furthermore, we showed that under a strong condition, the projected Hamiltonian in the lowest eight bands in the first or second chiral-flat limit becomes similar to a stabilizer code Hamiltonian, thus allowing one to exactly solve all the many-body eigenstates, which we will study in Ref. [109].

A U(4) symmetry in the flat band limit is also discussed in Ref. [71], which is constructed based on a non-maximally-symmetric Wannier basis. (These Wannier functions break the $C_{2z}T$ and $C_{2z}TP$ symmetries, which protect the fragile topology [43–45] and stable topology [108] in TBG, respectively.) The U(4) symmetry in Ref. [71] is closest to our first chiral-nonflat U(4) symmetry that we introduce in Eq. (37) since they have the same generators $\tau^a s^b$ $(a, b = 0, x, y, z)$. However, Ref. [71] does not assume the $CC_{2z}P$ symmetry but requires the flatness of the two bands, which is in contradiction to our first chiral-nonflat U(4), which assumes the $CC_{2z}P$ symmetry and does not require flat bands. The reason Ref. [71] needs flat bands is the absence of exact $CC_{2z}P$ symmetry. We show in Appendix F that, if the $CC_{2z}P$ symmetry is imposed to the Wannier functions, then the two U(4) symmetries become the same and do not require the flatness of bands.

The TBG interacting Hamiltonian, symmetries, and gauge fixings we derived here provide a solid ground for future theoretical studies. In the various limits we discussed, the many-body eigenstates of TBG should fall into irreps of U(4) or U(4)×U(4) groups. Besides, the generic PSDH form of the projected interaction H_I in Eq. (10) allows us to look for ground states of the Kang-Vafek type in the flat band limit. We will study the ground states and excitations of TBG in these limits analytically and numerically in separate papers [109–111]. The existence of several limits with identical large continuous symmetry groups (but different generators) of the BM interacting Hamiltonian, as shown in Fig. 3, suggests the presence of a yet to be found duality of this model.

ACKNOWLEDGMENTS

We thank Aditya Cowsik and Fang Xie for valuable discussions. B.A.B. thanks Oskar Vafek for fruitful discussions and for sharing similar results on this problem before publication [103]. This work was supported by DOE Grant No. DE-SC0016239, the Schmidt Fund for Innovative Research, Simons Investigator Grant No. 404513, the Packard Foundation, the Gordon and Betty Moore Foundation through Grant No. GBMF8685 toward the Princeton theory program, and a Guggenheim Fellowship from the John Simon Guggenheim Memorial Foundation. Further support was provided by NSF-EAGER Grant No. DMR 1643312, NSF-MRSEC Grants No. DMR-1420541 and No. DMR-2011750, ONR Grant No. N00014-20-1-2303, BSF Israel-US Foundation Grant No. 2018226, and the Princeton Global Network Funds. B.L. acknowledges the support of the Princeton Center for Theoretical Science at Princeton University during the early stage of this work.

APPENDIX A: REVIEW OF THE SINGLE-PARTICLE HAMILTONIAN

The quantitative and symmetry aspects of the single-particle Hamiltonian of TBG are discussed in detail in Refs. [107,108]. For completeness, here we briefly review the notations and conclusions for the single-particle Hamiltonian.

1. Bases

We denote the fermion operator in the plane-wave basis of graphene layer l as $c^\dagger_{\mathbf{p},\alpha,s,l}$. Here $\mathbf{p}$ is measured from the Γ point of the monolayer graphene Brillouin zone (BZ), $\alpha = A, B$ represents the AB sublattice, $s = \uparrow, \downarrow$ is the spin index, and $l = \pm$ is the layer index. We define $\mathbf{K}_+$ as the K point in the top-layer graphene BZ and $\mathbf{K}_-$ as the K point in the bottom-layer graphene BZ. $\mathbf{K}_+$ and $\mathbf{K}_-$ differ by a twist angle θ (Fig. 1). For concreteness, we assume $\mathbf{K}_l$ is along the direction with an angle $-l\theta/2$ to the p_x axis. Each graphene layer l contains two valleys, K and K′, at momenta $\eta\mathbf{K}_l$, where $\eta = \pm$ denotes graphene valleys K and K′, respectively.

For later use, we define the two-dimensional (2D) momenta

$$\mathbf{q}_1 = (\mathbf{K}_- - \mathbf{K}_+) = k_\theta(0, 1)^T,$$
$$\mathbf{q}_2 = C_{3z}\mathbf{q}_1 = k_\theta\left(-\frac{\sqrt{3}}{2}, -\frac{1}{2}\right)^T,$$
$$\mathbf{q}_3 = C^2_{3z}\mathbf{q}_1 = k_\theta\left(\frac{\sqrt{3}}{2}, -\frac{1}{2}\right)^T, \tag{A1}$$

where $k_\theta = |\mathbf{K}_- - \mathbf{K}_+| = 2|\mathbf{K}_+|\sin(\theta/2)$ for twist angle θ. We can then define the moiré BZ (MBZ) for the TBG moiré lattice, which is generated by the moiré reciprocal vectors

$$\mathbf{b}_{M1} = \mathbf{q}_3 - \mathbf{q}_1, \quad \mathbf{b}_{M2} = \mathbf{q}_3 - \mathbf{q}_2. \tag{A2}$$

2. Single-particle Hamiltonian

When the twist angle between the two graphene layers is small ($\theta \approx 1^\circ$), an approximate valley-U(1) symmetry and an approximate moiré translation symmetry emerge. Accordingly, the single-particle Hamiltonian is decoupled between two valleys $\eta = \pm$.

To concentrate on the low-energy physics of the two valleys, we define $\mathcal{Q}_0 = \mathbb{Z}\mathbf{b}_{M1} + \mathbb{Z}\mathbf{b}_{M2}$ as the triangular moiré reciprocal lattice sites generated by the moiré reciprocal vectors $\mathbf{b}_{M1}$ and $\mathbf{b}_{M2}$ in Eq. (A2). We then define two shifted momentum lattices $\mathcal{Q}_+ = \mathbf{q}_1 + \mathcal{Q}_0$ and $\mathcal{Q}_- = -\mathbf{q}_1 + \mathcal{Q}_0$. We then define the low-energy fermion operators $c^\dagger_{\mathbf{k},\mathbf{Q},\eta,\alpha,s}$ at valley η and $\mathbf{Q} \in \mathcal{Q}_\pm$ as

$$c^\dagger_{\mathbf{k},\mathbf{Q},+,\alpha,s} = \begin{cases} c^\dagger_{\mathbf{K}_+ + \mathbf{k} - \mathbf{Q},\alpha,s,+} & \mathbf{Q} \in \mathcal{Q}_+ \\ c^\dagger_{\mathbf{K}_- + \mathbf{k} - \mathbf{Q},\alpha,s,-} & \mathbf{Q} \in \mathcal{Q}_- \end{cases}, \tag{A3}$$

$$c^\dagger_{\mathbf{k},\mathbf{Q},-,\alpha,s} = \begin{cases} c^\dagger_{-\mathbf{K}_- + \mathbf{k} - \mathbf{Q},\alpha,s,-} & \mathbf{Q} \in \mathcal{Q}_+ \\ c^\dagger_{-\mathbf{K}_+ + \mathbf{k} - \mathbf{Q},\alpha,s,+} & \mathbf{Q} \in \mathcal{Q}_- \end{cases}, \tag{A4}$$

where $\mathbf{k}$ takes value in the MBZ, and $\mathbf{k} = \mathbf{0}$ is chosen at the center (Γ_M point) of the MBZ. In practice, we always take a finite cutoff for $\mathcal{Q}_{0,+,-}$; the largest $\mathbf{Q}$ in $\mathcal{Q}_\pm$ should have a norm much smaller than $|\mathbf{K}_+|$. We denote the number of points in $\mathcal{Q}_{0,+,-}$ as $|\mathcal{Q}_{0,+,-}|$.

The single-particle Hamiltonian of TBG for small twist angle θ is given by [1,107,108]

$$\hat{H}_0 = \sum_{\mathbf{k}\in \mathrm{MBZ}} \sum_{\eta\alpha\beta s} \sum_{\mathbf{Q}\mathbf{Q}'} \left[h^{(\eta)}_{\mathbf{Q},\mathbf{Q}'}(\mathbf{k})\right]_{\alpha\beta} c^\dagger_{\mathbf{k},\mathbf{Q},\eta,\alpha,s} c_{\mathbf{k},\mathbf{Q}',\eta,\beta,s}, \tag{A5}$$

where $h^{(\eta)}_{\mathbf{Q},\mathbf{Q}'}(\mathbf{k})$ is the first-quantized momentum space Hamiltonian at valley η in the sublattice space, and $\mathbf{Q}, \mathbf{Q}' \in \mathcal{Q}_\pm$. At valley K ($\eta = +$), we have

$$h^{(+)}_{\mathbf{Q},\mathbf{Q}'}(\mathbf{k}) = v_F(\mathbf{k} - \mathbf{Q}) \cdot \boldsymbol{\sigma} \delta_{\mathbf{Q},\mathbf{Q}'} + \sum_{j=1}^{3} T_j \delta_{\mathbf{Q},\mathbf{Q}'\pm\mathbf{q}_j}, \tag{A6}$$

where v_F is the graphene Fermi velocity, and the matrices

$$T_j = w_0\sigma_0 + w_1\left[\sigma_x \cos\frac{2\pi(j-1)}{3} + \sigma_y \sin\frac{2\pi(j-1)}{3}\right]. \tag{A7}$$

Here σ_0 and $\boldsymbol{\sigma} = (\sigma_x, \sigma_y)$ are the 2×2 identity matrix and Pauli matrices in the space of sublattice indices, while $w_0 \geqslant 0$ and $w_1 \geqslant 0$ are the interlayer hoppings at the AA and AB stacking centers of TBG, respectively. Generically, in realistic systems $w_0 < w_1$ due to the lattice relaxation. In the absence of lattice relaxation, one has $w_0 = w_1$.

At valley K′ ($\eta = -$), we have

$$h^{(-)}_{\mathbf{Q},\mathbf{Q}'}(\mathbf{k}) = \sigma_x h^{(+)}_{-\mathbf{Q},-\mathbf{Q}'}(-\mathbf{k})\sigma_x = -v_F(\mathbf{k} - \mathbf{Q}) \cdot \boldsymbol{\sigma}^* \delta_{\mathbf{Q},\mathbf{Q}'} + \sum_{j=1}^{3} (\sigma_x T_j \sigma_x) \delta_{\mathbf{Q},\mathbf{Q}'\pm\mathbf{q}_j}, \tag{A8}$$

where $\boldsymbol{\sigma}^* = (\sigma_x, -\sigma_y)$.

3. Symmetries

Here we summarize the symmetries of TBG, which can be found in Ref. [43] and are expanded on in Ref. [108].

1. *Discrete symmetries*. Since graphene has zero spin-orbit coupling (SOC), we can define a set of spinless symmetries for TBG. In TBG, there are spinless unitary discrete rotational symmetries C_{2z}, C_{3z}, and C_{2x}, and the spinless antiunitary time-reversal symmetry T, which satisfy

$$[C_{3z}, \hat{H}_0] = [C_{2z}, \hat{H}_0] = [C_{2x}, \hat{H}_0] = [T, \hat{H}_0] = 0. \tag{A9}$$

We denote the action of a spinless symmetry operator g on the fermion basis $c^\dagger_{\mathbf{k},\mathbf{Q},\eta,\alpha,s}$ as

$$g c^\dagger_{\mathbf{k},\mathbf{Q},\eta,\alpha,s} g^{-1} = \sum_{\mathbf{Q}'\eta'\beta} [D(g)]_{\mathbf{Q}'\eta'\beta,\mathbf{Q}\eta\alpha} c^\dagger_{g\mathbf{k},\mathbf{Q}',\eta',\beta,s}, \tag{A10}$$

where $D(g)$ is the representation matrix of the symmetry operation g in the space of indices $\{\mathbf{Q}, \eta, \alpha\}$, and $g\mathbf{k}$ is the momentum after acting g on momentum $\mathbf{k}$. In particular, $C_{2z}\mathbf{k} = T\mathbf{k} = -\mathbf{k}$. The representation matrices for the discrete symmetries of TBG are given by

$$[D(C_{3z})]_{\mathbf{Q}'\eta'\beta,\mathbf{Q}\eta\alpha} = \delta_{\mathbf{Q}',C_{3z}\mathbf{Q}} \delta_{\eta',\eta} \left(e^{i\eta\frac{2\pi}{3}\sigma_z}\right)_{\beta\alpha}, \tag{A11}$$

$$[D(C_{2x})]_{\mathbf{Q}'\eta'\beta,\mathbf{Q}\eta\alpha} = \delta_{\mathbf{Q}',C_{2x}\mathbf{Q}} \delta_{\eta',-\eta} (\sigma_x)_{\beta\alpha}, \tag{A12}$$

$$[D(C_{2z})]_{\mathbf{Q}'\eta'\beta,\mathbf{Q}\eta\alpha} = \delta_{\mathbf{Q}',-\mathbf{Q}} \delta_{\eta',-\eta} (\sigma_x)_{\beta\alpha}, \tag{A13}$$

$$[D(T)]_{\mathbf{Q}'\eta'\beta,\mathbf{Q}\eta\alpha} = \delta_{\mathbf{Q}',-\mathbf{Q}} \delta_{\eta',-\eta} \delta_{\beta,\alpha}, \tag{A14}$$

Moreover, T is antiunitary, so $TiT^{-1} = -i$.

In particular, the combined symmetry $C_{2z}T$ does not change $\mathbf{k}$, i.e., $C_{2z}T\mathbf{k} = \mathbf{k}$, and the representation matrix is

$$[D(C_{2z}T)]_{\mathbf{Q}'\eta'\beta,\mathbf{Q}\eta\alpha} = [D(C_{2z})D(T)]_{\mathbf{Q}'\eta'\beta,\mathbf{Q}\eta\alpha} = \delta_{\mathbf{Q}',\mathbf{Q}} \delta_{\eta',\eta} (\sigma_x)_{\beta,\alpha}. \tag{A15}$$

2. *U(2)×U(2) spin-charge rotation symmetry*. The graphene has zero (negligible) spin-orbit coupling (SOC). Since the single-particle Hamiltonian of TBG has two decoupled valleys $\eta = \pm$, and the SOC is zero, the electron SU(2) spins of each valley can be rotated freely. Each valley also has a charge U(1) rotation symmetry. This leads to a global U(2)×U(2) symmetry. The eight generators of the U(2)×U(2) symmetry are given by

$$\hat{S}^{ab} = \sum_{\mathbf{k}} (\tau^a)_{\eta\eta'} (s^b)_{ss'} c^\dagger_{\mathbf{k},\mathbf{Q},\eta,\alpha,s} c_{\mathbf{k},\mathbf{Q},\eta',\alpha,s'}, \quad (a = 0, z,\ b = 0, x, y, z), \tag{A16}$$

where we have defined τ^a and s^a ($a = 0, x, y, z$) as the 2×2 identity and Pauli matrices in the valley and spin spaces, respectively.

3. *Particle-hole (ph) transformation P*. In addition to the above symmetries, TBG also has a unitary particle-hole (ph) "symmetry" [43], which satisfies the anticommutation relation

$$\{P, \hat{H}_0\} = 0. \tag{A17}$$

The action of P is given by

$$Pc^\dagger_{\mathbf{k},\mathbf{Q},\eta,\alpha,s}P^{-1} = \sum_{\mathbf{Q}'\eta'\beta}[D(P)]_{\mathbf{Q}'\eta'\beta,\mathbf{Q}\eta\alpha}c^\dagger_{-\mathbf{k},\mathbf{Q}',\eta',\beta,s}\,, \quad \text{(A18)}$$

with the representation matrix

$$[D(P)]_{\mathbf{Q}'\eta'\beta,\mathbf{Q}\eta\alpha} = \delta_{\mathbf{Q}',-\mathbf{Q}}\delta_{\eta',\eta}\delta_{\beta,\alpha}\zeta_{\mathbf{Q}}\,, \quad \text{(A19)}$$

where $\zeta_{\mathbf{Q}} = \pm 1$ for $\mathbf{Q} \in \mathcal{Q}_\pm$, respectively. Note that P transforms creation operators to creation operators (rather than annihilation operators) and maps sites $\mathbf{Q} \in \mathcal{Q}_\pm$ into $-\mathbf{Q} \in \mathcal{Q}_\mp$. Since P flips the single-particle Hamiltonian $\hat{H}_0$, it is not a commuting symmetry of TBG but only reflects a relation between the positive and negative energy spectra. Furthermore, the ph transformation P satisfies

$$P^2 = -1, \quad [P, C_{3z}] = 0, \quad \{P, C_{2x}\} = 0,$$
$$\{P, C_{2z}\} = 0, \quad \{P, T\} = 0, \quad [P, C_{2z}T] = 0. \quad \text{(A20)}$$

4. Eigenstates

The solutions to the single-particle Hamiltonian $\hat{H}_0$ in Eq. (A5) allows us to define the energy band basis

$$c^\dagger_{\mathbf{k},n,\eta,s} = \sum_{\mathbf{Q}\alpha} u_{\mathbf{Q}\alpha;n\eta}(\mathbf{k})c^\dagger_{\mathbf{k},\mathbf{Q},\eta,\alpha s}, \quad \text{(A21)}$$

where $u_{\mathbf{Q}\alpha;n\eta}(\mathbf{k})$ is the eigenstate wave function of energy band n of the first quantized single-particle Hamiltonian $h^{(\eta)}_{\mathbf{Q},\mathbf{Q}'}(\mathbf{k})$ in valley η. It satisfies

$$\sum_{\mathbf{Q}',\beta}\left[h^{(\eta)}_{\mathbf{Q},\mathbf{Q}'}(\mathbf{k})\right]_{\alpha\beta}u_{\mathbf{Q}'\beta;n\eta}(\mathbf{k}) = \epsilon_{n,\eta}(\mathbf{k})u_{\mathbf{Q}\alpha;n\eta}(\mathbf{k}), \quad \text{(A22)}$$

where $\epsilon_{n,\eta}(\mathbf{k})$ is the single-particle energy of eigenstate $u_{\mathbf{Q}\alpha;n\eta}(\mathbf{k})$. Note that the wave function $u_{\mathbf{Q}\alpha;n\eta}(\mathbf{k})$ and energy $\epsilon_{n,\eta}(\mathbf{k})$ are independent of spin s, because of the absence of SOC. In each valley and spin, we shall use integers $n > 0$ to label the nth conduction band, and use integer $n < 0$ to label the $|n|$th valence band (thus $n \neq 0$). The lowest conduction and valence bands in each valley-spin flavor is thus labeled by $n = \pm 1$.

Since $c^\dagger_{\mathbf{k}+\mathbf{b}_{Mi},\mathbf{Q},\eta\alpha s} = c^\dagger_{\mathbf{k},\mathbf{Q}-\mathbf{b}_{Mi},\eta\alpha s}$ for reciprocal vector $\mathbf{b}_{Mi}$ ($i = 1, 2$), we generalize the eigenstate wave function to momenta $\mathbf{k}$ outside the MBZ by the embedding relation for shifting momentum $\mathbf{k}$ by a reciprocal vector $\mathbf{b}_{Mi}$:

$$u_{\mathbf{Q}\alpha;n\eta}(\mathbf{k} + \mathbf{b}_{Mi}) = u_{\mathbf{Q}-\mathbf{b}_{Mi},\alpha;n\eta}(\mathbf{k}). \quad \text{(A23)}$$

This ensures our energy band basis is defined periodically in the MBZ, namely, $c^\dagger_{\mathbf{k}+\mathbf{b}_{Mi},n\eta s} = c^\dagger_{\mathbf{k}n\eta s}$. Besides, due to the C_{2z} symmetry and ph symmetry P, the energy spectrum satisfies

$$\epsilon_{n,\eta}(\mathbf{k}) = \epsilon_{n,-\eta}(-\mathbf{k})\,, \quad \epsilon_{n,\eta}(\mathbf{k}) = -\epsilon_{-n,\eta}(-\mathbf{k})\,. \quad \text{(A24)}$$

The single-particle Hamiltonian can then be rewritten in the energy band basis as

$$\hat{H}_0 = \sum_{\mathbf{k}}\sum_{n\eta s}\epsilon_{n,\eta}(\mathbf{k})c^\dagger_{\mathbf{k}n\eta s}c_{\mathbf{k}n\eta s}. \quad \text{(A25)}$$

APPENDIX B: GAUGE FIXING AND THE CHERN BAND BASIS

In this Appendix, we fix the gauge for the energy band basis $c^\dagger_{\mathbf{k}n\eta s}$ in Eq. (A21), so that we are able to obtain an explicit form of the interaction Hamiltonian in Appendix C 3. We will also define a Chern band basis, whose gauge fixing was shown in Ref. [108], using the energy band basis.

1. Sewing matrices

The discrete symmetries in Appendix A 3 yield certain relations among the eigenstate wave functions related by these symmetries. For the purpose of gauge fixing, here we will discuss these relations among eigenstate wave functions for operators C_{2z}, T, and P.

For notation simplicity, we denote the wave function $u_{\mathbf{Q}\alpha;n\eta}(\mathbf{k})$ as a column vector $u_{n\eta}(\mathbf{k})$ in the space of indices $\{\mathbf{Q}, \alpha\}$. Furthermore, when a representation matrix $D(g)$ of an operation g [defined in Eqs. (A11) to (A19)] acts on a wave function $u_{n\eta'}(\mathbf{k})$, we denote the resulting wave function in valley η for short as $[D(g)]_{\eta\eta'}u_{n\eta'}(\mathbf{k})$, the components of which are given by $\sum_{\mathbf{Q}'\beta\eta'}[D(g)]_{\mathbf{Q}\alpha\eta,\mathbf{Q}'\beta\eta'}u_{\mathbf{Q}'\beta;n\eta'}(\mathbf{k})$. Namely, we suppress the indices $\{\mathbf{Q}, \alpha\}$ of the representation matrix $D(g)$ for short.

When g is a symmetry operator satisfying $[\hat{H}_0, g] = 0$ (or $\{\hat{H}_0, g\} = 0$), if $u_{n\eta'}(\mathbf{k})$ is an eigenstate wave function at momentum $\mathbf{k}$, the wave function $[D(g)]_{\eta\eta'}u_{n\eta'}(\mathbf{k})$ (an additional complex conjugation is needed if g is antiunitary) must also be an eigenstate wave function at momentum $g\mathbf{k}$ at the same (or opposite) single-particle energy. For symmetries C_{2z}, T, and P, this allows us to define the sewing matrices $B^g(\mathbf{k})$ in the band and valley space connecting the symmetry related eigenstates by

$$[D(C_{2z})]_{\eta\eta'}u_{n\eta'}(\mathbf{k}) = \sum_m [B^{C_{2z}}(\mathbf{k})]_{m\eta,n\eta'}u_{m\eta}(-\mathbf{k}), \quad \text{(B1)}$$

$$[D(T)]_{\eta\eta'}u^*_{n\eta'}(\mathbf{k}) = \sum_m [B^{T}(\mathbf{k})]_{m\eta,n\eta'}u_{m\eta}(-\mathbf{k}), \quad \text{(B2)}$$

$$[D(P)]_{\eta\eta'}u_{n\eta'}(\mathbf{k}) = \sum_m [B^{P}(\mathbf{k})]_{m\eta,n\eta'}u_{m\eta}(-\mathbf{k}). \quad \text{(B3)}$$

For nondegenerate wave function $u_{n\eta'}(\mathbf{k})$ in valley η', since C_{2z} and T commute with the $\hat{H}_0$ and flips the valley η, while P anticommutes with $\hat{H}_0$ and preserves the valley η, we generically have

$$[B^{C_{2z}}(\mathbf{k})]_{m\eta,n\eta'} = \delta_{\eta,-\eta'}\delta_{m,n}e^{i\varphi^{C_{2z}}_{n,\eta'}(\mathbf{k})},$$
$$[B^{T}(\mathbf{k})]_{m\eta,n\eta'} = \delta_{\eta,-\eta'}\delta_{m,n}e^{i\varphi^{T}_{n,\eta'}(\mathbf{k})},$$
$$[B^{P}(\mathbf{k})]_{m\eta,n\eta'} = \delta_{\eta,\eta'}\delta_{-m,n}e^{i\varphi^{P}_{n,\eta'}(\mathbf{k})}. \quad \text{(B4)}$$

Accordingly, the action of a symmetry operator g on the energy band fermion operators [defined in Eq. (A21)] is given by

$$gc^\dagger_{\mathbf{k},n,\eta',s}g^{-1} = \sum_{m\eta}[B^g(\mathbf{k})]_{m\eta,n\eta'}c^\dagger_{g\mathbf{k},m,\eta,s}. \quad \text{(B5)}$$

Since the three symmetries satisfy the relations

$$C^2_{2z} = 1, \; T^2 = 1, \; P^2 = -1, \; \{P, C_{2z}\} = 0,$$
$$\{P, T\} = 0, \; [C_{2z}, T] = 0, \quad \text{(B6)}$$

with the above notations, the symmetries C_{2z}, T, and P allow us to define

$$\begin{aligned} B^{C_{2z}}(-\mathbf{k})B^{C_{2z}}(\mathbf{k}) &= B^{T}(-\mathbf{k})B^{T*}(\mathbf{k}) = -B^{P}(-\mathbf{k})B^{P}(\mathbf{k}) = I, \\ B^{P}(-\mathbf{k})B^{C_{2z}}(\mathbf{k}) &= -B^{C_{2z}}(-\mathbf{k})B^{P}(\mathbf{k}), \\ B^{P}(-\mathbf{k})B^{T}(\mathbf{k}) &= -B^{T}(-\mathbf{k})B^{P*}(\mathbf{k}), \\ B^{T}(-\mathbf{k})B^{C_{2z}*}(\mathbf{k}) &= -B^{C_{2z}}(-\mathbf{k})B^{T}(\mathbf{k}), \end{aligned} \tag{B7}$$

where $B^{g*}(\mathbf{k})$ stands for the complex conjugation of matrix $B^{g}(\mathbf{k})$, and I is the identity matrix in the n, η space. More discussions on the sewing matrices can be found in Ref. [108].

The combination of the three symmetries yields two independent symmetry operations $C_{2z}T$ and $C_{2z}P$, which do not change $\mathbf{k}$. Note that $C_{2z}T$ is antiunitary and $C_{2z}P$ is unitary. Their sewing matrices are defined by

$$[D(C_{2z})D(T)]_{\eta\eta'}u^{*}_{n\eta'}(\mathbf{k}) = \sum_{m}[B^{C_{2z}T}(\mathbf{k})]_{m\eta,n\eta'}u_{m\eta}(\mathbf{k}), \tag{B8}$$

$$[D(P)D(C_{2z})]_{\eta\eta'}u_{n\eta'}(\mathbf{k}) = \sum_{m}[B^{C_{2z}P}(\mathbf{k})]_{m\eta,n\eta'}u_{m\eta}(\mathbf{k}). \tag{B9}$$

For nondegenerate eigenstates at momentum $\mathbf{k}$ (nondegenerate within one valley), they are given by

$$\begin{aligned} [B^{C_{2z}T}(\mathbf{k})]_{m\eta,n\eta'} &= \delta_{\eta,\eta'}\delta_{m,n}e^{i\varphi^{C_{2z}T}_{n,\eta'}(\mathbf{k})}, \\ [B^{C_{2z}P}(\mathbf{k})]_{m\eta,n\eta'} &= \delta_{-\eta,\eta'}\delta_{-m,n}e^{i\varphi^{C_{2z}P}_{n,\eta'}(\mathbf{k})}, \end{aligned} \tag{B10}$$

where by definition we have $\varphi^{C_{2z}T}_{n,\eta'}(\mathbf{k}) = \varphi^{T}_{n,\eta'}(\mathbf{k}) + \varphi^{C_{2z}}_{n,-\eta'}(-\mathbf{k})$ and $\varphi^{C_{2z}P}_{n,\eta'}(\mathbf{k}) = \varphi^{C_{2z}}_{n,\eta'}(\mathbf{k}) + \varphi^{P}_{n,-\eta'}(-\mathbf{k})$. The sewing matrices of $C_{2z}T$ and $C_{2z}P$ are subject to the constraint that

$$(C_{2z}T)^2 = (C_{2z}P)^2 = 1, \quad [C_{2z}T, C_{2z}P] = 1, \tag{B11}$$

and thus they satisfy

$$\begin{aligned} B^{C_{2z}T}(\mathbf{k})B^{C_{2z}T*}(\mathbf{k}) &= [B^{C_{2z}P}(\mathbf{k})]^2 = I, \\ B^{C_{2z}P}(\mathbf{k})B^{C_{2z}T}(\mathbf{k}) &= B^{C_{2z}T}(\mathbf{k})B^{C_{2z}P*}(\mathbf{k}). \end{aligned} \tag{B12}$$

2. Gauge fixing

We will now gauge fix the wave functions and sewing matrices of the $\mathbf{k}$-preserving symmetry operations $C_{2z}T$ and $C_{2z}P$. By Eqs. (B10) and (B12), we are able to choose the following $\mathbf{k}$-independent choices for the sewing matrices:

$$\begin{aligned} [B^{C_{2z}T}(\mathbf{k})]_{m\eta,n\eta'} &= \delta_{\eta,\eta'}\delta_{m,n}, \\ [B^{C_{2z}P}(\mathbf{k})]_{m\eta,n\eta'} &= -\mathrm{sgn}(n)\eta'\delta_{-\eta,\eta'}\delta_{-m,n}. \end{aligned} \tag{B13}$$

Accordingly, the symmetry actions on the band basis fermion operators are given by

$$\begin{aligned} (C_{2z}T)c^{\dagger}_{\mathbf{k},n,\eta,s}(C_{2z}T)^{-1} &= c^{\dagger}_{\mathbf{k},n,\eta,s}, \\ (C_{2z}P)c^{\dagger}_{\mathbf{k},n,\eta,s}(C_{2z}P)^{-1} &= -\mathrm{sgn}(n)\eta c^{\dagger}_{\mathbf{k},-n,-\eta,s}. \end{aligned} \tag{B14}$$

This, however, does not yet fix the entire phases of the energy basis at momentum $\mathbf{k}$, since the sewing matrices in Eq. (B13) are invariant under the unitary transformation of wave functions $u_{n\eta}(\mathbf{k}) \to \mathrm{sgn}(n)\eta u_{n\eta}(\mathbf{k})$ at each individual $\mathbf{k}$. To further fix this gauge freedom for different $\mathbf{k} \in$ MBZ, we start by choosing a momentum $\mathbf{k} = \mathbf{k}_0$ where eigenstates within one valley are nondegenerate and choosing a fixing of the band basis at $\mathbf{k}_0$ satisfying Eq. (B13). We then fix the band basis of bands $\pm n$ at other $\mathbf{k} \neq \mathbf{k}_0$ by requiring

$$\begin{aligned} &f_{n,\eta}(\mathbf{k}+\mathbf{q}, \mathbf{k}) \\ &\quad = |u^{\dagger}_{n,\eta}(\mathbf{k}+\mathbf{q})u_{n,\eta}(\mathbf{k}) - u^{\dagger}_{-n,\eta}(\mathbf{k}+\mathbf{q})u_{-n,\eta}(\mathbf{k})| \end{aligned} \tag{B15}$$

to be a continuous function of $\mathbf{k}$ and $\mathbf{q}$ that satisfies

$$\lim_{\mathbf{q}\to\mathbf{0}} f_{n,\eta}(\mathbf{k}+\mathbf{q}, \mathbf{k}) = 0 \tag{B16}$$

for all $\mathbf{k}$. Meanwhile, we require the wave functions $u_{n,\eta}(\mathbf{k})$ at all $\mathbf{k}$ to satisfy Eq. (B13). This fixes the relative sign between wave functions $u_{n,\eta}(\mathbf{k})$ and $u_{-n,\eta}(\mathbf{k})$ in a way that is continuous in $\mathbf{k}$. Note that we do not require the wave function $u_{n,\eta}(\mathbf{k})$ itself to be globally continuous in $\mathbf{k}$ of the entire MBZ, which is impossible when the band n is topological. However, locally $u_{n,\eta}(\mathbf{k})$ can always be chosen to be continuous in $\mathbf{k}$, provided $u_{n,\eta}(\mathbf{k})$ is nondegenerate at momentum $\mathbf{k}$. We will see the importance of condition (B16) in Appendix B 3 again.

We also note that we could alternatively define the continuous condition between the same n but opposite η bands as $\lim_{\mathbf{q}\to\mathbf{0}} |u^{\dagger}_{n,\eta}(\mathbf{k}+\mathbf{q})u_{n,\eta}(\mathbf{k}) - u^{\dagger}_{n,-\eta}(\mathbf{k}+\mathbf{q})u_{n,-\eta}(\mathbf{k})| = 0$. Together with Eq. (B13), this is equivalent to condition (B16).

In particular, we see that all the sewing matrices in Eq. (B13) are closed within each pair of bands $n = \pm n_{\mathrm{B}}$ for any $n_{\mathrm{B}} \geqslant 1$. The same is true for all the sewing matrices we will consider in this paper, which are either commuting or anticommuting with the single-particle Hamiltonian $\hat{H}_0$. Within the space of each pair of ph symmetric bands with band indices $n = \pm n_{\mathrm{B}}$, if we use ζ^a and τ^a $(a = 0, x, y, z)$ to denote the identity and Pauli matrices in the energy band $n = \pm n_{\mathrm{B}}$ space and the valley space, respectively, the sewing matrices in Eq. (B13) can be rewritten as

$$B^{C_{2z}T}(\mathbf{k}) = \zeta^0\tau^0, \quad B^{C_{2z}P}(\mathbf{k}) = \zeta^y\tau^y. \tag{B17}$$

We also mention that for $n_{\mathrm{B}} = 1$ (i.e., within the lowest conduction and valence bands $n = \pm 1$ per spin per valley) when $\mathbf{k}$ is at K_M or K'_M point of the MBZ, bands $n = +1$ and $n = -1$ are degenerate. In this case, we still choose the eigenstate basis at K_M or K'_M point such that Eqs. (B17) and (B16) are satisfied.

Lastly, we note that we can further fix the relative gauge between wave functions at momenta $\mathbf{k}$ and $-\mathbf{k}$ by fixing the sewing matrices of C_{2z} and P. In particular, for $\mathbf{k}$ not at the P-invariant momenta, which are Γ_M and the three equivalent M_M in TBG, one can choose the sewing matrices of C_{2z}, T, and P between each pair of bands $n = \pm n_{\mathrm{B}}$ as

$$B^{C_{2z}}(\mathbf{k}) = \zeta^0\tau^x, \quad B^{T}(\mathbf{k}) = \zeta^0\tau^x, \quad B^{P}(\mathbf{k}) = -i\zeta^y\tau^z, \tag{B18}$$

which are consistent with Eq. (B17). As proven in the next subsection, with the gauge condition Eq. (B16), the sewing matrix $B^{P}(\mathbf{k})$ must have additional minus signs, i.e., $B^{P}(\mathbf{k}) = i\zeta^y\tau^z$, at an odd (even) number of the four P-invariant momenta if the two bands $n = \pm n_B$ have an odd (even) topological winding number protected by $C_{2z}T$, and at the other odd (even) P-invariant momenta $B^{P}(\mathbf{k})$ are $-i\zeta^y\tau^z$, the same as those at generic momenta. Accordingly, the sewing matrices $B^{C_{2z}}(\mathbf{k})$ and $B^{T}(\mathbf{k})$ also have the additional minus at momenta where $B^{P}(\mathbf{k})$ has the minus sign. In this work, we choose $B^{P}(\mathbf{k}_{\Gamma_M}) = -i\zeta^y\tau^z$ and $B^{P}(\mathbf{k}_{M_M}) = i\zeta^y\tau^z$. It should be

noticed that Eq. (B18) is incompatible with the second chiral symmetry, which we explain in Sec. D 5.

For the purpose of this paper, we will use the gauge conditions in Eqs. (B17) and (B18) for gauge fixing of the interaction Hamiltonian in Appendix C.

3. The Irrep band basis and Chern band basis

After we have gauge fixed the wave functions as shown in Eqs. (B17) and (B16), we have defined a new basis $d^{(n_B)\dagger}_{\mathbf{k},e_Y,\eta,s}$ in Eq. (26) within the band space of each pair of ph symmetric bands $n = \pm n_B$, which we call the irrep basis:

$$d^{(n_B)\dagger}_{\mathbf{k},e_Y,\eta,s} = \frac{c^\dagger_{\mathbf{k},n_B,\eta,s} + ie_Y c^\dagger_{\mathbf{k},-n_B,\eta,s}}{\sqrt{2}}, \quad (e_Y = \pm 1). \tag{B19}$$

In particular, for $n_B = 1$, we call them the Chern band basis within the lowest two bands (in each valley-spin flavor), which we denote for simplicity as $d^{(1)\dagger}_{\mathbf{k},e_Y,\eta,s} = d^\dagger_{\mathbf{k},e_Y,\eta,s}$, as given in Eq. (28), where $e_Y = \pm 1$. This basis will be useful when we discuss the symmetries in various limits in Appendix D.

In this Appendix, we briefly show that the basis $d^{(n_B)\dagger}_{\mathbf{k},e_Y,\eta,s}$ defines a band with well-defined Berry curvature, and for a fixed e_Y, η, s gives a band with Chern number

$$C^{n_B}_{e_Y,\eta,s} = e_Y e_{2,n_B}, \tag{B20}$$

where $e_{2,n_B} \in \mathbb{Z}$ is the Wilson loop winding number of the two bands $n = \pm n_B$, provided the pair of bands $n = \pm n_B$ are disconnected with other bands. More details can be found in Ref. [108].

The wave functions of the Chern band basis in Eq. (B19) are given by (denoted by wave functions with a prime)

$$u'_{e_Y,n_B,\eta}(\mathbf{k}) = \frac{u_{+n_B,\eta}(\mathbf{k}) + ie_Y u_{-n_B,\eta}(\mathbf{k})}{\sqrt{2}}. \tag{B21}$$

Due to the condition in Eq. (B16), we know that $\lim_{\mathbf{q}\to\mathbf{0}} u^\dagger_{+n_B,\eta}(\mathbf{k}+\mathbf{q})u_{+n_B,\eta}(\mathbf{k}) = \lim_{\mathbf{q}\to\mathbf{0}} u^\dagger_{-n_B,\eta}(\mathbf{k}+\mathbf{q})u_{-n_B,\eta}(\mathbf{k})$. Therefore, we find the Chern band wave functions satisfy the continuous condition

$$\begin{aligned}
&\lim_{\mathbf{q}\to 0} \left|u'^\dagger_{e_Y,n_B,\eta}(\mathbf{k}+\mathbf{q})u'_{e'_Y,n_B,\eta}(\mathbf{k})\right| \\
&= \frac{1}{2}\lim_{\mathbf{q}\to 0} \left|u^\dagger_{+n_B,\eta}(\mathbf{k}+\mathbf{q})u_{+n_B,\eta}(\mathbf{k})\right. \\
&\quad \left. + e_Y e'_Y u^\dagger_{-n_B,\eta}(\mathbf{k}+\mathbf{q})u_{-n_B,\eta}(\mathbf{k})\right| \\
&= \delta_{e_Y,e'_Y}.
\end{aligned} \tag{B22}$$

This continuous condition [which is due to condition (B16)] allows us to define a continuous Berry curvature for the Chern band wave function $u'_{e'_Y,n_B,\eta}(\mathbf{k})$.

We first focus in the valley $\eta = +$ sector. The sewing matrix for $C_{2z}T$ restricted in valley $\eta = +$ is given by $B^{C_{2z}T}(\mathbf{k}) = \zeta^0$ [see Eq. (B17)]. Under this gauge, according to Ref. [45], the non-Abelian Berry's connection $[\mathbf{A}(\mathbf{k})]_{mn} = iu^\dagger_{m,+}(\mathbf{k})\partial_{\mathbf{k}}u_{n,+}(\mathbf{k})$ will take the form

$$\mathbf{A}(\mathbf{k}) = \begin{pmatrix} 0 & i\mathbf{a}(\mathbf{k}) \\ -i\mathbf{a}(\mathbf{k}) & 0 \end{pmatrix} \tag{B23}$$

in the energy band basis $u_{n,+}(\mathbf{k})$ of $n = \pm n_B$. The sign of wave functions $u_{n,+}(\mathbf{k})$ is fixed in such a way that $\mathbf{a}(\mathbf{k})$ is globally continuous in the BZ, excluding the Dirac nodes between the two bands $\pm n_B$ (recall that we assume the bands $\pm n_B$ are disconnected from other bands, thus there can be Dirac nodes between them only if $n_B = 1$), which is always possible [45]. In particular, this way of sign fixing is consistent with Eq. (B16), since the vanishing of the diagonal Berry's connection requires $\lim_{\mathbf{q}\to 0} |u^\dagger_{m,\eta}(\mathbf{k}+\mathbf{q})u_{n,\eta}(\mathbf{k})| = \delta_{m,n}$.

It is known that the Wilson loop winding number of two bands isolated from other bands is given by the Euler class [45]:

$$e_{2,n_B} = \frac{1}{2\pi}\sum_i \oint_{\partial D_i} d\mathbf{k}\cdot\mathbf{a}(\mathbf{k}) = \frac{1}{2\pi}\int_{\mathrm{MBZ}-\sum_i D_i} d^2\mathbf{k}\ \Omega(\mathbf{k}), \tag{B24}$$

where D_i is a sufficiently small region containing the ith Dirac point in the BZ, and $\Omega(\mathbf{k}) = \nabla_{\mathbf{k}} \times \mathbf{a}(\mathbf{k})$.

With Eq. (B23), we can derive the Berry connection of the irrep band basis $d^\dagger_{\mathbf{k},e_Y,+,s}$ at $\mathbf{k}$ away from Dirac points as

$$\begin{aligned}
\mathbf{A}'_{e_Y}(\mathbf{k}) &= iu'^\dagger_{e_Y,n_B,+}(\mathbf{k})\partial_{\mathbf{k}}u'_{e_Y,n_B,+}(\mathbf{k}) \\
&= \frac{i}{2}\big[u^\dagger_{+n_B,+}(\mathbf{k})\partial_{\mathbf{k}}u_{+n_B,+}(\mathbf{k}) + ie_Y u^\dagger_{+n_B,+}(\mathbf{k})\partial_{\mathbf{k}}u_{-n_B,+}(\mathbf{k}) \\
&\quad - ie_Y u^\dagger_{-n_B,+}(\mathbf{k})\partial_{\mathbf{k}}u_{+n_B,+}(\mathbf{k}) + u^\dagger_{-n_B,+}(\mathbf{k})\partial_{\mathbf{k}}u_{-n_B,+}(\mathbf{k})\big] \\
&= e_Y\mathbf{a}(\mathbf{k}).
\end{aligned} \tag{B25}$$

Furthermore, the Berry curvature can be shown to be nondivergent at the Dirac points between the two bands $n = \pm n_B$ (see proof in Ref. [108]; if $n_B > 1$, there are no Dirac points between bands $n = \pm n_B$). Therefore, by Eq. (B24), we find the irrep basis $d^{(n_B)\dagger}_{\mathbf{k},e_Y,+,s}$ carries a Chern number given by Eq. (B20).

Further, note that the C_{2z} symmetry maps the irrep basis $d^{(n_B)\dagger}_{\mathbf{k},e_Y,+,s}$ into $d^{(n_B)\dagger}_{-\mathbf{k},e_Y,-,s}$ [see Eq. (B18)]. Since C_{2z} does not change the Chern number, we conclude that the Chern number of the irrep basis $d^{(n_B)\dagger}_{\mathbf{k},e_Y,\eta,s}$ in the MBZ is simply given by Eq. (B20).

In particular, for the lowest two bands $n_B = 1$, the bands are topological and carry a winding number $e_2 = 1$ [43–45]. Therefore, for the Chern band basis (the irrep basis with $n_B = 1$) $d^\dagger_{-\mathbf{k},e_Y,-,s}$, we have Chern number

$$C_{e_Y,\eta,s} = e_Y, \tag{B26}$$

and thus the name "Chern band basis" within the lowest two bands (see Ref. [108] for a more careful treatment at the Dirac points at CNP, which does not change the conclusion).

For $n_B > 1$, if the two bands $n = \pm n_B$ are isolated from other bands, they will be trivial, and thus $e_{2,n_B} = 0$ for $n_B > 1$ [43–45]. Therefore, they will have Chern number $C^{n_B}_{e_Y,\eta,s} = 0$.

Now we show that if e_{2,n_B} is odd, then the sign of the sewing matrix $B^P(\mathbf{k})$ must be $\mathbf{k}$ dependent: For $\eta = +$, $B^P(\mathbf{k})$ can be chosen as $-i\zeta^y$ at all the momenta except one or three of the P-invariant momenta, where $B^P(\mathbf{k})$ must be $i\zeta^y$. To see this, we assume $B^P(\mathbf{k}) = -i\chi(\mathbf{k})\zeta^y$, where $\chi(\mathbf{k}) = \pm 1$, and transform it into the Chern band basis Eq. (B21). We obtain

$$\begin{aligned}
B^{P'}_{e_Y,e'_Y}(\mathbf{k}) &= u'^\dagger_{e_Y,n_B,+}(-\mathbf{k})D(P)u'_{e_Y,n_B,+}(\mathbf{k}) \\
&= -i\chi(\mathbf{k})e_Y\delta_{e_Y,e'_Y}.
\end{aligned} \tag{B27}$$

Therefore, P leaves each branch of the Chern band basis, which has the Chern numbers $e_{2,n_B}e_Y$, invariant. iP can be equivalently thought as an inversion symmetry for each Chern band since it squares to 1 and changes $\mathbf{k}$ to $-\mathbf{k}$. The "inversion" eigenvalues of the Chern band e_Y are given by $\chi(\mathbf{k})e_Y$ for $\mathbf{k}$ being the P-invariant momentum. Due to the relation between Chern number and inversion eigenvalues, we have

$$(-1)^{e_{2,n_B}} = \prod_K \chi(K), \tag{B28}$$

where K indexes the four P-invariant momenta. Therefore, the right-hand side must be -1 (1) if e_{2,n_B} is odd (even), implying $\chi(K) = -1$ at one or three (zero, two, or four) of the four P-invariant momenta. The sign of $B^P(\mathbf{k})$ in the other valley $\eta = -$ can be obtained from the constraint between $B^{C_{2z}P}(\mathbf{k})$ and $B^P(\mathbf{k})$.

In the case when a pair of bands $n = \pm n_B$ are not isolated, the Chern number $C^{n_B}_{e_Y,\eta,s}$ is not clearly well defined. We leave this question for future studies.

APPENDIX C: INTERACTING HAMILTONIAN WITH COULOMB INTERACTION

In this Appendix, we write down the interaction Hamiltonian of TBG for the Coulomb interaction with screening from the top and bottom gates.

1. Low-energy interaction

We denote the (screened) Coulomb interaction in TBG between two electrons of distance $\mathbf{r}$ as $V(\mathbf{r})$. Usually, TBG samples in experiments feel the Coulomb screenings from the top and bottom gates. Here we assume the TBG has a top gate plate and bottom gate plate which are distance ξ away in the z direction. The screened Coulomb interaction is then given by

$$\widetilde{V}(\mathbf{r}) = U_\xi \sum_{n=-\infty}^{\infty} \frac{(-1)^n}{\sqrt{(r/\xi)^2 + n^2}}, \tag{C1}$$

where $U_\xi = e^2/(\epsilon\xi)$, with ϵ being the dielectric constant, and $r = |\mathbf{r}|$. We call ξ the screening length, which is usually around 10 nm and comparable to the moiré lattice constant. For $\epsilon \approx 6$ from typical hBN substrates, and $\xi \approx 10$ nm, we have $U_\xi \approx 24$ meV. Using the 2D Fourier transformation formula that

$$\begin{aligned}\int \frac{d^2\mathbf{q}}{(2\pi)^2}\cdot\frac{e^{-\xi q + i\mathbf{q}\cdot\mathbf{r}}}{q} &= \int_0^\infty dq \int_0^{2\pi} d\theta e^{-\xi q + iqr\cos\theta} \\ &= \int_0^{2\pi} d\theta \frac{1}{\xi - ir\cos\theta} \\ &= \oint_{|z|=1} \frac{dz}{\xi z - ir(z^2+1)/2} \\ &= \frac{1}{2\pi}\frac{1}{\sqrt{\xi^2 + r^2}}, \quad (\xi \geqslant 0),\end{aligned} \tag{C2}$$

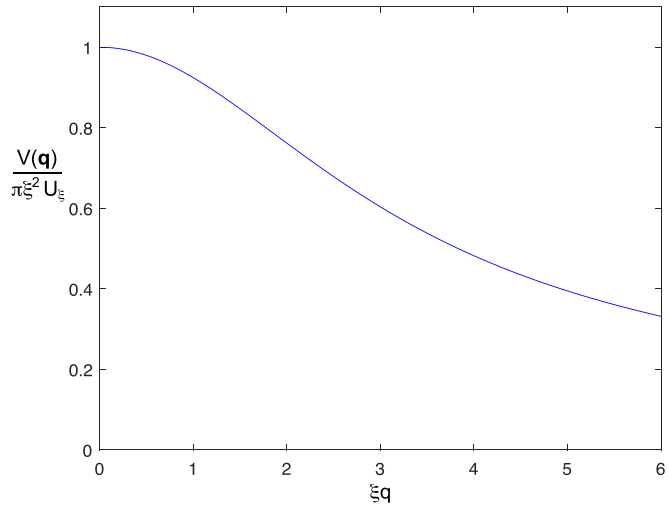

FIG. 4. The interaction $V(\mathbf{q})$ as a function of ξq given by Eq. (C3).

we find the Fourier transformation of the Coulomb interaction (C1) is

$$\begin{aligned}V(\mathbf{q}) &= \int d^2\mathbf{r} e^{-i\mathbf{q}\cdot\mathbf{r}}\widetilde{V}(\mathbf{r}) \\ &= \xi U_\xi \sum_{n=-\infty}^{\infty}\int d^2\mathbf{r}\frac{(-1)^n e^{-i\mathbf{q}\cdot\mathbf{r}}}{\sqrt{r^2+(n\xi)^2}} \\ &= 2\pi\xi U_\xi \sum_{n=-\infty}^{\infty}\int d^2\mathbf{r}\int\frac{d^2\mathbf{q}'}{(2\pi)^2}(-1)^{|n|}\frac{e^{-|n|\xi q' + i(\mathbf{q}'-\mathbf{q})\cdot\mathbf{r}}}{q'} \\ &= 2\pi\xi U_\xi \sum_{n=-\infty}^{\infty}\int d^2\mathbf{q}'\delta^2(\mathbf{q}-\mathbf{q}')(-1)^n\frac{e^{-|n|\xi q'}}{q'} \\ &= 2\pi\xi U_\xi \sum_{n=-\infty}^{\infty}(-1)^n\frac{e^{-|n|\xi q}}{q} = (\pi\xi^2 U_\xi)\frac{\tanh(\xi q/2)}{\xi q/2} \\ &= \frac{2\pi e^2}{\epsilon}\frac{\tanh(\xi q/2)}{q},\end{aligned} \tag{C3}$$

where $q = |\mathbf{q}|$, and we have used the formula $\sum_{n=-\infty}^{\infty} e^{-|n|x} = 1 - \frac{2e^{-x}}{1+e^{-x}} = \tanh\left(\frac{x}{2}\right)$. Note that $V(-\mathbf{q}) = V(\mathbf{q})$. The function $V(\mathbf{q})$ with respect to ζq is plotted in Fig. 4.

The Coulomb interaction of the 2D TBG electrons can be written in the momentum space under the graphene plane wave basis as $c^\dagger_{\mathbf{p},\alpha,s,l}$ as

$$\begin{aligned}\hat{H}_I = \frac{1}{2\Omega_{\rm tot}}\sum_{\mathbf{p},\mathbf{p}',\mathbf{q}\in{\rm GBZ}}\sum_{\alpha,\alpha',s,s',l,l'} V(\mathbf{q})\left(c^\dagger_{\mathbf{p}+\mathbf{q},\alpha,s,l}c_{\mathbf{p},\alpha,s,l} - \frac{1}{2}\delta_{\mathbf{q},\mathbf{0}}\right) \\ \times\left(c^\dagger_{\mathbf{p}'-\mathbf{q},\alpha',s',l'}c_{\mathbf{p}',\alpha',s',l'} - \frac{1}{2}\delta_{\mathbf{q},\mathbf{0}}\right),\end{aligned} \tag{C4}$$

where $\mathbf{p}$, $\mathbf{p}'$, $\mathbf{q}$ take values in the microscopic graphene BZ, and Ω_{tot} is the total area of TBG. Note that we did not normal order the interaction Hamiltonian $\hat{H}_I$ in Eq. (C4), and have subtracted a $\frac{1}{2}\delta_{\mathbf{q},\mathbf{0}}$ term in the two brackets of fermion operators. Normal ordering or removing the term

$\frac{1}{2}\delta_{\mathbf{q},\mathbf{0}}$ only shifts $\hat{H}_I$ by a chemical potential term of the form $\mu\sum_{\mathbf{p},\alpha,s,l} c^\dagger_{\mathbf{p},\alpha,s,l}c_{\mathbf{p},\alpha,s,l}$, which does not change the general physics. However, the advantage of the form in Eq. (C4) is that the Hamiltonian $\hat{H}_I$ is symmetric about the filling of the charge neutral point (CNP). In particular, this chemical potential shift allows us to easily obtain a many-body ph symmetric projected Hamiltonian, as we will derive below and discuss in more details in Appendix C 4. The derived many-body ph symmetric projected Hamiltonian is the most appropriate one, as it effectively properly includes the Hartree-Fock contributions from the passive bands (Appendix C 5).

The low-energy physics of TBG is concentrated at microscopic electron momenta $\mathbf{p}$ around the two valleys $\pm\mathbf{K}_l$. Since $V(\mathbf{q})$ decays quickly when $q \gg 1/\xi$, and in TBG $|\mathbf{K}_l| \gg 1/\xi$, we can ignore the terms in Eq. (C4) with $|\mathbf{q}| \sim |\mathbf{K}_l|$ connecting two valleys. After this approximation, at low energies we can assume $\mathbf{p}$ and $\mathbf{p}+\mathbf{q}$ ($\mathbf{p}'$ and $\mathbf{p}'+\mathbf{q}$) belong to the same graphene valley, namely, only intravalley scattering is preserved. Rewriting the fermion operators using Eqs. (A3) and (A4), we can rewrite the low-energy interaction Hamiltonian as

$$\hat{H}_I = \frac{1}{2\Omega_{\text{tot}}}\sum_{\mathbf{G}\in\mathcal{Q}_0}\sum_{\mathbf{q}\in\text{MBZ}} V(\mathbf{q}+\mathbf{G})\delta\rho_{-\mathbf{q}-\mathbf{G}}\delta\rho_{\mathbf{q}+\mathbf{G}}, \tag{C5}$$

where

$$\delta\rho_{\mathbf{q}+\mathbf{G}} = \sum_{\eta,\alpha,s}\sum_{\mathbf{k}\in\text{MBZ}}\sum_{\mathbf{Q}\in\mathcal{Q}_\pm}\left(c^\dagger_{\mathbf{k}+\mathbf{q},\mathbf{Q}-\mathbf{G},\eta,\alpha,s}c_{\mathbf{k},\mathbf{Q},\eta,\alpha,s} - \frac{1}{2}\delta_{\mathbf{q},\mathbf{0}}\delta_{\mathbf{G},\mathbf{0}}\right). \tag{C6}$$

Physically, $\delta\rho_{\mathbf{q}+\mathbf{G}}$ is the Fourier transform of the total electron density at momentum $\mathbf{q}+\mathbf{G}$ relative to the filling of the graphene CNP (since the CNP of TBG when the two layers are decoupled is at half filling $\langle c^\dagger_{\mathbf{k}+\mathbf{q},\mathbf{Q}-\mathbf{G},\eta,\alpha,s}c_{\mathbf{k},\mathbf{Q},\eta,\alpha,s}\rangle = \frac{1}{2}\delta_{\mathbf{q},\mathbf{0}}\delta_{\mathbf{G},\mathbf{0}}$ in both graphene layers).

2. Projected Hamiltonian

We now project the TBG Hamiltonian into the lowest $8n_{\max}$ bands $|n| \leqslant n_{\max}$ in each spin and valley. When the twist angle θ is close to the magic angle $\theta_M \approx 1.1^\circ$, a reasonable projected Hamiltonian is with $n_{\max} = 1$. To distinguish them from the unprojected Hamiltonians $\hat{H}_0$ and $\hat{H}_I$ in Eqs. (A5) and (C5), which have hats, we denote the projected kinetic and interaction Hamiltonians as H_0 and H_I (without hats), and the total projected Hamiltonian as $H = H_0 + H_I$.

From Eq. (A25), we can easily write down the projected kinetic Hamiltonian into $|n| \leqslant n_{\max}$ bands as

$$H_0 = \sum_{|n|\leqslant n_{\max}}\sum_{\eta s}\sum_{\mathbf{k}\in\text{MBZ}}\epsilon_{n,\eta}(\mathbf{k})c^\dagger_{\mathbf{k}n\eta s}c_{\mathbf{k}n\eta s}\,. \tag{C7}$$

To find the projected interaction Hamiltonian, we first note that due to Eq. (A21), the density operator in Eq. (C6) can be written as

$$\begin{aligned}\delta\rho_{\mathbf{G}+\mathbf{q}} &= \sum_{\eta\alpha s}\sum_{\mathbf{k}}\sum_{\mathbf{Q}\in\mathcal{Q}_\pm}\left(\left(\sum_{mn} u^*_{\mathbf{Q}-\mathbf{G},\alpha;m\eta}(\mathbf{k}+\mathbf{q})u_{\mathbf{Q},\alpha;n\eta}(\mathbf{k})c^\dagger_{\mathbf{k}+\mathbf{q},m,\eta,s}c_{\mathbf{k},n,\eta,s}\right) - \frac{1}{2}\delta_{\mathbf{q},0}\delta_{\mathbf{G},0}\right)\\ &= \sum_{\eta\alpha s}\sum_{\mathbf{k}}\sum_{\mathbf{Q}\in\mathcal{Q}_\pm}\sum_{m,n} u^*_{\mathbf{Q}-\mathbf{G},\alpha;m\eta}(\mathbf{k}+\mathbf{q})u_{\mathbf{Q},\alpha;n\eta}(\mathbf{k})\left(c^\dagger_{\mathbf{k}+\mathbf{q},m,\eta,s}c_{\mathbf{k},n,\eta,s} - \frac{1}{2}\delta_{\mathbf{q},0}\delta_{mn}\right),\end{aligned} \tag{C8}$$

where from the first line to the second line we have used the completeness relation

$$\delta_{\mathbf{G},\mathbf{0}} = \sum_{n\eta} u^*_{\mathbf{Q}-\mathbf{G},\alpha;n\eta}(\mathbf{k})u_{\mathbf{Q},\alpha;n\eta}(\mathbf{k}). \tag{C9}$$

We then define the form factor (overlap) matrix as given in Eq. (12), which we reprint here for convenience:

$$M^{(\eta)}_{m,n}(\mathbf{k},\mathbf{q}+\mathbf{G}) = \sum_{\alpha}\sum_{\mathbf{Q}\,\in\,\mathcal{Q}_\pm} u^*_{\mathbf{Q}-\mathbf{G},\alpha;m\eta}(\mathbf{k}+\mathbf{q})u_{\mathbf{Q},\alpha;n\eta}(\mathbf{k}). \tag{C10}$$

We note that if $\mathbf{k}+\mathbf{q}$ is outside the first BZ, it must be brought into the first BZ using the embedding relation in Eq. (A23). This further simplifies Eq. (C8) into

$$\delta\rho_{\mathbf{G}+\mathbf{q}} = \sum_{\mathbf{k}\eta s}\sum_{m,n} M^{\eta}_{m,n}(\mathbf{k},\mathbf{q}+\mathbf{G})\left(c^\dagger_{\mathbf{k}+\mathbf{q},m,\eta,s}c_{\mathbf{k},n,\eta,s} - \frac{1}{2}\delta_{\mathbf{q},0}\delta_{mn}\right). \tag{C11}$$

We can then define a projected density operator $\overline{\delta\rho}_{\mathbf{G}+\mathbf{q}}$ by restricting $|m|, |n| \leqslant n_{\max}$ in Eq. (C11):

$$\overline{\delta\rho}_{\mathbf{G}+\mathbf{q}} = \sum_{\mathbf{k}\eta s}\sum_{|m|,|n|\leqslant n_{\max}} M^{\eta}_{m,n}(\mathbf{k},\mathbf{q}+\mathbf{G})\left(c^\dagger_{\mathbf{k}+\mathbf{q},m,\eta,s}c_{\mathbf{k},n,\eta,s} - \frac{1}{2}\delta_{\mathbf{q},0}\delta_{mn}\right), \tag{C12}$$

and substitute $\overline{\delta\rho}_{\mathbf{G}+\mathbf{q}}$ into Eq. (C5) to obtain the projected interaction Hamiltonian H_I in the $n = \pm 1$ bands. To simplify the form of the interaction Hamiltonian, we define a set of operators

$$O_{\mathbf{q},\mathbf{G}} = \sqrt{V(\mathbf{q}+\mathbf{G})}\overline{\delta\rho}_{\mathbf{G}+\mathbf{q}} = \sum_{\mathbf{k}\eta s}\sum_{|m|,|n|\leqslant n_{\max}} \sqrt{V(\mathbf{q}+\mathbf{G})}M^{(\eta)}_{m,n}(\mathbf{k},\mathbf{q}+\mathbf{G})\left(\rho^{\eta}_{\mathbf{k},\mathbf{q},m,n,s} - \frac{1}{2}\delta_{\mathbf{q},\mathbf{0}}\delta_{m,n}\right), \tag{C13}$$

and the electron density operator within the flat bands

$$\rho^{\eta}_{\mathbf{k},\mathbf{q},m,n,s} = c^{\dagger}_{\mathbf{k}+\mathbf{q},m,\eta,s}c_{\mathbf{k},n,\eta,s}. \tag{C14}$$

We can then write the projected interaction Hamiltonian as

$$H_I = \frac{1}{2\Omega_{\text{tot}}}\sum_{\mathbf{q}\in\text{MBZ}}\sum_{\mathbf{G}\in\mathcal{Q}_0} O_{-\mathbf{q},-\mathbf{G}}O_{\mathbf{q},\mathbf{G}}\,, \tag{C15}$$

as given in the main text Eq. (10). In particular, we have

$$\begin{aligned}[O_{\mathbf{q},\mathbf{G}}, O_{\mathbf{q}',\mathbf{G}'}] = &\sum_{\mathbf{k},m,n,n',\eta,s}\sqrt{V(\mathbf{G}+\mathbf{q})V(\mathbf{G}'+\mathbf{q}')}\rho^{\eta}_{\mathbf{k},\mathbf{q}+\mathbf{q}',m,n,s}\\ &\times\left[M^{(\eta)}_{m,m'}(\mathbf{k}+\mathbf{q}',\mathbf{q}+\mathbf{G})M^{(\eta)}_{m',n}(\mathbf{k},\mathbf{q}'+\mathbf{G}') - M^{(\eta)}_{m',n}(\mathbf{k},\mathbf{q}+\mathbf{G})M^{(\eta)}_{m,m'}(\mathbf{k}+\mathbf{q},\mathbf{q}'+\mathbf{G}')\right],\end{aligned} \tag{C16}$$

which in general does not vanish if $\mathbf{q} \neq \mathbf{q}'$ or $\mathbf{G} \neq \mathbf{G}'$. Therefore, different terms in the interaction Hamiltonian H_I do not commute.

3. Gauge fixing of the interaction

Equation (C10) give the generic definition of the coefficient $M^{(\eta)}_{m,n}(\mathbf{k},\mathbf{q}+\mathbf{G})$. Here we fix the form of this coefficient under the gauge fixing of Eq. (B17). Under this gauge, the following constraints must be satisfied:

(I) Hermiticity condition:

$$M^{(\eta)*}_{mn}(\mathbf{k},\mathbf{q}+\mathbf{G}) = M^{(\eta)}_{nm}(\mathbf{k}+\mathbf{q},-\mathbf{q}-\mathbf{G})\,, \tag{C17}$$

which is trivially satisfied by the definition in Eq. (C10).

(II) The $C_{2z}T$ symmetry yields the real condition

$$\begin{aligned}M^{(\eta)}_{m,n}(\mathbf{k},\mathbf{q}+\mathbf{G}) &= \sum_{\alpha}\sum_{\mathbf{Q}\in\mathcal{Q}_{\pm}}[D(C_{2z}T)u_{m\eta}(\mathbf{k}+\mathbf{q})]_{\mathbf{Q}-\mathbf{G},\alpha}[D(C_{2z}T)u^{*}_{n\eta}(\mathbf{k})]_{\mathbf{Q},\alpha}\\ &= \sum_{\alpha}\sum_{\mathbf{Q}\in\mathcal{Q}_{\pm}}u^{*}_{\mathbf{Q},\bar{\alpha};n\eta}(\mathbf{k})u_{\mathbf{Q}-\mathbf{G}\bar{\alpha},m\eta}(\mathbf{k}+\mathbf{q}) = \sum_{\alpha}\sum_{\mathbf{Q}\in\mathcal{Q}_{\pm}}u^{*}_{\mathbf{Q}+\mathbf{G},\alpha;n\eta}(\mathbf{k})u_{\mathbf{Q}\alpha,m\eta}(\mathbf{k}+\mathbf{q})\\ &= M^{(\eta)*}_{mn}(\mathbf{k},\mathbf{q}+\mathbf{G}).\end{aligned} \tag{C18}$$

(III) Due to the combination operation $C_{2z}P$, which has the sewing matrix $D(C_{2z}P) = \zeta^{y}\tau^{y}$ in each pair of bands $n = \pm n_{\text{B}}$ [Eq. (B17)], we have

$$\begin{aligned}M^{(\eta)}_{mn}(\mathbf{k},\mathbf{q}+\mathbf{G}) &= \sum_{\alpha}\sum_{\mathbf{Q}\in\mathcal{Q}_{\pm}}[D(C_{2z}P)u^{*}_{m\eta}(\mathbf{k}+\mathbf{q})]_{\mathbf{Q}-\mathbf{G},\alpha}[D(C_{2z}P)u_{n\eta}(\mathbf{k})]_{\mathbf{Q},\alpha}\\ &= \sum_{\alpha}\sum_{\mathbf{Q}\in\mathcal{Q}_{\pm}}(\zeta_y)_{mm'}u^{*}_{\mathbf{Q}-\mathbf{G}\alpha,m',-\eta}(\mathbf{k}+\mathbf{q})u_{\mathbf{Q},\alpha;n',-\eta}(\mathbf{k})(\zeta_y)_{n'n}\\ &= [\zeta^{y}M^{(-\eta)}(\mathbf{k},\mathbf{q}+\mathbf{G})\zeta^{y}]_{m,n},\end{aligned} \tag{C19}$$

where we write $M^{(\eta)}_{mn}$ in short as a matrix $M^{(\eta)}$ in the band space, and ζ^{α} means the Pauli matrix within each pair of bands $\pm n$.

(IV) For momenta $\mathbf{k}$ and $\mathbf{k}+\mathbf{q}$ not at M_M points, due to the C_{2z} symmetry, which has the sewing matrix $B(C_{2z})(\mathbf{k}) = \zeta^{0}\tau^{x}$ [Eq. (B18)], we further have

$$M^{(\eta)}(\mathbf{k},\mathbf{q}+\mathbf{G}) = M^{(-\eta)}(-\mathbf{k},-\mathbf{q}-\mathbf{G}). \tag{C20}$$

For the case where $\mathbf{k}$ is at M_M and $\mathbf{k}+\mathbf{q}$ is not at M_M, the sewing matrices are given by $-B^{C_{2z}}(\mathbf{k}) = B^{C_{2z}}(\mathbf{k}+\mathbf{q}+\mathbf{G}) = i\zeta^{0}\tau^{x}$ due to the discussion in Appendix B 2, and hence the above condition changes to

$$M^{(\eta)}(\mathbf{k},\mathbf{q}+\mathbf{G}) = -M^{(-\eta)}(-\mathbf{k},-\mathbf{q}-\mathbf{G}). \tag{C21}$$

For the case where $\mathbf{k}$ is not at M_M and $\mathbf{k}+\mathbf{q}$ is at M_M, the M matrix also satisfies Eq. (C21) for the same reason. For the case where $\mathbf{k}$ is at M_M and $\mathbf{q} = 0$, the sewing matrices are given by $B^{C_{2z}}(\mathbf{k}) = B^{C_{2z}}(\mathbf{k}+\mathbf{G}) = -i\zeta^{0}\tau^{x}$ and hence the M matrix satisfies Eq. (C20).

We can generically parametrize $M^{\eta}_{m,n}(\mathbf{k},\mathbf{q})$ as

$$M^{\eta}_{m,n}(\mathbf{k},\mathbf{q}+\mathbf{G}) = \sum_{a=0,x,y,z}\sum_{b=0,z}(\zeta^a)_{mn}(\tau^b)_{\eta\eta}\alpha_{ab}(\mathbf{k},\mathbf{q}+\mathbf{G})\,, \tag{C22}$$

where only $b=0,z$ are allowed, since $M^{\eta}_{m,n}(\mathbf{k},\mathbf{q}+\mathbf{G})$ is diagonal in valley η. We have assumed $\alpha_{ab}(\mathbf{k},\mathbf{q}+\mathbf{G})$ are $n_{\max}\times n_{\max}$ matrices, and is tensor produced with ζ^a in each pair band basis $n=\pm n_{\mathrm{B}}$ and the valley Pauli matrix τ^b. Condition III requires M to be commutative with $\zeta^y\tau^y$ in the band and valley indices, which restricts M matrix to decompose into four terms

$$M(\mathbf{k},\mathbf{q}+\mathbf{G}) = \zeta^0\tau^0\alpha_0(\mathbf{k},\mathbf{q}+\mathbf{G}) + \zeta^x\tau^z\alpha_1(\mathbf{k},\mathbf{q}+\mathbf{G}) + i\zeta^y\tau^0\alpha_2(\mathbf{k},\mathbf{q}+\mathbf{G}) + \zeta^z\tau^z\alpha_3(\mathbf{k},\mathbf{q}+\mathbf{G}). \tag{C23}$$

We note that if $n_{\max}=1$, $\alpha_{0,1,2,3}(\mathbf{k},\mathbf{q}+\mathbf{G})$ are simply numbers, while if $n_{\max}>1$, $\alpha_{0,1,2,3}(\mathbf{k},\mathbf{q}+\mathbf{G})$ will be matrices. Condition II requires $M^{\eta}_{m,n}(\mathbf{k},\mathbf{q}+\mathbf{G})$ to be real, and thus $\alpha_{0,1,2,3}(\mathbf{k},\mathbf{q}+\mathbf{G})$ are all real (matrix) functions. We denote the matrix coefficient of $\alpha_j(\mathbf{k},\mathbf{q}+\mathbf{G})$ in Eq. (C23) as M_j. Besides, condition I requires

$$(1)\quad \alpha_a(\mathbf{k},\mathbf{q}+\mathbf{G}) = \alpha_a^T(\mathbf{k}+\mathbf{q},-\mathbf{q}-\mathbf{G}) \quad \text{for } a=0,1,3, \quad \alpha_2(\mathbf{k},\mathbf{q}+\mathbf{G}) = -\alpha_2^T(\mathbf{k}+\mathbf{q},-\mathbf{q}-\mathbf{G}). \tag{C24}$$

Finally, for $\mathbf{k}$ and $\mathbf{k}+\mathbf{q}$ not at M_M points, condition IV requires

$$(2)\quad \alpha_a(\mathbf{k},\mathbf{q}+\mathbf{G}) = \alpha_a(-\mathbf{k},-\mathbf{q}-\mathbf{G}) \quad \text{for } a=0,2, \quad \alpha_a(\mathbf{k},\mathbf{q}+\mathbf{G}) = -\alpha_a(-\mathbf{k},-\mathbf{q}-\mathbf{G}) \quad \text{for } a=1,3. \tag{C25}$$

In particular, the combination of Eqs. (C24) and (C25) implies that at $\mathbf{q}=\mathbf{0}$, we have

$$\alpha_0(\mathbf{k},\mathbf{G}) = \alpha_0^T(-\mathbf{k},\mathbf{G}), \quad \alpha_j(\mathbf{k},\mathbf{G}) = -\alpha_j^T(-\mathbf{k},\mathbf{G}), \quad (j=1,2,3). \tag{C26}$$

It is worth noting that even though Eq. (C25) is derived with assumption that $\mathbf{k}$ and $\mathbf{k}+\mathbf{q}$ are not at the M_M momentum, it is also true for $\mathbf{k}$ at M_M and $\mathbf{q}=0$ because condition IV [Eq. (C20)], from which Eq. (C25) is derived, is true for $\mathbf{k}$ at M_M and $\mathbf{q}=\mathbf{0}$. Therefore, Eq. (C26), the combination of Eqs. (C24) and (C25) at $\mathbf{q}=\mathbf{0}$, is true for $\mathbf{k}$ over the whole BZ.

4. Many-body charge conjugation symmetry of the Projected Hamiltonian

The full projected Hamiltonian $H=H_0+H_I$ has a many-body charge-conjugation symmetry, which ensures that all the physical phenomena is ph symmetric about the filling of the charge neutrality point (CNP) at $\nu=0$.

We define the *many-body charge conjugation* $\mathcal{P}_c$ as the single-particle transformation $C_{2z}TP$ followed by an interchange between electron annihilation operators c and creation operators $c^\dagger$, namely,

$$\mathcal{P}_c c^\dagger_{\mathbf{k},n,\eta,s}\mathcal{P}_c^{-1} = c_{-\mathbf{k},m,\eta',s}[B^{C_{2z}TP}(\mathbf{k})]_{m\eta',n\eta}(\mathbf{k}), \quad \mathcal{P}_c c_{\mathbf{k},n,\eta,s}\mathcal{P}_c^{-1} = c^\dagger_{-\mathbf{k},m,\eta',s}[B^{C_{2z}TP*}(\mathbf{k})]_{m\eta',n\eta}\,. \tag{C27}$$

Under the gauge fixings of Eq. (B17) and Eq. (B18), one has $B^{C_{2z}TP}_{m\eta',n\eta} = B^{P}_{m\eta',n\eta} = (-i\zeta^y\tau^z)_{m\eta',n\eta}$ [Eq. (B18)] within each pair of bands $n=\pm n_{\mathrm{B}}$. We now show $\mathcal{P}_c$ is a symmetry of the projected Hamiltonian.

Because of the relation $\epsilon_{n,\eta}(\mathbf{k}) = -\epsilon_{-n,\eta}(-\mathbf{k})$, the kinetic Hamiltonian is invariant under $\mathcal{P}_c$ up to a constant:

$$\mathcal{P}_c H_0\mathcal{P}_c^{-1} = \sum_{\mathbf{k},n\eta,s}\epsilon_{n,\eta}(\mathbf{k})c_{-\mathbf{k},-n,\eta}c^\dagger_{-\mathbf{k},-n,\eta} = \sum_{\mathbf{k},n\eta,s}\epsilon_{-n,\eta}(-\mathbf{k})c^\dagger_{-\mathbf{k},-n,\eta}c_{-\mathbf{k},-n,\eta} + \text{const.} = H_0 + \text{const.} \tag{C28}$$

Next, we note that the projected density operator $\overline{\delta\rho}_{\mathbf{q}+\mathbf{G}}$ in Eq. (C12) satisfies

$$\begin{aligned}
\mathcal{P}_c\overline{\delta\rho}_{\mathbf{q}+\mathbf{G}}\mathcal{P}_c^{-1} &= \sum_{\eta mns}\sum_{\mathbf{k}}[\zeta^y M^{\eta}(\mathbf{k},\mathbf{q}+\mathbf{G})\zeta^y]_{mn}\left(c_{-\mathbf{k}-\mathbf{q},m,\eta,s}c^\dagger_{-\mathbf{k},n,\eta,s} - \frac{1}{2}\delta_{\mathbf{q},0}\delta_{mn}\right)\\
&= \sum_{\eta mns}\sum_{\mathbf{k}}[\zeta^y M^{\eta}(\mathbf{k},\mathbf{q}+\mathbf{G})\zeta^y]_{mn}\left(-c^\dagger_{-\mathbf{k},n,\eta,s}c_{-\mathbf{k}-\mathbf{q},m,\eta,s} + \frac{1}{2}\delta_{\mathbf{q},0}\delta_{mn}\right)\\
&= \sum_{\eta mns}\sum_{\mathbf{k}}[\zeta^y M^{\eta}(-\mathbf{k}+\mathbf{q},\mathbf{q}+\mathbf{G})\zeta^y]_{mn}\left(-c^\dagger_{\mathbf{k}+\mathbf{q},n,\eta,s}c_{\mathbf{k},m,\eta,s} + \frac{1}{2}\delta_{\mathbf{q},0}\delta_{mn}\right)
\end{aligned} \tag{C29}$$

due to Eqs. (C23) and (C25), we have

$$M^{\eta}_{m,n}(\mathbf{k},\mathbf{q}+\mathbf{G}) = \sum_{m'n'}\zeta^y_{m',m}M^{\eta}_{m',n'}(-\mathbf{k},-\mathbf{q}-\mathbf{G})\zeta^y_{n'n}\,, \tag{C30}$$

and hence

$$\mathcal{P}_c\overline{\delta\rho}_{\mathbf{q}+\mathbf{G}}\mathcal{P}_c^{-1} = \sum_{\eta mns}\sum_{\mathbf{k}}M^{\eta}_{mn}(\mathbf{k}-\mathbf{q},-\mathbf{q}-\mathbf{G})\left(-c^\dagger_{\mathbf{k}+\mathbf{q},n,\eta,s}c_{\mathbf{k},m,\eta,s} + \frac{1}{2}\delta_{\mathbf{q},0}\delta_{mn}\right). \tag{C31}$$

Due to Eq. (C17), $M^{\eta}_{mn}(\mathbf{k}-\mathbf{q},-\mathbf{q}-\mathbf{G}) = M^{\eta}_{nm}(\mathbf{k},\mathbf{q}+\mathbf{G})$, and thus

$$\mathcal{P}_c \overline{\delta\rho}_{\mathbf{q}+\mathbf{G}} \mathcal{P}_c^{-1} = \sum_{\eta mns}\sum_{\mathbf{k}} M^{\eta}_{mn}(\mathbf{k},\mathbf{q}+\mathbf{G})\left(-c^{\dagger}_{\mathbf{k}+\mathbf{q},m,\eta,s}c_{\mathbf{k},n,\eta,s} + \frac{1}{2}\delta_{\mathbf{q},0}\delta_{mn}\right) = -\overline{\delta\rho}_{\mathbf{q}+\mathbf{G}}. \tag{C32}$$

Therefore, according to Eq. (C13), we have $\mathcal{P}_c O_{\mathbf{q},\mathbf{G}} \mathcal{P}_c^{-1} = -O_{\mathbf{q},\mathbf{G}}$, and thus the projected interaction in Eq. (C15) has the charge-conjugation symmetry $[\mathcal{P}_c, H_I] = 0$. In total, we have

$$\mathcal{P}_c H \mathcal{P}_c^{-1} = H - \sum_{|n|\leqslant n_{\max}}\sum_{\mathbf{k},\eta,s}\epsilon_{n,\eta}(\mathbf{k}) = H \tag{C33}$$

for $H = H_0 + H_I$, where we have used the fact that $\epsilon_{n,\eta}(\mathbf{k}) = -\epsilon_{-n,\eta}(-\mathbf{k})$ in Eq. (A24) due to the single-particle ph symmetry P. Note that $\mathcal{P}_c$ maps a many-body state at filling ν to filling $-\nu$, where ν is the number of electrons per moiré unit cell relative to the CNP. Therefore, one expects the TBG ground states at ν and $-\nu$ to be ph symmetric.

5. Contributions from the passive bands in the Projected Hamiltonian: Hartree-Fock Potential

We note that the projected interaction Hamiltonian H_I in Eq. (C15) is not normal ordered. We can rewrite H_I into normal-ordered part and some quadratic fermionic terms as

$$H_I = H_I^{\text{norm}} + \Delta H^{(1)} + \Delta H^{(2)} + \text{const.}, \tag{C34}$$

where H_I^{norm} is the normal ordered Hamiltonian, and $H^{(1)}$ and $\Delta H^{(2)}$ are specified below. By defining interaction parameters

$$U^{(\eta'\eta)}_{m'n';mn}(\mathbf{q};\mathbf{k}'\mathbf{k}) = \sum_{\mathbf{G}\in\mathcal{Q}_0} V(\mathbf{G}+\mathbf{q}) M^{(\eta')}_{m',n'}(\mathbf{k}',-\mathbf{q}-\mathbf{G}) M^{(\eta)}_{m,n}(\mathbf{k},\mathbf{q}+\mathbf{G}), \tag{C35}$$

we can rewrite each term as

$$H_I^{\text{norm}} = \frac{1}{2\Omega_{\text{tot}}}\sum_{\mathbf{q}\mathbf{k}\mathbf{k}'\in\text{MBZ}}\sum_{\eta\eta' ss'}\sum_{m,n;m',n'} U^{(\eta'\eta)}_{m'n';mn}(\mathbf{q};\mathbf{k}'\mathbf{k}) c^{\dagger}_{k+q,m,\eta,s} c^{\dagger}_{k'-q,m',\eta',s'} c_{k',n',\eta',s'} c_{k,n,\eta,s}, \tag{C36}$$

$$\Delta H^{(1)} = -\frac{1}{2\Omega_{\text{tot}}}\sum_{\mathbf{k}\mathbf{k}'}\sum_{\eta\eta' ss'}\sum_{m,n;m'} U^{(\eta'\eta)}_{m'm';mn}(\mathbf{0};\mathbf{k}'\mathbf{k}) c^{\dagger}_{k,m,\eta,s} c_{k,n,\eta,s}, \tag{C37}$$

and

$$\Delta H^{(2)} = \frac{1}{2\Omega_{\text{tot}}}\sum_{\mathbf{k},\mathbf{q}}\sum_{\eta,s}\sum_{m,n';m'} U^{(\eta\eta)}_{m'n';mm'}(\mathbf{q};\mathbf{k},\mathbf{k}-\mathbf{q}) c^{\dagger}_{k,m,\eta,s} c_{k,n',\eta,s}, \tag{C38}$$

where we have used the fact that $U^{(\eta'\eta)}_{m'n';mn}(\mathbf{q};\mathbf{k}'\mathbf{k}) = U^{(\eta\eta')}_{mn;m'n'}(-\mathbf{q};\mathbf{k}\mathbf{k}')$ which trivially holds by exchanging the two M matrices in the definition (C35). By summing over only $|m|, |n| \leqslant n_{\max}$, H_I gives the projected Hamiltonian. In the following, we prove that $H_I^{(1)}$ and $H_I^{(2)}$ can be heuristically understood as the Hartree and Fock potential of the higher passive bands $|n| > n_{\max}$ which are projected out. We emphasize that the difference between the H_I and its normal-ordered version is not just a simple chemical potential shift, contrary to the unprojected interaction Hamiltonian $\hat{H}_I$.

We first note that the full interaction Hamiltonian $\hat{H}_I$ before projection is simply given by Eqs. (C36)–(C38) with summation over all band indices m, n, m', n'. We now derive the Hartree-Fock Hamiltonian of the full Hamiltonian $\hat{H}_I$ at filling $\nu = -4n_{\max}$ (number of electrons per moiré unit cell relative to the CNP). The occupied single-particle bands at $\nu = -4n_{\max}$ produce a mean field

$$\langle c^{\dagger}_{\mathbf{k},m,\eta,s} c_{\mathbf{k}',n,\eta',s'}\rangle = \Theta(-n_{\max}-m)\delta_{\mathbf{k},\mathbf{k}'}\delta_{m,n}\delta_{\eta,\eta'}\delta_{s,s'}, \tag{C39}$$

where we define $\Theta(x) = 1$ if $x > 0$, and $\Theta(x) = 0$ if $x \leqslant 0$. We shall use the property of interaction parameter $U^{(\eta'\eta)}_{m'n';mn}(\mathbf{q};\mathbf{k}'\mathbf{k}) = \text{sgn}(mn) U^{(\eta'-\eta)}_{m'n';-m,-n}(\mathbf{q};\mathbf{k}'\mathbf{k}) = \text{sgn}(m'n') U^{(-\eta'\eta)}_{-m'-n';m,n}(\mathbf{q};\mathbf{k}'\mathbf{k}) = U^{(\eta\eta')}_{mn;m'n'}(-\mathbf{q};\mathbf{k}\mathbf{k}')$, which can be verified by the properties of the M matrices through Eq. (C23)–(C25). We then find the Hartree term

$$\begin{aligned} H_H^{\nu=-4n_{\max}} &= \frac{1}{2\Omega_{\text{tot}}}\sum_{\mathbf{k}\mathbf{k}'}\sum_{\eta\eta' ss'}\sum_{m,n;m'}[2\Theta(-n_{\max}-m')-1] U^{(\eta'\eta)}_{m'm';mn}(\mathbf{0};\mathbf{k}'\mathbf{k}) c^{\dagger}_{k,m,\eta,s} c_{k,n,\eta,s} \\ &= -\frac{1}{2\Omega_{\text{tot}}}\sum_{\mathbf{k}\mathbf{k}'}\sum_{\eta\eta' ss',m,n}\sum_{|m'|\leqslant n_{\max}} U^{(\eta'\eta)}_{m'm';mn}(\mathbf{0};\mathbf{k}'\mathbf{k}) c^{\dagger}_{k,m,\eta,s} c_{k,n,\eta,s}, \end{aligned} \tag{C40}$$

and the Fock term

$$\begin{aligned} H_F^{\nu=-4n_{\max}} &= -\frac{1}{2\Omega_{\rm tot}}\sum_{\mathbf{k},\mathbf{q}}\sum_{\eta,s}\Bigg[\sum_{m,n';m'}\Theta(-n_{\max}-m')U^{(\eta\eta)}_{m'n';mm'}(\mathbf{q};\mathbf{k}+\mathbf{q},\mathbf{k})c^\dagger_{k+q,m,\eta,s}c_{k+q,n',\eta,s} \\ &\quad+\sum_{m',n;m}\Theta(-n_{\max}-m)U^{(\eta\eta)}_{m'm;mn}(\mathbf{q};\mathbf{k}+\mathbf{q},\mathbf{k})c^\dagger_{k,m',\eta,s}c_{k,n,\eta,s}\Bigg] \\ &= -\frac{1}{2\Omega_{\rm tot}}\sum_{\mathbf{k},\mathbf{q}}\sum_{\eta,s}\sum_{m,n';m'}\Theta(-n_{\max}-m')\left[U^{(\eta\eta)}_{m'n;mm'}(\mathbf{q};\mathbf{k}+\mathbf{q},\mathbf{k})+U^{(\eta\eta)}_{mm';m'n}(-\mathbf{q};\mathbf{k},\mathbf{k}+\mathbf{q})\right]c^\dagger_{k+q,m,\eta,s}c_{k+q,n,\eta,s} \\ &= -\frac{1}{2\Omega_{\rm tot}}\sum_{\mathbf{k},\mathbf{q}}\sum_{\eta,s}\sum_{m,n';m'}2\Theta(-n_{\max}-m')U^{(\eta\eta)}_{m'n;mm'}(\mathbf{q};\mathbf{k},\mathbf{k}-\mathbf{q})c^\dagger_{k,m,\eta,s}c_{k,n,\eta,s}. \end{aligned} \tag{C41}$$

Similarly, one can show the Hartree term at $\nu = 4n_{\max}$ is given by

$$H_H^{\nu=4n_{\max}} = -H_H^{\nu=-4n_{\max}}, \tag{C42}$$

and the Fock term at $\nu = 4n_{\max}$ is

$$H_F^{\nu=4n_{\max}} = -\frac{1}{2\Omega_{\rm tot}}\sum_{\mathbf{k},\mathbf{q}}\sum_{\eta,s}\sum_{m,n';m'}2\Theta(n_{\max}+1-m')U^{(\eta\eta)}_{m'n;mm'}(\mathbf{q};\mathbf{k},\mathbf{k}-\mathbf{q})c^\dagger_{k,m,\eta,s}c_{k,n,\eta,s}. \tag{C43}$$

Therefore, when projected into the lowest $8n_{\max}$ bands ($2n_{\max}$ per spin-valley), we find the difference between our particle-hole symmetric Hamiltonian and its normal-ordered version:

$$\Delta H^{(1)} = H_H^{\nu=-4n_{\max}} = -H_H^{\nu=4n_{\max}}, \qquad \Delta H^{(2)} = \tfrac{1}{2}\left(H_F^{\nu=-4n_{\max}} - H_F^{\nu=4n_{\max}}\right). \tag{C44}$$

Note that the interaction satisfies the orthonormal condition $\sum_{m'} U^{(\eta\eta)}_{m'n;mm'}(\mathbf{q};\mathbf{k},\mathbf{k}-\mathbf{q}) = \sum_{\mathbf{G}} V(\mathbf{q}+\mathbf{G})\delta_{m,n}$, so under the single-particle ph transformation P which takes $Pc^\dagger_{k,m,\eta,s}P^{-1} = -\mathrm{sgn}(m)\eta c^\dagger_{-k,-m,\eta,s}$, we have

$$\begin{aligned} PH_F^{\nu=-4n_{\max}}P^{-1} &= -\frac{1}{2\Omega_{\rm tot}}\sum_{\mathbf{k},\mathbf{q}}\sum_{\eta,s}\sum_{m,n';m'}2\Theta(-n_{\max}-m')\mathrm{sgn}(mn)U^{(\eta\eta)}_{m'n;mm'}(\mathbf{q};\mathbf{k},\mathbf{k}-\mathbf{q})c^\dagger_{-k,-m,\eta,s}c_{-k,-n,\eta,s} \\ &= -\frac{1}{2\Omega_{\rm tot}}\sum_{\mathbf{k},\mathbf{q}}\sum_{\eta,s}\sum_{m,n';m'}2\Theta(n_{\max}+1+m')U^{(\eta\eta)}_{m'n;mm'}(\mathbf{q};\mathbf{k},\mathbf{k}-\mathbf{q})c^\dagger_{k,m,\eta,s}c_{k,n,\eta,s} \\ &= -\frac{1}{2\Omega_{\rm tot}}\sum_{\mathbf{k},\mathbf{q}}\sum_{\eta,s}\sum_{m,n';m'}2[1-\Theta(n_{\max}+1-m')]U^{(\eta\eta)}_{m'n;mm'}(\mathbf{q};\mathbf{k},\mathbf{k}-\mathbf{q})c^\dagger_{k,m,\eta,s}c_{k,n,\eta,s} \\ &= -H_F^{\nu=4n_{\max}} - \mu_V\sum_{\mathbf{k},m,\eta,s}c^\dagger_{k,m,\eta,s}c_{k,m,\eta,s}, \end{aligned} \tag{C45}$$

where we have used the ph symmetry of interaction $U^{(\eta\eta')}_{mn;m'n'}(\mathbf{q};\mathbf{k},\mathbf{k}') = \mathrm{sgn}(mnm'n')U^{(\eta\eta')}_{-m,-n;-m',-n'}(-\mathbf{q};-\mathbf{k},-\mathbf{k}')$. The constant μ_V is defined by $\mu_V = \frac{1}{\Omega_{\rm tot}}\sum_{\mathbf{q},\mathbf{G}}V(\mathbf{q}+\mathbf{G})$, which is a coefficient of a chemical potential term.

6. U(2)×U(2) spin-charge rotational symmetry

In Eq. (A16), we have given the generators of the U(2)×U(2) symmetry of the single-particle Hamiltonian H_0 from the spin-charge rotational symmetry in each valley. Here we show that the projected interaction Hamiltonian also respects the U(2)×U(2) symmetry. Hereafter, with the understanding that we assume the gauge fixing given by Eqs. (B17) and (B16) [we note that Eq. (B16) is only used for defining the irrep band basis in Eq. (B19), which will be useful in the discussion of nonchiral-flat U(4) irreps in Appendix D 2 b], we shall use ζ^a, τ^a, s^a to denote the identity matrix ($a = 0$) and Pauli matrices ($a = x, y, z$) in the each pair of bands $n = \pm n_{\rm B}$, valley $\eta = \pm$, and spin $s = \uparrow, \downarrow$ bases, respectively.

When projected into the $8n_{\max}$ flat bands of $|n| \leqslant n_{\max}$, the eight generators S^{ab} ($a = 0, z$, $b = 0, x, y, z$) of the U(2)×U(2) symmetry in Eq. (A16) take the form

$$S^{ab} = \sum_{\mathbf{k},m,\eta,s;n,\eta',s'}(s^{ab})_{m,\eta,s;n,\eta',s'}c^\dagger_{\mathbf{k},m,\eta,s}c_{\mathbf{k},n,\eta',s'}, \qquad (a = 0, z, \quad b = 0, x, y, z), \tag{C46}$$

where the matrices within each pair of bands $n = \pm n_{\rm B}$ are given by

$$s^{0b} = \zeta^0\tau^0 s^b, \quad s^{zb} = \zeta^0\tau^z s^b, \quad (b = 0, x, y, z). \tag{C47}$$

In particular, S^{0b} and S^{zb} give the global spin-charge U(2) rotations and the valley spin-charge U(2) rotations, respectively.

It is easy to see that both S^{0b} and S^{zb} are diagonal in valley η and only act on spin s. Since the operator $O_{\mathbf{q},\mathbf{G}}$ defined in Eq. (C13) is diagonal in valley η, and all the coefficients are

independent of spin s, we conclude that

$$[O_{\mathbf{q},\mathbf{G}}, S^{0b}] = [O_{\mathbf{q},\mathbf{G}}, S^{zb}] = 0. \tag{C48}$$

Accordingly, the interaction H_I in Eq. (C15) respects the U(2)×U(2) symmetry, and so does the full projected Hamiltonian $H = H_0 + H_I$.

APPENDIX D: ENHANCED SYMMETRIES IN VARIOUS LIMITS

In this Appendix, we will show that the U(2)×U(2) symmetry [Eq. (C46)] of the full Hamiltonian $H = H_0 + H_I$ is enhanced into higher symmetries in various limits of TBG. Since all these higher symmetries involve the U(4) group, we first briefly review the algebra of the U(4) group.

1. Brief Review of the U(4) group

The U(N) group is defined by all the $N \times N$ unitary matrices U satisfying $U^\dagger U = I_N$, where I_N is the identity matrix. The matrices U are generated by all the linearly independent $N \times N$ Hermitian matrices, and thus the total number of generators is N^2. In particular, for the U(4) group, the 16 generators can be represented by the tensor product of two sets of 2×2 identity and Pauli matrices τ^a and s^a ($a = 0, x, y, z$) as

$$s_0^{ab} = \tau^a s^b, \quad (a, b = 0, x, y, z). \tag{D1}$$

We denote their commutation relations as

$$\left[s_0^{ab}, s_0^{cd}\right] = f_{ef}^{ab,cd} s_0^{ef}. \tag{D2}$$

Then $f_{ef}^{ab,cd}$ are the group structure constants, which are the same for all representations of U(4) group.

The set of all the 4×4 matrices U defines the four-dimensional fundamental irreducible representation (irrep) of the U(4) group, and the representation matrices of the generators are exactly given by Eq. (D1). There is also a one-dimensional trivial identity irrep, in which the representation matrices of all generators $s_0^{ab} = 0$. We shall use the following notation to denote the fundamental irrep and trivial identity irrep of the U(4) group:

$$\begin{aligned} &\text{U(4) fundamental irrep:} \quad [1]_4, \\ &\text{U(4) trivial identity irrep:} \quad [0]_4. \end{aligned} \tag{D3}$$

We will not explain the meaning of these notations, except that we mention they are consistent with the Young tableau notations for U(4) irreps we explain and adopt in Ref. [109].

2. U(4) symmetry in the nonchiral-flat limit

a. The symmetry

We now assume the magic angle TBG is in the nonchiral-flat limit, where the projected kinetic Hamiltonian in Eq. (C7) becomes exactly $H_0 = 0$, while both $w_0 > 0$ and $w_1 > 0$ in Eq. (A7). In this case, the total projected Hamiltonian is $H = H_I$. We will show that there is an enhanced U(4) symmetry.

To see this, we first show that $C_{2z}P$ is a symmetry of $H = H_I$. With the sewing matrix of $C_{2z}P$ given by $B^{C_{2z}P}(\mathbf{k}) = \zeta^y \tau^y$ in Eq. (B17), we have

$$\begin{aligned} (C_{2z}P) O_{\mathbf{q},\mathbf{G}} (C_{2z}P)^{-1} &= \sum_{\mathbf{k}\eta s} \sum_{m,n=\pm 1} \sqrt{V(\mathbf{q}+\mathbf{G})} M_{m,n}^{(\eta)}(\mathbf{k}, \mathbf{q}+\mathbf{G}) \left((C_{2z}P) c^\dagger_{\mathbf{k}+\mathbf{q},m,\eta,s} c_{\mathbf{k},n,\eta,s} (C_{2z}P)^{-1} - \frac{1}{2}\delta_{\mathbf{q},\mathbf{0}}\delta_{m,n} \right) \\ &= \sum_{\mathbf{k}\eta s} \sum_{|m|,|n| \leqslant n_{\max}} \sqrt{V(\mathbf{q}+\mathbf{G})} \left([\zeta^y M^{(-\eta)}(\mathbf{k}, \mathbf{q}+\mathbf{G}) \zeta^y]_{mn} c^\dagger_{\mathbf{k}+\mathbf{q},m,\eta,s} c_{\mathbf{k},n,\eta,s} - \frac{1}{2} M_{m,n}^{(\eta)}(\mathbf{k}, \mathbf{q}+\mathbf{G}) \delta_{\mathbf{q},\mathbf{0}}\delta_{m,n} \right) \\ &= \sum_{\mathbf{k}\eta s} \sum_{|m|,|n| \leqslant n_{\max}} \sqrt{V(\mathbf{q}+\mathbf{G})} M_{m,n}^{(\eta)}(\mathbf{k}, \mathbf{q}+\mathbf{G}) \left(c^\dagger_{\mathbf{k}+\mathbf{q},m,\eta,s} c_{\mathbf{k},n,\eta,s} - \frac{1}{2}\delta_{\mathbf{q},\mathbf{0}}\delta_{m,n} \right) = O_{\mathbf{q},\mathbf{G}}, \end{aligned} \tag{D4}$$

where we have used Eq. (C19). Therefore, we have $[C_{2z}P, O_{\mathbf{q},\mathbf{G}}] = 0$, and thus the interaction Hamiltonian H_I in Eq. (C15) satisfies

$$[C_{2z}P, H_I] = 0. \tag{D5}$$

Besides, since $[C_{2z}, H_0] = 0$ and $\{P, H_0\} = 0$, we have $\{C_{2z}P, H_0\} = 0$, which implies $\epsilon_{n,\eta}(\mathbf{k}) = -\epsilon_{-n,-\eta}(\mathbf{k})$. If we want to have $[C_{2z}P, H_0] = 0$, we would have to require $\epsilon_{n,\eta}(\mathbf{k}) = \epsilon_{-n,-\eta}(\mathbf{k})$, which is only possible when $\epsilon_{n,\eta}(\mathbf{k}) = 0$, namely, only in the exact flat band limit with projected kinetic term $H_0 = 0$.

The $C_{2z}P$ symmetry allows us to define the following operator as a commuting symmetry of the projected Hamiltonian $H = H_I$:

$$S^{y0} = \sum_{\mathbf{k},s} \sum_{nn'\eta\eta'} [B^{C_{2z}P}(\mathbf{k})]_{n\eta,n'\eta'} c^\dagger_{\mathbf{k},n,\eta,s} c_{\mathbf{k},n',\eta',s} = \sum_{\mathbf{k},s} \sum_{nn'\eta\eta'} [\zeta^y \tau^y]_{n\eta,n'\eta'} c^\dagger_{\mathbf{k},n,\eta,s} c_{\mathbf{k},n',\eta',s}, \tag{D6}$$

where we have used the gauge fixing of Eq. (B17), and ζ^y only acts within each pair of bands $n = \pm n_{\mathrm{B}}$. We note that when S^{y0} acts on single-electron states $c^\dagger_{\mathbf{k},n,\eta,s}|0\rangle$ where $|0\rangle$ is the vacuum, it is the same as the operation of $C_{2z}P$. To see this is a symmetry, we note that

$$[S^{y0}, O_{\mathbf{q},\mathbf{G}}] = \sum_{\mathbf{k},s} \sum_{nn'\eta\eta'} ([\zeta^y \tau^y, M(\mathbf{k}, \mathbf{q}+\mathbf{G})])_{n\eta,n'\eta'} c^\dagger_{\mathbf{k},n,\eta,s} c_{\mathbf{k},n',\eta',s} = 0, \tag{D7}$$

where we have used the fact that the $M(\mathbf{k}, \mathbf{q}+\mathbf{G})$ matrix commutes with $\zeta^y\tau^y$ from condition (C23), a result of the $C_{2z}P$ symmetry. Therefore, S^{y0} is a commuting symmetry of the interaction Hamiltonian H_I in Eq. (C15), namely,

$$[S^{y0}, H_I] = 0. \tag{D8}$$

Recall that H_I has a U(2)×U(2) symmetry with eight generators S^{0b} and S^{zb} ($b = 0, x, y, z$) in Eq. (C46). The commutators of S^{y0} in Eq. (D6) with the eight U(2)×U(2) generators then yields 16 Hermitian operators in total:

$$S^{ab} = \sum_{\mathbf{k},m,\eta,s;n,\eta',s'} (s^{ab})_{m,\eta,s;n,\eta',s'} c^\dagger_{\mathbf{k},m,\eta,s} c_{\mathbf{k},n,\eta',s'}, \quad (a, b = 0, x, y, z), \tag{D9}$$

where within each pair of bands $n = \pm n_{\mathrm{B}}$

$$s^{ab} = \{\zeta^0\tau^0 s^b,\ \zeta^y\tau^x s^b,\ \zeta^y\tau^y s^b,\ \zeta^0\tau^z s^b\}, \quad (a, b = 0, x, y, z). \tag{D10}$$

More specifically, the new generators are given by

$$S^{xb} = -\frac{i}{2}[S^{y0}, S^{zb}], \quad S^{yb} = \frac{i}{2}[S^{x0}, S^{zb}]. \tag{D11}$$

It is then easy to see that the 16 operators S^{ab} satisfy the commutation relations of U(4) generators,

$$[S^{ab}, S^{cd}] = f^{ab,cd}_{ef} S^{ef}, \tag{D12}$$

where $f^{ab,cd}_{ef}$ are the U(4) structure constants defined in Eq. (D2). Therefore, we find in the nonchiral-flat limit, the projected interaction Hamiltonian H_I has an enhanced U(4) symmetry.

The Cartan subalgebra of the U(4) generators in Eq. (D10) can be chosen as

$$\text{Cartan:} \quad \zeta^0\tau^0 s^0, \quad \zeta^0\tau^0 s^z, \quad \zeta^0\tau^z s^0, \quad \zeta^0\tau^z s^z. \tag{D13}$$

We note that although we proved the symmetry of S^{y0} under the fixed gauge (B17), the definition of $S^{y0} = \sum_{\mathbf{k},s}\sum_{nn'\eta\eta'}[B^{C_{2z}P}(\mathbf{k})]_{n\eta,n'\eta'} c^\dagger_{\mathbf{k},n,\eta,s} c_{\mathbf{k},n',\eta',s}$ in Eq. (D6) is gauge invariant. This can be seen by noting that under a gauge transformation $c^\dagger_{\mathbf{k},n,\eta,s} \to e^{i\phi_{n,\eta}} c^\dagger_{\mathbf{k},n,\eta,s}$, the sewing matrix elements change according to $[B^{C_{2z}P}(\mathbf{k})]_{n\eta,n'\eta'} \to e^{-i\phi_{n,\eta}+i\phi_{n',\eta'}}[B^{C_{2z}P}(\mathbf{k})]_{n\eta,n'\eta'}$.

b. The single-electron irreps

The $\mathbf{k}$-independent representation matrices of Eq. (D10) at each momentum $\mathbf{k}$ can be decomposed into fundamental U(4) irreps. This can be done by transforming into a new basis where ζ^y is diagonalized. This turns out to be exactly the irrep band basis $d^{(n_{\mathrm{B}})\dagger}_{\mathbf{k},e_Y,\eta,s} = \frac{1}{\sqrt{2}}(c^\dagger_{\mathbf{k},+n_{\mathrm{B}},\eta,s} + ie_Y c^\dagger_{\mathbf{k},-n_{\mathrm{B}},\eta,s})$ we defined earlier in Eq. (26) (see also Ref. [108]). For $n_{\mathrm{B}} = 1$, $e_Y = \pm 1$ gives the Chern number of the band basis. The single-electron state in irrep band e_Y

$$d^{(n_{\mathrm{B}})\dagger}_{\mathbf{k},e_Y,\eta,s}|0\rangle \tag{D14}$$

has eigenvalue $\zeta^y = e_Y$. It is then easy to see that the representations of the U(4) generators S^{ab} for the single-electron state (D14) are given by

$$s^{ab}(e_Y) = \{\tau^0 s^b,\ e_Y\tau^x s^b,\ e_Y\tau^y s^b,\ \tau^z s^b\}. \tag{D15}$$

Therefore, the single-electron state (D14) for a fixed e_Y, or equivalently the irrep band fermion operator $d^\dagger_{\mathbf{k},e_Y,\eta,s}$ for a fixed e_Y, occupies a fundamental irrep $[1]_4$ of the U(4) group. However, we note that the $e_Y = +1$ and $e_Y = -1$ irreps differ by a π valley rotation $e^{i\pi\tau^z/2}$ about the z axis.

For many-body Fock states created by multiple $d^{(n_{\mathrm{B}})\dagger}_{\mathbf{k},e_Y,\eta,s}$, the U(4) representation is given by the tensor product of the U(4) fundamental irreps $[1]_4$ of each $d^{(n_{\mathrm{B}})\dagger}_{\mathbf{k},e_Y,\eta,s}$. Such tensor product representations can be further decomposed into U(4) irreps, which we will not discuss here but rather in our upcoming paper of the many-body states of the PSDHs [109].

3. U(4)×U(4) symmetry in the (first) chiral-flat limit

In this Appendix, we demonstrate that by setting $w_0 = 0 < w_1$ (the chiral condition) and setting the projected kinetic Hamiltonian H_0 to zero (flat condition), the system has a unitary U(4)×U(4) symmetry. We call this limit the first chiral-flat limit.

a. The chiral symmetry at $w_0 = 0$

In the first chiral-flat limit, since $w_0 = 0$, the single-particle Hamiltonian of TBG acquires an additional unitary chiral symmetry C, which satisfies the anticommutation relation with the full single-particle Hamiltonian $\hat{H}_0$ in Eq. (A5):

$$\{C, \hat{H}_0\} = 0. \tag{D16}$$

The action of C is given by

$$C c^\dagger_{\mathbf{k},\mathbf{Q},\eta,\alpha,s} C^{-1} = \sum_{\mathbf{Q}'\eta'\beta} [D(C)]_{\mathbf{Q}'\eta'\beta,\mathbf{Q}\eta\alpha} c^\dagger_{\mathbf{k},\mathbf{Q}',\eta',\beta,s}, \tag{D17}$$

with the representation matrix

$$[D(C)]_{\mathbf{Q}'\eta'\beta,\mathbf{Q}\eta\alpha} = \delta_{\mathbf{Q}',\mathbf{Q}}\delta_{\eta',\eta}(\sigma_z)_{\beta,\alpha}. \tag{D18}$$

Note that C preserves the electron momentum $\mathbf{k}$. Since C flips the single-particle Hamiltonian $\hat{H}_0$, it is not a commuting symmetry of TBG, but only reflects a relation between the positive- and negative-energy spectra. The transformation C satisfies

$$C^2 = 1, \quad \{C, C_{2z}\} = 0, \quad [C, T] = 0,$$
$$[C, P] = 0, \quad \{C, C_{2z}T\} = 0, \quad \{C, C_{2z}P\} = 0. \tag{D19}$$

b. The full symmetry

When transformed into the energy band basis, the chiral symmetry C implies

$$\epsilon_{n,\eta}(\mathbf{k}) = -\epsilon_{-n,\eta}(\mathbf{k}), \tag{D20}$$

$$[D(C)]_{\eta\eta'}u_{n\eta'}(\mathbf{k}) = \sum_m [B^C(\mathbf{k})]_{m\eta,n\eta'}u_{m\eta}(\mathbf{k}), \tag{D21}$$

where

$$[B^C(\mathbf{k})]_{m\eta,n\eta'} = \delta_{\eta,\eta'}\delta_{-m,n}e^{i\varphi^C_{n,\eta'}(\mathbf{k})}. \tag{D22}$$

This implies the transformation

$$Cc^\dagger_{\mathbf{k},n,\eta',s}C^{-1} = \sum_{m\eta}[B^C(\mathbf{k})]_{m\eta,n\eta'}c^\dagger_{\mathbf{k},m,\eta,s}. \tag{D23}$$

By the relations $\{C, C_{2z}T\} = \{C, C_{2z}P\} = 0$, the sewing matrix of C satisfies

$$\begin{aligned} B^C(\mathbf{k})B^{C_{2z}T}(\mathbf{k}) &= -B^{C_{2z}T}(\mathbf{k})B^{C*}(\mathbf{k}), \\ B^C(\mathbf{k})B^{C_{2z}P}(\mathbf{k}) &= -B^{C_{2z}P}(\mathbf{k})B^C(\mathbf{k}). \end{aligned} \tag{D24}$$

Under the gauge fixing of Eq. (B17), we have $B^{C_{2z}T}(\mathbf{k}) = \zeta^0\tau^0$, and $B^{C_{2z}P}(\mathbf{k}) = \zeta^y\tau^y$. The only $\mathbf{k}$-independent gauge for sewing matrix of C in consistency with Eqs. (D22) and (D24) within each pair of bands $n = \pm n_B$ is then (up to a global minus sign)

$$B^C(\mathbf{k}) = \zeta^y\tau^z. \tag{D25}$$

In particular, this $\mathbf{k}$-independent gauge fixing (D25) of C automatically ensures the continuous gauge fixing condition (B16), which is crucial for defining the irrep band basis in Eq. (26). To see this, note that Eq. (D25) tells us that $u_{-n,\eta}(\mathbf{k}) = i\mathrm{sgn}(n)\eta u_{n,\eta}(\mathbf{k})$ for band $n = \pm n_B$, and thus we have

$$\begin{aligned} f_{n,\eta}(\mathbf{k}+\mathbf{q},\mathbf{k}) &= |u^\dagger_{n,\eta}(\mathbf{k}+\mathbf{q})u_{n,\eta}(\mathbf{k}) - u^\dagger_{-n,\eta}(\mathbf{k}+\mathbf{q})u_{-n,\eta}(\mathbf{k})| \\ &= |u^\dagger_{n,\eta}(\mathbf{k}+\mathbf{q})u_{n,\eta}(\mathbf{k})[1-\mathrm{sgn}(n)^2\eta^2]| = 0 \end{aligned} \tag{D26}$$

for any $\mathbf{k}$ and $\mathbf{q}$, satisfying Eq. (B16).

We also note that this gauge fixing of C is consistent with the gauge fixings of both C_{2z} and P separately in Eq. (B18). Basically, the relations $\{C, C_{2z}\} = 0$ and $[C, P] = 0$ require

$$\begin{aligned} B^C(-\mathbf{k})B^{C_{2z}}(\mathbf{k}) &= -B^{C_{2z}}(\mathbf{k})B^C(\mathbf{k}), \\ B^C(-\mathbf{k})B^P(\mathbf{k}) &= B^P(\mathbf{k})B^C(\mathbf{k}), \end{aligned} \tag{D27}$$

which is satisfied by Eq. (D25).

For the projected Hamiltonian $H = H_0 + H_I$, we now show that C is a symmetry of the interaction Hamiltonian H_I and further constrains the matrix $M(\mathbf{k}, \mathbf{q}+\mathbf{G})$ in Eq. (C23). To see this, we note that with the relation (D21) due to C symmetry, the definition of $M(\mathbf{k}, \mathbf{q}+\mathbf{G})$ in Eq. (C10) satisfies (written as a matrix in the n, η space)

$$\begin{aligned} M^{(\eta)}_{m,n}(\mathbf{k},\mathbf{q}+\mathbf{G}) &= \sum_\alpha \sum_{\mathbf{Q}\in\mathcal{Q}_\pm} u^*_{\mathbf{Q}-\mathbf{G},\alpha;m\eta}(\mathbf{k}+\mathbf{q})u_{\mathbf{Q},\alpha;n\eta}(\mathbf{k}) \\ &= \sum_\alpha \sum_{\mathbf{Q}\in\mathcal{Q}_\pm} [u^\dagger_{m\eta}(\mathbf{k}+\mathbf{q})D^\dagger(C)]_{\mathbf{Q}-\mathbf{G},\alpha}[D(C)u_{n\eta}(\mathbf{k})]_{\mathbf{Q},\alpha} \\ &= [B^C(\mathbf{k}+\mathbf{q})^\dagger]_{m\eta,m'\eta'}\sum_\alpha \sum_{\mathbf{Q}\in\mathcal{Q}_\pm} u^*_{\mathbf{Q}-\mathbf{G},\alpha;m'\eta'}(\mathbf{k}+\mathbf{q})u_{\mathbf{Q},\alpha;n'\eta'}(\mathbf{k})[B^C(\mathbf{k})]_{n'\eta',n\eta}, \end{aligned} \tag{D28}$$

or in matrix form,

$$M(\mathbf{k},\mathbf{q}+\mathbf{G}) = B^C(\mathbf{k}+\mathbf{q})^\dagger M(\mathbf{k},\mathbf{q}+\mathbf{G})B^C(\mathbf{k}). \tag{D29}$$

We note that Eq. (D29) is independent of gauge fixings. If we take the gauge fixed form of $M(\mathbf{k}, \mathbf{q}+\mathbf{G})$ in Eq. (C23) and the gauge fixing of C in Eq. (D25), we find $M(\mathbf{k}, \mathbf{q}+\mathbf{G})$ has to commute with $\zeta^y\tau^z$. Thus, when there is the chiral symmetry C, the gauge fixed $M(\mathbf{k}, \mathbf{q}+\mathbf{G})$ has to take the form

$$M(\mathbf{k},\mathbf{q}+\mathbf{G}) = \zeta^0\tau^0\alpha_0(\mathbf{k},\mathbf{q}+\mathbf{G}) + i\zeta^y\tau^0\alpha_2(\mathbf{k},\mathbf{q}+\mathbf{G}). \tag{D30}$$

In particular, the functions $\alpha_1(\mathbf{k}, \mathbf{q}+\mathbf{G}) = \alpha_3(\mathbf{k}, \mathbf{q}+\mathbf{G}) = 0$.

By Eqs. (D23) and (D29), it is easy to see that

$$\begin{aligned} CO_{\mathbf{q},\mathbf{G}}C^{-1} &= \sum_{\mathbf{k}\eta s}\sum_{m,n=\pm1}\sqrt{V(\mathbf{q}+\mathbf{G})}M^{(\eta)}_{m,n}(\mathbf{k},\mathbf{q}+\mathbf{G})\left(Cc^\dagger_{\mathbf{k}+\mathbf{q},m,\eta,s}c_{\mathbf{k},n,\eta,s}C^{-1} - \frac{1}{2}\delta_{\mathbf{q},\mathbf{0}}\delta_{m,n}\right) \\ &= \sum_{\mathbf{k}\eta s}\sum_{m,n=\pm1}\sqrt{V(\mathbf{q}+\mathbf{G})}\left([B^C(\mathbf{k}+\mathbf{q})^\dagger M(\mathbf{k},\mathbf{q}+\mathbf{G})B^C(\mathbf{k})]_{m\eta;n\eta}c^\dagger_{\mathbf{k}+\mathbf{q},m,\eta,s}c_{\mathbf{k},n,\eta,s} - \frac{1}{2}M^{(\eta)}_{m,n}(\mathbf{k},\mathbf{q}+\mathbf{G})\delta_{\mathbf{q},\mathbf{0}}\delta_{m,n}\right) \\ &= \sum_{\mathbf{k}\eta s}\sum_{m,n=\pm1}\sqrt{V(\mathbf{q}+\mathbf{G})}M^{(\eta)}_{m,n}(\mathbf{k},\mathbf{q}+\mathbf{G})\left(c^\dagger_{\mathbf{k}+\mathbf{q},m,\eta,s}c_{\mathbf{k},n,\eta,s} - \frac{1}{2}\delta_{\mathbf{q},\mathbf{0}}\delta_{m,n}\right) = O_{\mathbf{q},\mathbf{G}}. \end{aligned} \tag{D31}$$

Therefore, $[C, O_{\mathbf{q},\mathbf{G}}] = 0$, and accordingly the projected interaction H_I satisfies

$$[C, H_I] = 0, \tag{D32}$$

implying C is a symmetry of H_I.

The C symmetry allows us to define the following operator as a commuting symmetry of H_I:

$$S'^{z0} = \sum_{\mathbf{k},s} \sum_{nn'\eta\eta'} [B^C(\mathbf{k})]_{n\eta,n'\eta'} c^\dagger_{\mathbf{k},n,\eta,s} c_{\mathbf{k},n',\eta',s} = \sum_{\mathbf{k},s} \sum_{nn'\eta\eta'} [\zeta^y \tau^z]_{n\eta,n'\eta'} c^\dagger_{\mathbf{k},n,\eta,s} c_{\mathbf{k},n',\eta',s}, \tag{D33}$$

where we have gauge fixed its representation by Eq. (D25). We note that when S^{y0} acts on single-electron states $c^\dagger_{\mathbf{k},n,\eta,s}|0\rangle$ where $|0\rangle$ is the vacuum, it is the same as the operation of C. To see this is a symmetry, we note that

$$[S'^{z0}, O_{\mathbf{q},\mathbf{G}}] = \sum_{\mathbf{k},s} \sum_{nn'\eta\eta'} ([\zeta^y\tau^z, M(\mathbf{k}, \mathbf{q}+\mathbf{G})])_{n\eta,n'\eta'} \times c^\dagger_{\mathbf{k},n,\eta,s} c_{\mathbf{k},n',\eta',s} = 0. \tag{D34}$$

Therefore, S'^{z0} is a commuting symmetry of the interaction Hamiltonian H_I in Eq. (C15), namely,

$$[S'^{z0}, H_I] = 0. \tag{D35}$$

Note that S'^{z0} does not commute with the single-particle Hamiltonian H_0 unless $\epsilon_{n,\eta}(\mathbf{k}) = \epsilon_{-n,\eta}(\mathbf{k})$. Due to Eq. (D20), this is only possible when $\epsilon_{n,\eta}(\mathbf{k}) = 0$, namely, in the exact flat band limit $H_0 = 0$.

Recall that H_I already has a U(4) symmetry generated by S^{ab} in Eq. (D9). The commutation of S^{ab} with S'^{z0} then produces another 16 Hermitian operators:

$$S'^{ab} = \sum_{\mathbf{k},m,\eta,s;n,\eta',s'} (s'^{ab})_{m,\eta,s;n,\eta',s'} c^\dagger_{\mathbf{k},m,\eta,s} c_{\mathbf{k},n,\eta',s'}, \quad (a, b = 0, x, y, z), \tag{D36}$$

where for each pair of bands $n = \pm n_{\mathrm{B}}$

$$s'^{ab} = \{\zeta^y\tau^0 s^b,\ \zeta^0\tau^x s^b,\ \zeta^0\tau^y s^b,\ \zeta^y\tau^z s^b\}, \quad (a, b{=}0, x, y, z). \tag{D37}$$

In summary, the single-particle representation matrices of all the generators S^{ab} and S'^{ab} can be reorganized into

$$\{\zeta^0\tau^a s^b, \quad \zeta^y\tau^a s^b\}, \quad (a, b = 0, x, y, z). \tag{D38}$$

It is more convenient to linear combine the U(4)×U(4) generators as

$$S^{ab}_\pm = \sum_{\mathbf{k},m,\eta,s;n,\eta',s'} (s^{ab}_\pm)_{m,\eta,s;n,\eta',s'} c^\dagger_{\mathbf{k},m,\eta,s} c_{\mathbf{k},n,\eta',s'}, \tag{D39}$$

where we define

$$s^{ab}_\pm = \tfrac{1}{2}(\zeta^0 \pm \zeta^y)\tau^a s^b, \quad (a, b = 0, x, y, z). \tag{D40}$$

In this form, it is easier to see that the 16 generators S^{ab}_+ generate one U(4), the 16 generators S^{ab}_- generate another U(4), and $[S^{ab}_+, S^{cd}_-] = 0$. Therefore, in total they give a U(4)×U(4) symmetry in the first chiral-flat limit.

We note that the U(4) group in the nonchiral-flat limit in Eq. (D10) is a subgroup of the U(4)×U(4) group in the first chiral-flat limit in Eq. (D40), but it is not one of the two tensor-producted U(4) groups.

The Cartan subalgebra of the first chiral-flat $U(4) \times U(4)$ generators in Eq. (D38) can be chosen as

Cartan of first chiral $U(4) \times U(4)$:

$$\zeta^0\tau^0 s^0, \quad \zeta^0\tau^0 s^z, \quad \zeta^0\tau^z s^0, \quad \zeta^0\tau^z s^z, \quad \zeta^y\tau^0 s^0, \quad \zeta^y\tau^0 s^z, \quad \zeta^y\tau^z s^0, \quad \zeta^y\tau^z s^z. \tag{D41}$$

c. The single-electron irreps

The irreps of the U(4)×U(4) group can be obtained by the tensor product of the irreps of the first U(4) and the second U(4), respectively. We shall use

$$([\lambda_1]_4, [\lambda_2]_4) \tag{D42}$$

to represent a U(4)×U(4) irrep, which is the tensor product of an irrep $[\lambda_1]_4$ of the first U(4) and an irrep $[\lambda_2]_4$ of the second U(4).

At each momentum $\mathbf{k}$, the $\mathbf{k}$-independent representation matrices in Eq. (D40) can be decomposed into U(4)×U(4) irreps. This can be done again by transforming into a new basis where ζ^y is diagonalized, which is exactly the irrep band basis $d^{(n_{\mathrm{B}})\dagger}_{\mathbf{k},e_Y,\eta,s} = \frac{1}{\sqrt{2}}(c^\dagger_{\mathbf{k},+n_{\mathrm{B}},\eta,s} + ie_Y c^\dagger_{\mathbf{k},-n_{\mathrm{B}},\eta,s})$ we defined earlier in Eq. (26), where $e_Y = \pm 1$ gives the irrep number of the band basis. The single-electron state in irrep band e_Y

$$d^{(n_{\mathrm{B}})\dagger}_{\mathbf{k},e_Y,\eta,s}|0\rangle \tag{D43}$$

has eigenvalue $\zeta^y = e_Y$. It is then easy to see that the representation matrices of the U(4)×U(4) generators $S^{ab}_\pm$ for the single-electron state (D43) are given by the 4 × 4 matrices

$$s^{ab}_\pm = \tfrac{1}{2}(1 \pm e_Y)\tau^a s^b. \tag{D44}$$

Therefore, the single-electron state (D43) for a fixed e_Y, or equivalently the irrep band fermion operator $d^{(n_{\mathrm{B}})\dagger}_{\mathbf{k},e_Y,\eta,s}$ for a fixed e_Y, occupies an irrep of the U(4)×U(4) group. The U(4)×U(4) irrep of $d^{(n_{\mathrm{B}})\dagger}_{\mathbf{k},+1,\eta,s}$ is given by $([1]_4, [0]_4)$, while the U(4)×U(4) irrep of $d^\dagger_{\mathbf{k},-1,\eta,s}$ is $([0]_4, [1]_4)$, where we recall that $[1]_4$ and $[0]_4$ are the four-dimensional fundamental irrep and the one-dimensional trivial identity irrep of U(4) group, respectively.

We also note that the operator $O_{\mathbf{q},\mathbf{G}}$ in the first chiral limit can be rewritten under irrep band basis as

$$O_{\mathbf{q},\mathbf{G}} = \sum_{\mathbf{k},e_Y,\eta,s} \sqrt{V(\mathbf{G}+\mathbf{q})}[M_{e_Y}(\mathbf{k}, \mathbf{q}+\mathbf{G})]_{n_{\mathrm{B}},n'_{\mathrm{B}}} \times \sum_{\eta,s} \left(d^{(n_{\mathrm{B}})\dagger}_{\mathbf{k}+\mathbf{q},e_Y,\eta,s} d^{(n'_{\mathrm{B}})}_{\mathbf{k},e_Y,\eta,s} - \frac{1}{2}\delta_{\mathbf{q},\mathbf{0}}\delta_{n_{\mathrm{B}},n'_{\mathrm{B}}} \right), \tag{D45}$$

where

$$M_{e_Y}(\mathbf{k}, \mathbf{q}+\mathbf{G}) = \alpha_0(\mathbf{k}, \mathbf{q}+\mathbf{G}) + ie_Y\alpha_2(\mathbf{k}, \mathbf{q}+\mathbf{G}). \quad \text{(D46)}$$

Therefore, the interaction H_I in Eq. (10) is diagonal in the index e_Y.

For many-body Fock states created by multiple $d^{(n_B)\dagger}_{\mathbf{k},e_Y,\eta,s}$, the U(4)×U(4) representation is given by the tensor product of the U(4)×U(4) irreps $([1]_4, [0]_4)$ or $([0]_4, [1]_4)$ of each $d^{(n_B)\dagger}_{\mathbf{k},e_Y,\eta,s}$. Such tensor product representations can be further decomposed into U(4)×U(4) irreps, which will be discussed in a separate paper [109].

4. U(4) symmetry in the (first) chiral-nonflat limit

We have seen that the first chiral-flat limit has a U(4)×U(4) symmetry in the projected Hamiltonian $H = H_I$. Here we show that if $w_0 = 0 < w_1$ but $H_0 \neq 0$, which we define as the nonchiral-flat limit, there is still a remaining U(4) symmetry.

a. The symmetry

When $H_0 \neq 0$, namely, when $\epsilon_{n\eta}(\mathbf{k})$ is not constantly zero, we have $H = H_0 + H_I$, and neither $C_{2z}P$ nor C is a commuting symmetry of H. However, their combination $CC_{2z}P$ is still a commuting symmetry, namely,

$$[CC_{2z}P, H] = [CC_{2z}P, H_0] + [CC_{2z}P, H_I] = 0. \quad \text{(D47)}$$

Therefore, the symmetry is still enhanced compared to the nonchiral-nonflat case. This can be most easily seen as follows: Among the 32 generators in Eq. (D38), only those with a single-particle representation matrix proportional ζ^0 is still a symmetry when $H_0 \neq 0$. This is because the kinetic Hamiltonian in the first chiral limit (denoted by H_0^+) can be written as

$$H_0 = H_0^+ = \sum_{\mathbf{k}} \epsilon_{|n|,\eta}(\mathbf{k})(\zeta^z\tau^0 s^0)_{m,\eta,s;n,\eta',s'} c^\dagger_{\mathbf{k},m,\eta,s} c_{\mathbf{k},n,\eta',s'}, \quad \text{(D48)}$$

where we have used the constraint $\epsilon_{n,\eta}(\mathbf{k}) = -\epsilon_{-n,\eta}(\mathbf{k})$ due to the chiral symmetry C. It is then clear that the generators in Eq. (D38) proportional to ζ^y will flip the pair of single-particle bands $n = \pm n_B$ and do not commute with H_0. Therefore, we are left with 16 generators commuting with $H = H_0 + H_I$. We redefine their notations as follows:

$$\widetilde{S}^{ab} = \sum_{\mathbf{k},m,\eta,s;n,\eta',s'} (\tilde{s}^{ab})_{m,\eta,s;n,\eta',s'} c^\dagger_{\mathbf{k},m,\eta,s} c_{\mathbf{k},n,\eta',s'}, \quad \text{(D49)}$$

where for each pair of bands $n = \pm n_B$

$$\tilde{s}^{ab} = \zeta^0\tau^a s^b, \quad (a, b = 0, x, y, z). \quad \text{(D50)}$$

They form the generators of a U(4) symmetry group. In particular, $\zeta^0\tau^x s^0$ is the sewing matrix of $iCC_{2z}P$.

We note that this U(4) symmetry group in the first chiral-nonflat limit is different from the U(4) symmetry group in the nonchiral-flat limit [Eq. (D10)]. Here the generators $\widetilde{S}^{ab}$ are simply the full unitary rotations in the valley-spin space, while the band space is not transformed.

b. The single-electron irreps

Since the generators in Eq. (D50) is proportional to ζ^0, any fixed band basis of all valleys and spins form a fundamental U(4) irrep. For example, we still consider the single-electron state in the irrep band basis

$$d^{(n_B)\dagger}_{\mathbf{k},e_Y,\eta,s}|0\rangle. \quad \text{(D51)}$$

For a fixed $\mathbf{k}$ and e_Y, the states in Eq. (D51) occupies a fundamental irrep $[1]_4$ of the first chiral-nonflat U(4), and the representation matrices of the generators are given by

$$\tau^a s^b, \quad (a, b = 0, x, y, z) \quad \text{(D52)}$$

for either $e_Y = \pm 1$. Similarly, the many-body Fock states created by $d^{(n_B)\dagger}_{\mathbf{k},e_Y,\eta,s}$ are given by the tensor product of the fundamental irreps $[1]_4$ of each $d^{(n_B)\dagger}_{\mathbf{k},e_Y,\eta,s}$ [109].

5. U(4)×U(4) symmetry in the second chiral-flat limit

We now consider an opposite limit where $w_1 = 0 < w_0$, which we define as the second chiral limit. Although this limit is far from experimental reality and the band structure contains no flat bands over the full MBZ (but they are flat in some directions of the MBZ) and is a perfect metal (see Fig. 2, proof is given in Ref. [108]), the interaction Hamiltonian enjoys a enhanced U(4)×U(4) symmetry of different physical origin from the first chiral limit. One cannot help but hope there is some hidden duality in the TBG problem.

a. The second chiral symmetry

When $w_1 = 0$, we can define a second chiral transformation C', which anticommutes with the full single-particle Hamiltonian $\hat{H}_0$ in Eq. (A5):

$$\{C', \hat{H}_0\} = 0. \quad \text{(D53)}$$

The operation of C' is given by

$$C' c^\dagger_{\mathbf{k},\mathbf{Q},\eta,\alpha,s} C'^{-1} = \sum_{\mathbf{Q}'\eta'\beta} [D(C')]_{\mathbf{Q}'\eta'\beta,\mathbf{Q}\eta\alpha} c^\dagger_{\mathbf{k},\mathbf{Q}',\eta',\beta,s}, \quad \text{(D54)}$$

with the representation matrix

$$[D(C')]_{\mathbf{Q}'\eta'\beta,\mathbf{Q}\eta\alpha} = \zeta_{\mathbf{Q}}\delta_{\mathbf{Q}',\mathbf{Q}}\delta_{\eta',\eta}(\sigma_z)_{\beta,\alpha}, \quad \text{(D55)}$$

where $\zeta_{\mathbf{Q}} = \pm 1$ for $\mathbf{Q} \in \mathcal{Q}_\pm$. Note that C' preserves the electron momentum $\mathbf{k}$. Since C' flips the single-particle Hamiltonian $\hat{H}_0$, it is not a commuting symmetry of TBG but only reflects a relation between the positive- and negative-energy spectra. The transformation C' satisfies

$$C'^2 = 1, \quad [C', C_{2z}] = 0, \quad \{C', T\} = 0,$$
$$\{C', P\} = 0, \quad \{C', C_{2z}T\} = 0, \quad \{C', C_{2z}P\} = 0. \quad \text{(D56)}$$

b. The full symmetry

When transformed into the energy band basis, the second chiral symmetry C' implies

$$\epsilon_{n,\eta}(\mathbf{k}) = -\epsilon_{-n,\eta}(\mathbf{k}), \quad \text{(D57)}$$

$$[D(C')]_{\eta\eta'}u_{n\eta'}(\mathbf{k}) = \sum_m [B^{C'}(\mathbf{k})]_{m\eta,n\eta'}u_{m\eta}(\mathbf{k}), \quad \text{(D58)}$$

where

$$[B^{C'}(\mathbf{k})]_{m\eta,n\eta'} = \delta_{\eta,\eta'}\delta_{-m,n}e^{i\varphi^{C'}_{n,\eta'}(\mathbf{k})}. \tag{D59}$$

This implies the transformation

$$C' c^\dagger_{\mathbf{k},n,\eta',s} C'^{-1} = \sum_{m\eta}[B^{C'}(\mathbf{k})]_{m\eta,n\eta'} c^\dagger_{\mathbf{k},m,\eta,s}. \tag{D60}$$

By the relations $\{C', C_{2z}T\} = \{C', C_{2z}P\} = 0$, the sewing matrix of C' satisfies

$$\begin{aligned} B^{C'}(\mathbf{k})B^{C_{2z}T}(\mathbf{k}) &= -B^{C_{2z}T}(\mathbf{k})B^{C'*}(\mathbf{k}), \\ B^{C'}(\mathbf{k})B^{C_{2z}P}(\mathbf{k}) &= -B^{C_{2z}P}(\mathbf{k})B^{C'}(\mathbf{k}). \end{aligned} \tag{D61}$$

Note that this constraint for the sewing matrix of C' is exactly the same as that for C in Eq. (D24). Therefore, within each pair of bands $n = \pm n_{\mathrm{B}}$, if we impose the gauge fixing of Eq. (B17), we similarly find the only consistent $\mathbf{k}$-independent gauge for sewing matrix of C' is (up to a global minus sign)

$$B^{C'}(\mathbf{k}) = \zeta^y\tau^z. \tag{D62}$$

This $\mathbf{k}$-independent gauge fixing (D62) of C' also automatically ensures the continuous gauge fixing condition (B16), which is crucial for defining the irrep band basis in Eq. (26). This is because Eq. (D62) tells us that $u_{-n,\eta}(\mathbf{k}) = i\mathrm{sgn}(n)\eta u_{n,\eta}(\mathbf{k})$ for band $n = \pm n_{\mathrm{B}}$, which implies

$$\begin{aligned} f_{n,\eta}(\mathbf{k}+\mathbf{q},\mathbf{k}) &= |u^\dagger_{n,\eta}(\mathbf{k}+\mathbf{q})u_{n,\eta}(\mathbf{k}) - u^\dagger_{-n,\eta}(\mathbf{k}+\mathbf{q})u_{-n,\eta}(\mathbf{k})| \\ &= |u^\dagger_{n,\eta}(\mathbf{k}+\mathbf{q})u_{n,\eta}(\mathbf{k})[1-\mathrm{sgn}(n)^2\eta^2]| = 0 \end{aligned} \tag{D63}$$

for any $\mathbf{k}$ and $\mathbf{q}$, satisfying Eq. (B16).

However, the gauge fixing of C' in Eq. (D62) is inconsistent with the $\mathbf{k}$-independent gauge fixings of both C_{2z} and P separately in Eq. (B18). This is because $[C', C_{2z}] = 0$ and $\{C', P\} = 0$ require

$$\begin{aligned} B^{C'}(-\mathbf{k})B^{C_{2z}}(\mathbf{k}) &= B^{C_{2z}}(\mathbf{k})B^{C'}(\mathbf{k}), \\ B^{C'}(-\mathbf{k})B^{P}(\mathbf{k}) &= B^{P}(\mathbf{k})B^{C'}(\mathbf{k}), \end{aligned} \tag{D64}$$

which are, however, not satisfied by the simultaneous gauge fixings of Eqs. (D62) and (B18). If we fix the sewing matrix of C' to be $\mathbf{k}$ independent as given in Eq. (D62), the sewing matrices of C_{2z} and P have to be $\mathbf{k}$ dependent. In this Appendix, we shall choose the gauge fixing of Eq. (D62) and give up the separate gauge fixing of C_{2z} and P in Eq. (B18), since only their combination $C_{2z}P$ is used for the U(4) symmetries discussed here.

However, we note that if a momentum $\mathbf{k}$ is C_{2z} invariant (the Γ_M point and the three M_M points in MBZ), the above gauge fixing problem appears to imply the absence of well-defined sewing matrices of C_{2z} and P. In fact, this is because at $w_1 = 0$, the TBG band structure is protected to be doubly degenerate at C_{2z} invariant momenta, which leads to a perfect metal (see Fig. 2 and Ref. [108] for proof). Therefore, the pair of bands $n = \pm n_{\mathrm{B}}$ are connected with the other bands at Γ_M and M_M points, where the projection within the two bands $n = \pm n_{\mathrm{B}}$ is ill defined. The sewing matrices of C_{2z} and P at such C_{2z} invariant momenta can only be written down when the additional degenerate states at these momenta from other bands are included. We shall not discuss this matter here, since we will not use the sewing matrices of C_{2z} and P in this Appendix.

Nevertheless, we note that one could fix the gauge of C_{2z} and P in a simple $\mathbf{k}$-dependent way, provided $\mathbf{k}$ is not a C_{2z} invariant point. First, we divide all the C_{2z}-noninvariant $\mathbf{k}$ points into two sets $\mathcal{K}_1, \mathcal{K}_2$ related by C_{2z}, namely, $C_{2z}\mathcal{K}_1 = \mathcal{K}_2$. For instance, $\mathcal{K}_1$ and $\mathcal{K}_2$ can be two half-MBZs related by C_{2z}. Then we can fix the sewing matrices of C_{2z} and P (and T given that C_{2z} and $C_{2z}T$ are fixed) at C_{2z}-noninvariant $\mathbf{k}$ within each pair of bands $n = \pm n_{\mathrm{B}}$ as

$$\begin{aligned} B^{C_{2z}}(\mathbf{k}) &= (-1)^j\zeta^0\tau^x, \quad B^T(\mathbf{k}) = -(-1)^j\zeta^0\tau^x, \\ B^P(\mathbf{k}) &= i(-1)^j\zeta^y\tau^z, \quad (\text{for } \mathbf{k}\in\mathcal{K}_j). \end{aligned} \tag{D65}$$

Since the gauge fixed sewing matrix of C' in Eq. (D62) is exactly the same as that of C in Eq. (D25), we can follow a similar derivation as that from Eqs. (D28) to (D40), which gives us the following.

First, C' is a symmetry of H_I satisfying $[C', H_I] = 0$, and the $M(\mathbf{k},\mathbf{q}+\mathbf{G})$ matrix is restricted to have the form

$$M(\mathbf{k},\mathbf{q}+\mathbf{G}) = \zeta^0\tau^0\alpha_0(\mathbf{k},\mathbf{q}+\mathbf{G}) + i\zeta^y\tau^0\alpha_2(\mathbf{k},\mathbf{q}+\mathbf{G}). \tag{D66}$$

The Hermitian condition of the $M(\mathbf{k},\mathbf{q}+\mathbf{G})$ [Eq. (C17)] requires that

$$\begin{aligned} \alpha_0(\mathbf{k},\mathbf{q}+\mathbf{G}) &= \alpha_0^T(\mathbf{k}+\mathbf{q},-\mathbf{q}-\mathbf{G}), \\ \alpha_2(\mathbf{k},\mathbf{q}+\mathbf{G}) &= -\alpha_2^T(\mathbf{k}+\mathbf{q},-\mathbf{q}-\mathbf{G}). \end{aligned} \tag{D67}$$

For $\mathbf{q} = 0$, the $B^{C_{2z}}(\mathbf{k})$ sewing matrix implies $M^\eta(\mathbf{k},\mathbf{G}) = M^{-\eta}(-\mathbf{k},-\mathbf{G})$ and hence

$$\alpha_0(\mathbf{k},\mathbf{G}) = \alpha_0(-\mathbf{k},-\mathbf{G}), \quad \alpha_2(\mathbf{k},\mathbf{G}) = \alpha_2(-\mathbf{k},-\mathbf{G}). \tag{D68}$$

Combining the above two constraints, we obtain

$$\alpha_0(\mathbf{k},\mathbf{G}) = \alpha_0^T(-\mathbf{k},\mathbf{G}), \quad \alpha_2(\mathbf{k},\mathbf{G}) = -\alpha_2^T(-\mathbf{k},\mathbf{G}). \tag{D69}$$

Second, the C' symmetry yields a U(4)×U(4) symmetry with generators

$$S'^{ab}_\pm = \sum_{\mathbf{k},m,\eta,s;n,\eta',s'} (s'^{ab}_\pm)_{m,\eta,s;n,\eta',s'} c^\dagger_{\mathbf{k},m,\eta,s} c_{\mathbf{k},n,\eta',s'}, \tag{D70}$$

where we define

$$s'^{ab}_\pm = \tfrac{1}{2}(\zeta^0 \pm \zeta^y)\tau^a s^b, \quad (a,b = 0,x,y,z). \tag{D71}$$

We note, however, although these generators take the same gauge-fixed form as those in the first chiral-flat limit [Eq. (D71)], their physical origins are different: Here the U(4)×U(4) generators are generated by the sewing matrix of the second chiral symmetry C', while in the first chiral-flat limit, the U(4)×U(4) generators are generated by the sewing matrix of the first chiral symmetry C.

c. The single-electron irreps

We have shown that under the gauge fixings (B17) and (D62), the U(4)×U(4) generators of the second chiral-flat limit is exactly the same as that of the first chiral-flat limit. Therefore, exactly parallel to the first chiral-flat limit, the single-electron irreps in the second chiral-flat limit

are given by the irrep band basis $d^{(n_B)\dagger}_{\mathbf{k},e_Y,\eta,s} = \frac{1}{\sqrt{2}}(c^\dagger_{\mathbf{k},+n_B,\eta,s} + ie_Y c^\dagger_{\mathbf{k},-n_B,\eta,s})$ we defined earlier in Eq. (26), where $e_Y = \pm 1$ gives the irrep number of the band basis. The single-electron state

$$d^{(n_B)\dagger}_{\mathbf{k},e_Y,\eta,s}|0\rangle \tag{D72}$$

with a fixed e_Y and $\mathbf{k}$ occupies a U(4)×U(4) irrep of $([1]_4, [0]_4)$ if $e_Y = +1$, and $([0]_4, [1]_4)$ if $e_Y = -1$. The representation matrices of the U(4)×U(4) generators $S^{ab}_\pm$ for the single-electron state (D43) are given by the 4×4 matrices

$$s'^{ab}_\pm = \tfrac{1}{2}(1 \pm e_Y)\tau^a s^b. \tag{D73}$$

However, in this second chiral limit, we note that the basis $d^\dagger_{\mathbf{k},e_Y,\eta,s} = d^{(1)\dagger}_{\mathbf{k},e_Y,\eta,s}$ when $n_B = 1$ no longer give a well-defined Chern band in the MBZ with a definite Chern number as illustrated in Sec. B 3, since the lowest two bands $n = \pm 1$ are gapless with the higher bands when $w_1 = 0$ (see Fig. 2). Neither are the bands flat, possibly giving rise to interesting, gapless phases.

6. U(4) symmetry in the second chiral-nonflat limit

If $w_1 = 0 < w_0$, taking into account the kinetic term $H_0 \neq 0$, we are still left with a U(4) symmetry. We call this limit the second chiral-nonflat limit. Since the U(4)×U(4) generators in the second chiral-flat limit are exactly the same as those in the first chiral-flat limit, the case here is mathematically exactly the same as the first chiral-nonflat limit in Appendix D 4. Therefore, we conclude that the second chiral-nonflat limit has a remaining U(4) symmetry with generators given by

$$\widetilde{S}'^{ab} = \sum_{\mathbf{k},m,\eta,s;n,\eta',s'} (\tilde{s}'^{ab})_{m,\eta,s;n,\eta',s'} c^\dagger_{\mathbf{k},m,\eta,s} c_{\mathbf{k},n,\eta',s'}, \tag{D74}$$

where within each pair of bands $n = \pm n_B$

$$\tilde{s}'^{ab} = \zeta^0 \tau^a s^b, \quad (a, b = 0, x, y, z), \tag{D75}$$

under the gauge fixings of Eqs. (B17) and (D62). The only difference is that here the U(4) symmetry is generated by the sewing matrix of $iC'C_{2z}P$, which reads $\zeta^0\tau^x s^0$.

This second chiral-nonflat limit is more physical, since when $w_1 = 0 < w_0$, the bands are never too flat (Fig. 2).

APPENDIX E: THE STABILIZER CODE LIMIT

The projected interacting Hamiltonian in Eq. (10) is generically a quantum Hamiltonian, where the terms $O_{-\mathbf{q},-\mathbf{G}}O_{\mathbf{q},\mathbf{G}}$ do not commute, since the commutator $[O_{\mathbf{q},\mathbf{G}}, O_{\mathbf{q}',\mathbf{G}'}]$ given in Eq. (C16) does not vanish for generic form factors (overlaps) $M^{(\eta)}_{m,n}(\mathbf{k}, \mathbf{q}+\mathbf{G})$. Thus, although it gives a PSDH, which allows us to find exact ground states at certain fillings in the flat band limit (for which $H = H_I$) as we will demonstrate in a separate paper [109], it is impossible to analytically solve all the many-body eigenstates of $H = H_I$.

However, in the case where we are projecting only into the eight lowest $n = \pm 1$ bands (i.e., $n_{\max} = 1$), in the first (or second) chiral-flat limit $w_0 = 0$ (or $w_1 = 0$) and $H_0 = 0$, if we further have $M^{(\eta)}_{m,n}(\mathbf{k}, \mathbf{q}+\mathbf{G})$ independent of $\mathbf{k}$, we would have $[O_{\mathbf{q},\mathbf{G}}, O_{\mathbf{q}',\mathbf{G}'}] = 0$. We call this limit the *stabilizer code limit*:

$$\begin{aligned}&\text{stabilizer code limit}\\ &= \text{1st/2nd chiral-flat limit}\\ &+ \mathbf{k}\text{-independent form factors } M(\mathbf{k}, \mathbf{q}+\mathbf{G}).\end{aligned} \tag{E1}$$

Indeed, Eq. (D30) or (D66) and our $\mathbf{k}$-independent assumption lead to a $\mathbf{k}$-independent form factor matrix:

$$\begin{aligned}M(\mathbf{k}, \mathbf{q}+\mathbf{G}) &= M(\mathbf{0}, \mathbf{q}+\mathbf{G})\\ &= \zeta^0\tau^0\alpha_0(\mathbf{0}, \mathbf{q}+\mathbf{G}) + i\zeta^y\tau^0\alpha_2(\mathbf{0}, \mathbf{q}+\mathbf{G}).\end{aligned} \tag{E2}$$

In particular, if $n_{\max} = 1$, both $\alpha_0(\mathbf{0}, \mathbf{q}+\mathbf{G})$ and $\alpha_2(\mathbf{0}, \mathbf{q}+\mathbf{G})$ are not matrices but just numbers, and thus they commute among each other. Therefore, by Eq. (C16), we have

$$\begin{aligned}[O_{\mathbf{q},\mathbf{G}}, O_{\mathbf{q}',\mathbf{G}'}] \propto\ & M(\mathbf{k}+\mathbf{q}', \mathbf{q}+\mathbf{G})M(\mathbf{k}, \mathbf{q}'+\mathbf{G}')\\ & - M(\mathbf{k}+\mathbf{q}, \mathbf{q}'+\mathbf{G}')M(\mathbf{k}, \mathbf{q}+\mathbf{G}) = 0.\end{aligned} \tag{E3}$$

This yields a Hamiltonian similar to a stabilizer code Hamiltonian

$$H = H_I = \frac{1}{2\Omega_{\text{tot}}} \sum_{\mathbf{q}\in \text{MBZ}} \sum_{\mathbf{G}\in\mathcal{Q}_0} O_{-\mathbf{q},-\mathbf{G}}O_{\mathbf{q},\mathbf{G}}, \tag{E4}$$

where all the terms commute:

$$[O_{-\mathbf{q},-\mathbf{G}}O_{\mathbf{q},\mathbf{G}}, O_{-\mathbf{q}',-\mathbf{G}'}O_{\mathbf{q}',\mathbf{G}'}] = 0. \tag{E5}$$

Therefore, all the terms $O_{-\mathbf{q},-\mathbf{G}}O_{\mathbf{q},\mathbf{G}}$ can be simultaneously diagonalized, which makes all the many-body eigenstates of the Hamiltonian exactly solvable. Note that Eq. (E4) is not strictly a stabilizer code Hamiltonian since the terms $O_{-\mathbf{q},-\mathbf{G}}O_{\mathbf{q},\mathbf{G}}$ do not have a spectrum equal to 0 or 1 (moreover their spectrum depends on $\mathbf{q}$ and $\mathbf{G}$). Nevertheless, Eq. (E4) has the crucial feature that makes the spectrum of a stabilizer code solvable (namely a sum of commuting operators), thus its name.

As we will prove in Ref. [109], the Hamiltonian $H = H_I$ in the stabilizer code limit is an extended Hubbard model with extended interactions and zero hoppings. Therefore, although far from physical, the stabilizer code limit provides a Hubbard-model understanding of the TBG physics, as suggested by the recent experimental observations [22,23].

We will solve the stabilizer code limit Hamiltonian in Ref. [109].

APPENDIX F: COMPARISON WITH THE U(4)x SYMMETRY OF REF. [71]

In this Appendix, we discuss the interaction Hamiltonian of Ref. [71] and compare it with ours. In Ref. [71], Kang and Vafek were the first to show the appearance of a U(4) approximate symmetry in their Hamiltonian, which is a type of PSDH obtained by projecting into a Wannier basis.

1. The Wannier gauge

The $s = \uparrow\downarrow$ sectors are related by an SU(2) rotation. Thus, we only need to construct Wannier functions in the $s = \uparrow$ sector; the Wannier functions in the $s = \downarrow$ sector can then be

symmetrically generated. Before we introduce the Wannier functions, let us first write the Bloch states of TBG as linear combinations of plane waves

$$|\psi_{\mathbf{k},n,\eta}\rangle = \frac{1}{\sqrt{N}} \sum_{\mathbf{Q}\in\mathcal{Q}_\pm} \sum_{\mathbf{R}\alpha} u_{\mathbf{Q},\alpha;n\eta}(\mathbf{k}) e^{i(\mathbf{k}+\mathbf{Q})\cdot(\mathbf{R}+\mathbf{t}_\alpha)} |\mathbf{R}\alpha\rangle, \quad \text{(F1)}$$

where summations over $\mathbf{R}, \alpha$ are limited to sites in the top layer (bottom layer) graphene for $\mathbf{Q} \in \mathcal{Q}_+$ ($\mathbf{Q} \in \mathcal{Q}_-$), $|\mathbf{R}\alpha\rangle$ is the atomic orbital at $\mathbf{R}+\mathbf{t}_\alpha$, and N is the number of unit cells in each of the two graphene layers. Generally, the Wannier functions are linear combinations of the Bloch states

$$\begin{aligned} \left|w_{\mathbf{R}_M,\mu,\eta}\right\rangle &= \frac{1}{\sqrt{N_M}} \sum_{\mathbf{k}} e^{-i\mathbf{k}\cdot\mathbf{R}_M} |\widetilde{\psi}_{\mathbf{k},\mu,\eta}\rangle, \\ |\widetilde{\psi}_{\mathbf{k},\mu,\eta}\rangle &= \sum_{n=\pm1} |\psi_{\mathbf{k},n,\eta}\rangle W^\eta_{n,\mu}(\mathbf{k}), \end{aligned} \quad \text{(F2)}$$

where N_M is the number of moiré unit cells and $W^\eta(\mathbf{k})$ at each $\mathbf{k}$ is a two-by-two matrix. We denote the center of the Wannier function $|w_{\mathbf{R}_M,\mu,\eta}\rangle$ as $\mathbf{R}_M + \mathbf{t}_{M,\mu}$, with $\mathbf{R}_M = l_1\mathbf{a}_{M1} + l_2\mathbf{a}_{M2}$ being a moiré lattice and $\mathbf{t}_{M,\mu}$ ($\mu = 1, 2$) being the sublattice vectors. Here we take the unit cell basis as $\mathbf{a}_{M1} = (0, -1)$ and $\mathbf{a}_{M2} = (\frac{\sqrt{3}}{2}, \frac{1}{2})$. Notice that the Bloch states are periodic in momentum space, so the transformation coefficient is $e^{-i\mathbf{k}\cdot\mathbf{R}}$ rather than $e^{-i\mathbf{k}\cdot(\mathbf{R}+\mathbf{t}_\mu)}$. The sewing matrices of $|\widetilde{\psi}_{\mathbf{k},\mu,\eta}\rangle$ are defined as

$$B^g_{\mu\eta,\nu\eta'}(\mathbf{k}) = \langle\widetilde{\psi}_{g\mathbf{k},\mu,\eta}|g|\widetilde{\psi}_{\mathbf{k},\nu,\eta'}\rangle. \quad \text{(F3)}$$

The two bands in each valley have a fragile topology protected by $C_{2z}T$ symmetry and a stable topology protected by the $PC_{2z}T$ symmetry [108]. Thus, in order to obtain the Wannier functions, we have to abandon smooth $C_{2z}T$ gauge and smooth P gauge of $|\widetilde{\psi}_{\mathbf{k},\mu,\eta}\rangle$. It is possible to choose a smooth gauge for the remaining symmetries $g = C_{3z}, C_{2y}, T$ since they do not protect a topology. According to Kang and Vafek [42], the two Wannier states ($\mu = 1, 2$) in each valley locate at the honeycomb lattice, i.e., $\mathbf{t}_{M,1} = \frac{1}{3}\mathbf{a}_{M,1} + \frac{2}{3}\mathbf{a}_{M,2} = (\frac{1}{\sqrt{3}}, 0)$, and $\mathbf{t}_{M,2} = -\mathbf{t}_{M,1}$, and one can choose the Wannier functions to satisfy

$$C'_{3z}\left|w_{\mathbf{R}_M,\mu,\eta}\right\rangle = e^{i\eta\frac{2\pi}{3}}\left|w_{\mathbf{R}'_M,\mu,\eta}\right\rangle, \quad [\mathbf{R}'_M + \mathbf{t}_{M,\mu} = C'_{3z}(\mathbf{R}_M + \mathbf{t}_{M,\mu})], \quad \text{(F4)}$$

$$C_{2y}\left|w_{\mathbf{R}_M,\mu,\eta}\right\rangle = \sum_\beta \gamma^x_{\nu\alpha}\tau^x_{\eta',\eta}\left|w_{\mathbf{R}'_M,\nu,\eta'}\right\rangle, \quad [\mathbf{R}'_M + \mathbf{t}_{M,\nu} = C_{2y}(\mathbf{R}_M + \mathbf{t}_{M,\mu})], \quad \text{(F5)}$$

$$T|w_{\mathbf{R}_M,\mu,\eta}\rangle = \left|w_{\mathbf{R}_M,\mu,-\eta}\right\rangle, \quad \text{(F6)}$$

where γ^x is the first Pauli matrix in the moiré sublattice space, and τ^x is the first Pauli matrix in the valley space. Kang and Vafek's $|w_{1,2,3,4}\rangle$ are our $|w_{\mathbf{R}_M,1,+}\rangle$, $|w_{\mathbf{R}_M,1,-}\rangle$, $|w_{\mathbf{R}_M,2,-}\rangle$, $|w_{\mathbf{R}_M,2,+K}\rangle$, respectively. Here we have used C'_{3z} to represent the $2\pi/3$ rotation microscopically centered at honeycomb vertex of graphene. In this work, we use C_{3z} to denote the $2\pi/3$ rotation microscopically centered at the honeycomb center of graphene. One should notice that the C'_{3z} eigenvalues, which are $e^{i\eta\frac{2\pi}{3}}$ at Γ_M, are different from the C_{3z} in the BM model, which are 1 at Γ_M [43]. We will discuss the relation between C_{3z} and C'_{3z} in the end of this subsection.

The sewing matrices of C_{3z}, C_{2y}, T on $|\widetilde{\psi}_{\mathbf{k},\mu,\eta}\rangle$ can be obtained from the actions of C_{3z}, C_{2y}, T on the Wannier functions. We have

$$\begin{aligned} C'_{3z}|\widetilde{\psi}_{\mathbf{k},\mu,\eta}\rangle &= \frac{1}{\sqrt{N_M}} \sum_{\mathbf{R}_M} e^{i\mathbf{k}\cdot\mathbf{R}_M} C'_{3z}\left|W_{\mathbf{R}_M,\mu,\eta}\right\rangle \\ &= e^{i\eta\frac{2\pi}{3}} \frac{1}{\sqrt{N_M}} \sum_{\mathbf{R}_M} e^{i\mathbf{k}\cdot\mathbf{R}_M}\left|W_{\mathbf{R}'_M,\mu,\eta}\right\rangle \\ &= e^{i\eta\frac{2\pi}{3}} \frac{1}{\sqrt{N_M}} \sum_{\mathbf{R}'_M} e^{i\mathbf{k}\cdot(C'^{-1}_{3z}\mathbf{R}'_M + C'^{-1}_{3z}\mathbf{t}_{M,\mu} - \mathbf{t}_{M,\mu})}\left|W_{\mathbf{R}'_M,\mu,\eta}\right\rangle \\ &= e^{i\eta\frac{2\pi}{3}} e^{i(C'_{3z}\mathbf{k}-\mathbf{k})\cdot\mathbf{t}_{M,\mu}}\left|\widetilde{\psi}_{C'_{3z}\mathbf{k},\mu,\eta}\right\rangle, \end{aligned} \quad \text{(F7)}$$

where $\mathbf{R}'_M = C'_{3z}(\mathbf{R}_M + \mathbf{t}_{M,\mu}) - \mathbf{t}_{M,\mu}$. Thus, the C'_{3z} sewing matrix is

$$B^{C'_{3z}}_{\mu\eta,\nu\eta'}(\mathbf{k}) = \delta_{\mu\nu}\delta_{\eta\eta'} e^{i\eta\frac{2\pi}{3}} e^{i(C_{3z}\mathbf{k}-\mathbf{k})\cdot\mathbf{t}_\mu}. \quad \text{(F8)}$$

We also have

$$\begin{aligned} C_{2y}|\widetilde{\psi}_{\mathbf{k},\mu,\eta}\rangle &= \frac{1}{\sqrt{N_M}} \sum_{\mathbf{R}_M} e^{i\mathbf{k}\cdot\mathbf{R}_M} C_{2y}\left|w_{\mathbf{R}_M,\mu,\eta}\right\rangle \\ &= \sum_{\beta\eta'} \gamma^x_{\nu,\mu}\tau^x_{\eta'\eta} \frac{1}{\sqrt{N_M}} \sum_{\mathbf{R}_M} e^{i\mathbf{k}\cdot\mathbf{R}_M}\left|w_{\mathbf{R}'_M,\nu,\eta'}\right\rangle \\ &= \sum_{\beta\eta'} \gamma^x_{\beta,\alpha}\tau^x_{\eta'\eta} \frac{1}{\sqrt{N_M}} \\ &\quad \times \sum_{\mathbf{R}'_M} e^{i\mathbf{k}\cdot(C^{-1}_{2y}\mathbf{R}'_M + C^{-1}_{2y}\mathbf{t}_{M,\nu} - \mathbf{t}_{M,\mu})}\left|w_{\mathbf{R}'_M,\nu,\eta'}\right\rangle \\ &= \sum_{\nu\eta'} \gamma^x_{\nu,\mu}\tau^x_{\eta'\eta}\left|\widetilde{\psi}_{C_{2y}\mathbf{k},\mu,\eta'}\right\rangle, \end{aligned} \quad \text{(F9)}$$

where $C_{2y}\mathbf{t}_{M,\nu} = \mathbf{t}_{M,\mu}$ and $\mathbf{R}'_M = C_{2y}(\mathbf{R}_M + \mathbf{t}_{M,\mu}) - \mathbf{t}_{M,\nu}$. Thus, the C_{2y} sewing matrix is

$$B^{C_{2y}}_{\mu\eta,\nu\eta'}(\mathbf{k}) = \gamma^x_{\mu\nu}\tau^x_{\eta\eta'}. \quad \text{(F10)}$$

For the time-reversal, we have

$$T|\widetilde{\psi}_{\mathbf{k},\mu,\eta}\rangle = \frac{1}{\sqrt{N_M}} \sum_{\mathbf{R}_M} e^{-i\mathbf{k}\cdot\mathbf{R}_M}|w_{\mathbf{R},\mu,-\eta}\rangle = |\widetilde{\psi}_{-\mathbf{k},\mu,-\eta}\rangle. \quad \text{(F11)}$$

Thus, the time-reversal sewing matrix is

$$B^T_{\mu\eta,\nu\eta'}(\mathbf{k}) = \delta_{\mu\nu}\tau^x_{\eta,\eta'}. \quad \text{(F12)}$$

In this gauge, the $C_{2z}T$ sewing matrix $B^{C_{2z}T}(\mathbf{k})$ and the P sewing matrix $B^{(P)}(\mathbf{k})$ must have be discontinuous at some momenta due to the topology protected by $C_{2z}T$ and/or $PC_{2z}T$ of the two lowest bands. Correspondingly, in the Wannier basis the $C_{2z}T$ and P representations must be nonlocal. Usually, an Wannier function at $\mathbf{r}$ ($\mathbf{r} \neq \mathbf{0}$) would be transformed to another Wannier function at $-\mathbf{r}$ under $C_{2z}T$ or P. In the nonlocal case, the Wannier function at $\mathbf{r}$ ($\mathbf{r} \neq \mathbf{0}$) will be transformed to a linear combination of all the Wannier functions in the whole 2D space under $C_{2z}T$ or P. Any tight-binding model in this Wannier representation that has finite-range hopping will break the $C_{2z}T$ and the P symmetries.

a. Another choice of C_{3z} center

We find that the C'_{3z} operation, which is a $2\pi/3$ rotation at the honeycomb vertex of graphene, is the $2\pi/3$ centered at honeycomb center of graphene followed by a microscopic translation, i.e., $C'_{3z} = \{1|-\mathbf{a}_1\}C_{3z}$. Here $\mathbf{a}_1$ is the lattice basis of single-layer graphene. The microscopic model of TBG cannot have both C'_{3z} and C_{3z}. For example, we choose the twisting center at the honeycomb center, and then C_{3z} is an exact symmetry but C'_{3z} is only an approximate symmetry; however, the microscopic error of C'_{3z} should be negligible, diminishing at small angle. The translation $-\mathbf{a}_1$ will lead to factors $e^{i\frac{2\pi}{3}}$ and $e^{-i\frac{2\pi}{3}}$ for the two valleys K and K', respectively. Thus, the representation matrix of C'_{3z} in the BM model is given by

$$D(C'_{3z}) = e^{i\frac{2\pi}{3}\tau^z} D(C_{3z}), \tag{F13}$$

where $D(C_{3z})$ is given by Eq. (A11). Thus, C_{3z} acts on the Wannier functions as

$$C_{3z}\left|w_{\mathbf{R}_M,\mu,\eta}\right\rangle = \left|w_{\mathbf{R}'_M,\mu,\eta}\right\rangle, \quad \left[\mathbf{R}'_M + \mathbf{t}_{M,\mu} = C_{3z}(\mathbf{R}_M + \mathbf{t}_{M,\mu})\right]. \tag{F14}$$

It follows that the C_{3z} sewing matrix is

$$B^{C_{3z}}_{\mu\eta,\nu\eta'}(\mathbf{k}) = \delta_{\mu\nu}\delta_{\eta\eta'} e^{i(C_{3z}\mathbf{k}-\mathbf{k})\cdot\mathbf{t}_\mu}. \tag{F15}$$

Notice that the C_{2y} axis of Kang and Vafek's model is same as ours, so we do not need to change the C_{2y} sewing matrix.

2. Interaction

Now that we have implement the Kang and Vafek Wannier symmetries, we transform their interaction [71] into momentum space. Let us denote the fermion annihilation operator of the Wannier states as $c_{\mathbf{R}_M,\mu,\eta,s}$. Then the Kang-Vafek interaction has the form

$$H_I = \frac{V_0}{2}\sum_{\mathbf{R}_M} O_{\mathbf{R}_M} O_{\mathbf{R}_M}, \tag{F16}$$

$$O_{\mathbf{R}_M} = \frac{1}{3} Q_{\mathbf{R}_M} + \kappa T_{\mathbf{R}_M}, \tag{F17}$$

where $\mathbf{R}_M$ sums over all the lattice vectors (honeycomb centers), and $Q_{\mathbf{R}_M}$ and $T_{\mathbf{R}_M}$ are given by

$$Q_{\mathbf{R}_M} = \sum_{\eta,s}\sum_{j\in\hexagon} c^\dagger_{\mathbf{R}_M+\mathbf{d}_{M,j}-\mathbf{t}_{M,[j]},[j],\eta,s} c_{\mathbf{R}_M+\mathbf{d}_{M,j}-\mathbf{t}_{M,[j]},[j],\eta,s}, \tag{F18}$$

$$T_{\mathbf{R}_M} = \sum_{\eta,s}\sum_{j\in\hexagon} \left((-1)^{j-1} e^{i(-1)^{j-1}\eta\vartheta} c^\dagger_{\mathbf{R}_M+\mathbf{d}_{M,j+1}-\mathbf{t}_{M,[j+1]},[j+1],\eta,s} c_{\mathbf{R}_M+\mathbf{d}_{M,j}-\mathbf{t}_{M,[j]},[j],\eta,s} + \text{H.c.}\right). \tag{F19}$$

Here j sums over the six hexagon vertex around the triangle site $\mathbf{R}_M$, $[j] = j \bmod 2$ is the sublattice index, and ϑ is a phase factor. The vectors are given by $\mathbf{d}_{M,1} = \mathbf{t}_{M,1}$, $\mathbf{d}_{M,4} = \mathbf{t}_{M,2} = -\mathbf{t}_{M,1}$, and $\mathbf{d}_{M,j+2} = C_{3z}\mathbf{d}_{M,j}$. To match our convention of Wannier functions, we have decomposed the position $(\mathbf{R}_M + \mathbf{d}_{M,j})$ of the operator $c^\dagger_{\mathbf{R}_M+\mathbf{d}_{M,j}-\mathbf{t}_{M,[j]},[j],\eta,s}$ into a lattice vector $\mathbf{R}_M + \mathbf{d}_{M,j} - \mathbf{t}_{M,[j]}$ and a sublattice vector $\mathbf{t}_{M,[j]}$. $Q_{\mathbf{R}_M}$ is the total charge on the six vertices of the honeycomb centered at $\mathbf{R}_M$. $T_{\mathbf{R}_M}$ is a hopping-like term where each term annihilates an electron at the vertex j and create an electron at the vertex $j+1$ or $j-1$. The phase factor associated with the hopping is $e^{i\eta\vartheta}$ if $j = 1, 3, 5$ and is $-e^{-j\eta\vartheta}$ if $j = 2, 4, 6$. κ is a factor determining the strength of the hopping-like term and is estimated as 0.16 in Ref. [71]. (κ is originally denoted as α_1 in Ref. [71]. We changed the notation to avoid confusion with the $\alpha_1(\mathbf{k}, \mathbf{q}+\mathbf{G})$ function [Eq. (C23)] in this paper.) We can write $O_{\mathbf{R}_M}$ as

$$\begin{aligned} O_{\mathbf{R}_M} = &\sum_{\eta,s}\sum_{j\in\hexagon} \frac{1}{3} c^\dagger_{\mathbf{R}_M+\mathbf{d}_{M,j}-\mathbf{t}_{M,[j]},[j],\eta,s} c_{\mathbf{R}_M+\mathbf{d}_{M,j}-\mathbf{t}_{M,[j]},[j],\eta,s} \\ &+ \kappa\left((-1)^{j-1} e^{i(-1)^{j-1}\eta\vartheta} c^\dagger_{\mathbf{R}_M+\mathbf{d}_{M,j+1}-\mathbf{t}_{M,[j+1]},[j+1],\eta,s} c_{\mathbf{R}_M+\mathbf{d}_{M,j}-\mathbf{t}_{M,[j]},[j],\eta,s} + \text{H.c.}\right). \end{aligned} \tag{F20}$$

Now we apply the transformation

$$O_{\mathbf{R}_M} = \frac{1}{N_M}\sum_{\mathbf{q}} e^{-i\mathbf{q}\cdot\mathbf{R}_M} O_{\mathbf{q}} \tag{F21}$$

such that the interaction can be written as our interaction form (already present in Vafek and Kang)

$$H_I = \frac{V_0}{2N_M}\sum_{\mathbf{q}} O_{-\mathbf{q}} O_{\mathbf{q}}. \tag{F22}$$

We transform the three terms, i.e., the $Q_{\mathbf{R}_M}$ term, the first term in $T_{\mathbf{R}_M}$ term, and the second term in $T_{\mathbf{R}_M}$, in $O_{\mathbf{R}_M}$ one by one. First, we have

$$\begin{aligned} O^1_{\mathbf{q}} &= \frac{1}{N_M}\sum_{\mathbf{R}_M} e^{i\mathbf{R}_M\cdot\mathbf{q}} O^1_{\mathbf{R}_M} = \frac{1}{3N_M}\sum_{\mathbf{R}_M} e^{i\mathbf{R}_M\cdot\mathbf{q}} \sum_{\eta,s}\sum_{j\in\hexagon} c^\dagger_{\mathbf{R}_M+\mathbf{d}_{M,j}-\mathbf{t}_{M,[j]},[j],\eta,s} c_{\mathbf{R}_M+\mathbf{d}_{M,j}-\mathbf{t}_{M,[j]},[j],\eta,s} \\ &= \frac{1}{3N_M}\sum_{\mathbf{R}_M} e^{i\mathbf{R}_M\cdot\mathbf{q}} \sum_{\eta,s}\sum_{j\in\hexagon}\sum_{\mathbf{pk}} e^{-i(\mathbf{R}_M+\mathbf{d}_{M,j}-\mathbf{t}_{M,[j]})\cdot\mathbf{p}} e^{i(\mathbf{R}_M+\mathbf{d}_{M,j}-\mathbf{t}_{M,[j]})\cdot\mathbf{k}} c^\dagger_{\mathbf{p},[j],\eta,s} c_{\mathbf{k},[j],\eta,s} \\ &= \frac{1}{3}\sum_{\eta s}\sum_{j\in\hexagon}\sum_{\mathbf{k}} c^\dagger_{\mathbf{k}+\mathbf{q},[j],\eta,s} c_{\mathbf{k},[j],\eta,s} = \sum_{\mu\eta s}\sum_{\mathbf{k}} c^\dagger_{\mathbf{k}+\mathbf{q},\mu,\eta,s} c_{\mathbf{k},\mu,\eta,s}. \end{aligned} \tag{F23}$$

Second, we have

$$\begin{aligned} O^2_{\mathbf{q}} &= \frac{\kappa}{N_M}\sum_{\mathbf{R}_M} e^{i\mathbf{R}_M\cdot\mathbf{q}} \sum_{\eta,s}\sum_{j\in\hexagon} (-1)^{j-1} e^{i(-1)^{j-1}\eta\vartheta} c^\dagger_{\mathbf{R}_M+\mathbf{d}_{M,j+1}-\mathbf{t}_{M,[j+1]},[j+1],\eta,s} c_{\mathbf{R}_M+\mathbf{d}_{M,j}-\mathbf{t}_{M,[j]},[j],\eta,s} \\ &= \frac{\kappa}{N_M}\sum_{\mathbf{R}_M} e^{i\mathbf{R}_M\cdot\mathbf{q}} \sum_{\eta,s}\sum_{j\in\hexagon} (-1)^{j-1} e^{i(-1)^{j-1}\eta\vartheta} \sum_{\mathbf{pk}} e^{-i(\mathbf{R}_M+\mathbf{d}_{M,j+1}-\mathbf{t}_{M,[j+1]})\cdot\mathbf{p}} e^{i(\mathbf{R}_M+\mathbf{d}_{M,j}-\mathbf{t}_{M,[j]})\cdot\mathbf{k}} c^\dagger_{\mathbf{p},[j+1],\eta,s} c_{\mathbf{k},[j],\eta,s} \\ &= \kappa\sum_{\eta,s}\sum_{j\in\hexagon} (-1)^{j-1} e^{i(-1)^{j-1}\eta\vartheta} \sum_{\mathbf{k}} e^{-i(\mathbf{d}_{M,j+1}-\mathbf{t}_{M,[j+1]})\cdot(\mathbf{k}+\mathbf{q})} e^{i(\mathbf{d}_{M,j}-\mathbf{t}_{M,[j]})\cdot\mathbf{k}} c^\dagger_{\mathbf{k}+\mathbf{q},[j+1],\eta,s} c_{\mathbf{k},[j],\eta,s}. \end{aligned} \tag{F24}$$

We split the summation $\sum_{j\in\hexagon}$ into $\sum_{j=1,3,5}$ and $\sum_{j=2,4,6}$, and then

$$\begin{aligned} O^2_{\mathbf{q}} &= \kappa\sum_{\eta,s}\sum_{j=1,3,5} e^{i\eta\vartheta}\sum_{\mathbf{k}} e^{i(-\mathbf{d}_{M,j+1}+\mathbf{t}_{M,2})\cdot\mathbf{q}} e^{i(\mathbf{d}_{M,j}-\mathbf{t}_{M,1}-\mathbf{d}_{M,j+1}+\mathbf{t}_{M,2})\cdot\mathbf{k}} c^\dagger_{\mathbf{k}+\mathbf{q},2,\eta,s} c_{\mathbf{k},1,\eta,s} \\ &\quad - \kappa\sum_{\eta,s}\sum_{j=2,4,6} e^{-i\eta\vartheta}\sum_{\mathbf{k}} e^{i(-\mathbf{d}_{M,j+1}+\mathbf{t}_{M,1})\cdot\mathbf{q}} e^{i(\mathbf{d}_{M,j}-\mathbf{t}_{M,2}-\mathbf{d}_{M,j+1}+\mathbf{t}_{M,1})\cdot\mathbf{k}} c^\dagger_{\mathbf{k}+\mathbf{q},1,\eta,s} c_{\mathbf{k},2,\eta,s}. \end{aligned} \tag{F25}$$

Since $\mathbf{t}_{M,1} = -\mathbf{t}_{M,2}$ and $\mathbf{d}_{M,j+3} = -\mathbf{d}_{M,j}$, the phase factors of the second term are the complex conjugations of those of the first term, and thus we can rewrite $O^2_{\mathbf{q}}$ as

$$O^2_{\mathbf{q}} = \kappa\sum_{\eta s}\sum_{\mathbf{k}} e^{i\eta\vartheta}\omega(\mathbf{k},\mathbf{q}) c^\dagger_{\mathbf{k}+\mathbf{q},2,\eta,s} c_{\mathbf{k},1,\eta,s} - e^{-i\eta\vartheta}\omega^*(\mathbf{k},\mathbf{q}) c^\dagger_{\mathbf{k}+\mathbf{q},1,\eta,s} c_{\mathbf{k},2,\eta,s} \tag{F26}$$

with

$$\omega(\mathbf{k},\mathbf{q}) = \sum_{j=1,3,5} e^{i(-\mathbf{d}_{M,j+1}+\mathbf{t}_{M,2})\cdot\mathbf{q}} e^{i(\mathbf{d}_{M,j}-\mathbf{t}_{M,1}-\mathbf{d}_{M,j+1}+\mathbf{t}_{M,2})\cdot\mathbf{k}}. \tag{F27}$$

Now we list all the involved vectors in the phase factors ($\mathbf{t}_{M,1} = \mathbf{d}_{M,1}$, $\mathbf{t}_{M,2} = \mathbf{d}_{M,4}$):

$$j = 1, \quad -\mathbf{d}_{M,j+1} + \mathbf{d}_{M,4} = -\mathbf{a}_{M2}, \quad \mathbf{d}_{M,j} - \mathbf{d}_{M,1} - \mathbf{d}_{M,j+1} + \mathbf{d}_{M,4} = -\mathbf{a}_{M2}, \tag{F28}$$

$$j = 3, \quad -\mathbf{d}_{M,j+1} + \mathbf{d}_{M,4} = 0, \quad \mathbf{d}_{M,j} - \mathbf{d}_{M,1} - \mathbf{d}_{M,j+1} + \mathbf{d}_{M,4} = -\mathbf{a}_{M1} - \mathbf{a}_{M2}, \tag{F29}$$

$$j = 5, \quad -\mathbf{d}_{M,j+1} + \mathbf{d}_{M,4} = -\widetilde{\mathbf{a}}_1 - \mathbf{a}_{M2}, \quad \mathbf{d}_j - \mathbf{d}_1 - \mathbf{d}_{M,j+1} + \mathbf{d}_{M,4} = -\mathbf{a}_{M1} - 2\mathbf{a}_{M2}. \tag{F30}$$

Thus, we have

$$\omega(\mathbf{k},\mathbf{q}) = e^{-i\mathbf{a}_{M2}\cdot\mathbf{q}} e^{-i\mathbf{a}_{M2}\cdot\mathbf{k}} + e^{-i(\mathbf{a}_{M1}+\mathbf{a}_{M2})\cdot\mathbf{k}} + e^{-i(\mathbf{a}_{M1}+\mathbf{a}_{M2})\cdot\mathbf{q}} e^{i(\mathbf{a}_{M1}-2\mathbf{a}_{M2})\cdot\mathbf{k}}. \tag{F31}$$

Since the third term in $O_{\mathbf{R}_M}$ is the Hermitian conjugation of the second term, we have

$$\begin{aligned} O^3_{\mathbf{q}} = Q^{2\dagger}_{-\mathbf{q}} &= \kappa\sum_{\eta s}\sum_{\mathbf{k}} \left(-e^{i\eta\vartheta}\omega(\mathbf{k},-\mathbf{q}) c^\dagger_{\mathbf{k},2,\eta,s} c_{\mathbf{k}-\mathbf{q},1,\eta,s} + e^{-i\eta\vartheta}\omega^*(\mathbf{k},-\mathbf{q}) c^\dagger_{\mathbf{k},1,\eta,s} c_{\mathbf{k}-\mathbf{q},2,\eta,s}\right) \\ &= \kappa\sum_{\eta s}\sum_{\mathbf{k}} \left(-e^{i\eta\vartheta}\omega(\mathbf{k}+\mathbf{q},-\mathbf{q}) c^\dagger_{\mathbf{k}+\mathbf{q},2,\eta,s} c_{\mathbf{k},1,\eta,s} + e^{-i\eta\vartheta}\omega^*(\mathbf{k}+\mathbf{q},-\mathbf{q}) c^\dagger_{\mathbf{k}+\mathbf{q},1,\eta,s} c_{\mathbf{k},2,\eta,s}\right). \end{aligned} \tag{F32}$$

We define

$$\beta(\mathbf{k},\mathbf{q}) = \omega(\mathbf{k},\mathbf{q}) - \omega(\mathbf{k}+\mathbf{q},-\mathbf{q}). \tag{F33}$$

Thus, $O^2_{\mathbf{q}} + O^3_{\mathbf{q}}$ can be written as

$$O^2_{\mathbf{q}} + O^3_{\mathbf{q}} = \sum_{\eta s} \sum_{\mathbf{k}} e^{i\eta\vartheta}\beta(\mathbf{k},\mathbf{q}) c^\dagger_{\mathbf{k}+\mathbf{q},2,\eta,s} c_{\mathbf{k},1,\eta,s} - e^{-i\eta\vartheta}\beta^*(\mathbf{k},\mathbf{q}) c^\dagger_{\mathbf{k}+\mathbf{q},1,\eta,s} c_{\mathbf{k},2,\eta,s}. \tag{F34}$$

Now we write the total $O_{\mathbf{q}}$ operator as

$$O_{\mathbf{q}} = \sum_{\eta s} \sum_{\mathbf{k}} M^\eta_{\mu,\nu}(\mathbf{k},\mathbf{q}) c^\dagger_{\mathbf{k}+\mathbf{q},\mu,\eta,s} c_{\mathbf{k},\nu,\eta,s}, \tag{F35}$$

where M is

$$M^\eta(\mathbf{k},\mathbf{q}) = \gamma^0 - i\kappa\gamma^y \mathrm{Re}[e^{i\eta\vartheta}\beta(\mathbf{k},\mathbf{q})] + i\kappa\gamma^x \mathrm{Im}[e^{i\eta\vartheta}\beta(\mathbf{k},\mathbf{q})]. \tag{F36}$$

We can also express M as a 4×4 matrix (in the sublattice and valley spaces) as

$$\begin{aligned} M(\mathbf{k},\mathbf{q}) =& \gamma^0\tau^0 - i\kappa\gamma^y \mathrm{Re}[(\cos\vartheta\,\tau^0 + i\sin\vartheta\,\tau^z)\beta(\mathbf{k},\mathbf{q})] + i\kappa\gamma^x \mathrm{Im}[(\cos\vartheta\,\tau^0 + i\sin\vartheta\,\tau^z)\beta(\mathbf{k},\mathbf{q})] \\ =& \gamma^0\tau^0 - i\kappa\gamma^y\tau^0 \mathrm{Re}[\cos\vartheta\,\beta(\mathbf{k},\mathbf{q})] + i\kappa\gamma^x\tau^0 \mathrm{Im}[\cos\vartheta\,\beta(\mathbf{k},\mathbf{q})] + i\kappa\gamma^y\tau^z \mathrm{Im}[\sin\vartheta\,\beta(\mathbf{k},\mathbf{q})] + i\kappa\gamma^x\tau^z \mathrm{Re}[\sin\vartheta\,\beta(\mathbf{k},\mathbf{q})]. \end{aligned} \tag{F37}$$

With this, we have brought the Kang-Vafek interaction to the same form as our momentum-space interactions.

3. The Kang-Vafek U(4) symmetry

It is obvious that the Kang-Vafek interaction have spin-valley U(2)×U(2) symmetry, whose generators are

$$\gamma^0\tau^0 s^a, \quad \gamma^0\tau^z s^a, \quad a = 0, x, y, z. \tag{F38}$$

Now we show that it indeed has a U(4) symmetry. Our proof is the momentum-space version of the original proof [71]. We introduce two matrices

$$\Sigma^x = \gamma^x\tau^0\cos\vartheta + \gamma^y\tau^z\sin\vartheta, \quad \Sigma^y = -\gamma^x\tau^z\sin\vartheta + \gamma^y\tau^0\cos\vartheta, \tag{F39}$$

and rewrite the M matrix as

$$M(\mathbf{k},\mathbf{q}) = \gamma^0\tau^0 + i\kappa\Sigma^x \mathrm{Im}[\beta(\mathbf{k},\mathbf{q})] + i\kappa\Sigma^y \mathrm{Re}[\beta(\mathbf{k},\mathbf{q})]. \tag{F40}$$

One can verify that $\{\Sigma^x, \Sigma^y\} = 0$. We then apply a $\mathbf{k}$-*independent* gauge transformation $e^{i\frac{\vartheta}{2}\gamma^z\tau^z}$ such that $e^{i\frac{\vartheta}{2}\gamma^z\tau^z}\Sigma^x e^{-i\frac{\vartheta}{2}\gamma^z\tau^z} = \gamma^x\tau^0$ and $e^{i\frac{\vartheta}{2}\gamma^z\tau^z}\Sigma^y e^{-i\frac{\vartheta}{2}\gamma^z\tau^z} = \gamma^y\tau^0$. After the transformation, M becomes

$$M(\mathbf{k},\mathbf{q}) = \gamma^0\tau^0 + i\kappa\gamma^x\tau^0 \mathrm{Im}[\beta(\mathbf{k},\mathbf{q})] - i\kappa\gamma^y\tau^0 \mathrm{Re}[\beta(\mathbf{k},\mathbf{q})]. \tag{F41}$$

Therefore, the M matrix is invariant under the U(4) generators

$$\gamma^0\tau^a s^b, \quad a, b = 0, x, y, z. \tag{F42}$$

This gauge transformation seems equivalent to setting $\vartheta = 0$ [71]. However, after the gauge transformation, the sewing matrices might change.

4. Relation between Kang-Vafek U(4) and the $C_{2z}P$-implied U(4) symmetry

Let us first fix the $C_{2z}P$ gauge of the Wannier functions. According to Eq. (A20), we have

$$(C_{2z}P)^2 = 1, \quad [C_{3z}, C_{2z}P] = 0, \quad [C_{2y}, C_{2z}P] = 0, \quad \{T, C_{2z}P\} = 0, \tag{F43}$$

and hence

$$[B^{C_{2z}P}(\mathbf{k})]^2 = 1, \quad B^{C_{3z}}(\mathbf{k})B^{C_{2z}P}(\mathbf{k}) = B^{C_{2z}P}(C_{3z}\mathbf{k})B^{C_{3z}}(\mathbf{k}), \tag{F44}$$

$$B^{C_{2y}}(\mathbf{k})B^{C_{2z}P}(\mathbf{k}) = B^{C_{2z}P}(C_{2y}\mathbf{k})B^{C_{2y}}(\mathbf{k}), \quad B^T(\mathbf{k})B^{C_{2z}P*}(\mathbf{k}) = -B^{C_{2z}P}(-\mathbf{k})B^T(\mathbf{k}). \tag{F45}$$

Since both T and $C_{2z}TP$ (the charge conjugation) are local in real space, as shown in Appendix C 4, $C_{2z}P$ must also be a local operator in real space. Thus, we want $C_{2z}P$ to be local in the Wannier representation. However, this is incompatible with the crystalline and time-reversal symmetries. In order to be local in the Wannier representation, $C_{2z}P$ must leave the center of each Wannier function invariant and hence will be $\mathbf{k}$ independent. Since $C_{2z}P$ does not change the sublattice, the sewing matrix $B^{C_{2z}P}(\mathbf{k})$ should be diagonal in the sublattice index and thus does not contain $\gamma^{x,y}$ terms. Since $C_{2z}P$ changes valley, it must not contain τ^0 and τ^z. Thus, $B^{C_{2z}P}$ can only have four possible terms: $\gamma^{0,z}\tau^{x,y}$. All the four terms commute with $B^{C_{3z}}(\mathbf{k})$, which only contains the terms $\gamma^{0,z}\tau^0$. In order to commute with $B^{C_{2y}}(\mathbf{k})$ ($\gamma^x\tau^x$), only $\gamma^0\tau^x$ and $\gamma^z\tau^y$

are possible. However, both commute with $T = \tau^x K$, whereas Eq. (F43) shows that $C_{2z}P$ anticommutes with T. Thus, a local representation of $C_{2z}P$ is not compatible with the C_{3z}, C_{2y}, T symmetries. In other words, $C_{2z}P$ in the Wannier representation that respects C_{3z}, C_{2y}, T symmetries must be nonlocal.

The above analysis leads to two conclusions: (i) Our charge-conjugation symmetry must be nonlocal in the Kang-Vafek Wannier representation, and (ii) Kang and Vafek U(4) symmetry, which is local in the Wannier representation, is not equivalent to the $C_{2z}P$-implied U(4) symmetry, which is nonlocal in their Wannier representation.

5. Kang-Vafek U(4) as our U(4) chiral-nonflat limit symmetry

We now ask: Is the Kang and Vafek U(4) consistent with our U(4) implied by the $C_{2z}PC$? We assume that the Kang and Vafek model (at least approximately) preserves the $C_{2z}PC$ symmetry. Here C is the chiral symmetry:

$$D(C)h(\mathbf{k})D^{-1}(C) = -h(\mathbf{k}), \quad D(C)_{\mathbf{Q},\alpha;\mathbf{Q}',\alpha'} = \delta_{\mathbf{Q},\mathbf{Q}'}\sigma^z_{\alpha\alpha'}, \quad C^2 = 1. \tag{F46}$$

Commutations between C and $T, C_{3z}, C_{2y}, C_{2z}P$ are

$$[T, C] = 0, \quad [C_{3z}, C] = 0, \quad [C_{2y}, C] = 0, \quad \{C, C_{2z}P\} = 0. \tag{F47}$$

Thus, we have

$$(C_{2z}PC)^2 = -1, \quad [C_{3z}, C_{2z}PC] = 0, \quad [C_{2y}, C_{2z}PC] = 0, \quad \{T, C_{2z}PC\} = 0, \tag{F48}$$

and hence

$$[B^{C_{2z}PC}(\mathbf{k})]^2 = -1,$$
$$B^{C_{3z}}(\mathbf{k})B^{C_{2z}PC}(\mathbf{k}) = B^{C_{2z}PC}(C_{3z}\mathbf{k})B^{C_{3z}}(\mathbf{k}), \tag{F49}$$

$$B^{C_{2y}}(\mathbf{k})B^{C_{2z}PC}(\mathbf{k}) = B^{C_{2z}PC}(C_{2y}\mathbf{k})B^{C_{2y}}(\mathbf{k}),$$
$$B^{T}(\mathbf{k})B^{C_{2z}PC*}(\mathbf{k}) = -B^{C_{2z}PC}(-\mathbf{k})B^{T}(\mathbf{k}). \tag{F50}$$

We try to find a $\mathbf{k}$-independent solution, which means $C_{2z}PC$ is local in the Wannier representation. Since $C_{2z}PC$ preserves the sublattice (local) and changes valley, $B^{C_{2z}PC}$ can only have four terms $i\gamma^{0,z}\tau^{x,y}$, each of which squares to -1. All the four terms commute with C_{3z} ($\gamma^{0,z}$). Two terms commute with C_{2y} ($\gamma^x\tau^x$): $i\gamma^0\tau^x$, $i\gamma^z\tau^y$, and the two terms also anticommute with T. Therefore, there are two solutions of $B^{C_{2z}PC}$:

$$B^{C_{2z}PC(1)} = i\gamma^0\tau^x, \quad B^{C_{2z}PC(2)} = i\gamma^z\tau^y. \tag{F51}$$

If we can understand M [Eq. (F36)] as the inner product of periodic part of Bloch wave functions, i.e.,

$$M^{\eta}_{\mu\nu}(\mathbf{k}, \mathbf{q}) \sim \sqrt{V(\mathbf{q})}\langle u_{\mathbf{k}+\mathbf{q},\mu,\eta}|u_{\mathbf{k},\nu,\eta}\rangle, \tag{F52}$$

then M must commute with $B^{C_{2z}PC}$. Applying $B^{C_{2z}PC(1)}$ and $B^{C_{2z}PC(2)}$ to Eq. (F37), we obtain $\vartheta = 0, \pi$ and $\vartheta = \pm\frac{\pi}{2}$, respectively. For $\vartheta = 0, \pi$, the U(4) generators are

$$\gamma^0\tau^a s^b, \quad a, b = 0, x, y, z; \tag{F53}$$

for $\vartheta = \pm\frac{\pi}{2}$, the U(4) generators are

$$\gamma^z\tau^{x,y}s^a, \quad \gamma^0\tau^{0,z}s^a, \quad a = 0, x, y, z. \tag{F54}$$

Now we show that the two representations Eqs. (F53) and (F54) are equivalent. Under the gauge transformation $\begin{pmatrix}\tau^0 & 0\\ 0 & i\tau^z\end{pmatrix}$, Eq. (F54) becomes Eq. (F53) and $B^{C_{3z}}$, $B^{C_{2y}}$, B^T remain unchanged.

We summarize: (i) The $C_{2z}PC$ can be chosen as local in the Wannier representation. (ii) If Kang and Vafek's model does not have an exact $C_{2z}PC$ symmetry (which remains to be checked), then, if we continuously recover the $C_{2z}PC$ symmetry, their U(4) continuously changes to our U(4) implied by the $C_{2z}PC$ symmetry; this U(4) is implied by the chiral, nonflat limit. Hence, we conjecture that the Kang and Vafek U(4) is also invariant to the addition of *some* kinetic terms. (iii) The U(4) symmetry implied by $C_{2z}PC$ is also local in the Wannier representation because the U(2)×U(2) part is already local, and the additional generator is just the $C_{2z}PC$ operation.

If we impose the $CC_{2z}P$ symmetry to the Kang and Vafek's tight-binding model, their U(4) symmetry would become the chiral-nonflat U(4) symmetry, since the two U(4) symmetries share the same generators $\tau^a s^b$ ($a, b = 0, x, y, z$).

[1] R. Bistritzer and A. H. MacDonald, Moiré bands in twisted double-layer graphene, Proc. Natl. Acad. Sci. USA **108**, 12233 (2011).

[2] Y. Cao, V. Fatemi, A. Demir, S. Fang, S. L. Tomarken, J. Y. Luo, J. D. Sanchez-Yamagishi, K. Watanabe, T. Taniguchi, E. Kaxiras, R. C. Ashoori, and P. Jarillo-Herrero, Correlated insulator behaviour at half-filling in magic-angle graphene superlattices, Nature (London) **556**, 80 (2018).

[3] Y. Cao, V. Fatemi, S. Fang, K. Watanabe, T. Taniguchi, E. Kaxiras, and P. Jarillo-Herrero, Unconventional superconductivity in magic-angle graphene superlattices, Nature (London) **556**, 43 (2018).

[4] X. Lu, P. Stepanov, W. Yang, M. Xie, M. A. Aamir, I. Das, C. Urgell, K. Watanabe, T. Taniguchi, G. Zhang *et al.*, Superconductors, orbital magnets and correlated states in magic-angle bilayer graphene, Nature (London) **574**, 653 (2019).

[5] M. Yankowitz, S. Chen, H. Polshyn, Y. Zhang, K. Watanabe, T. Taniguchi, D. Graf, A. F. Young, and C. R. Dean, Tuning superconductivity in twisted bilayer graphene, Science **363**, 1059 (2019).

[6] A. L. Sharpe, E. J. Fox, A. W. Barnard, J. Finney, K. Watanabe, T. Taniguchi, M. A. Kastner, and D. Goldhaber-Gordon, Emergent ferromagnetism near three-quarters filling in twisted bilayer graphene, Science **365**, 605 (2019).

[7] Y. Saito, J. Ge, K. Watanabe, T. Taniguchi, and A. F. Young, Independent superconductors and correlated insulators in twisted bilayer graphene, Nat. Phys. **16**, 926 (2020).

[8] P. Stepanov, I. Das, X. Lu, A. Fahimniya, K. Watanabe, T. Taniguchi, F. H. L. Koppens, J. Lischner, L. Levitov, and D. K. Efetov, Untying the insulating and superconducting orders in magic-angle graphene, Nature (London) **583**, 375 (2020).

[9] X. Liu, Z. Wang, K. Watanabe, T. Taniguchi, O. Vafek, and J. Li, Tuning electron correlation in magic-angle twisted bilayer graphene using coulomb screening, Science **371**, 1261 (2021).

[10] H. S. Arora, R. Polski, Y. Zhang, A. Thomson, Y. Choi, H. Kim, Z. Lin, I. Z. Wilson, X. Xu, J.-H. Chu *et al.*, Superconductivity in metallic twisted bilayer graphene stabilized by WSe_2, Nature (London) **583**, 379 (2020).

[11] M. Serlin, C. L. Tschirhart, H. Polshyn, Y. Zhang, J. Zhu, K. Watanabe, T. Taniguchi, L. Balents, and A. F. Young, Intrinsic quantized anomalous Hall effect in a moiré heterostructure, Science **367**, 900 (2019).

[12] Y. Cao, D. Chowdhury, D. Rodan-Legrain, O. Rubies-Bigorda, K. Watanabe, T. Taniguchi, T. Senthil, and P. Jarillo-Herrero, Strange Metal in Magic-Angle Graphene with Near Planckian Dissipation, Phys. Rev. Lett. **124**, 076801 (2020).

[13] H. Polshyn, M. Yankowitz, S. Chen, Y. Zhang, K. Watanabe, T. Taniguchi, C. R. Dean, and A. F. Young, Large linear-in-temperature resistivity in twisted bilayer graphene, Nat. Phys. **15**, 1011 (2019).

[14] Y. Saito, J. Ge, L. Rademaker, K. Watanabe, T. Taniguchi, D. A. Abanin, and A. F. Young, Hofstadter subband ferromagnetism and symmetry-broken Chern insulators in twisted bilayer graphene, Nat. Phys. **17**, 478 (2021).

[15] I. Das, X. Lu, J. Herzog-Arbeitman, Z.-D. Song, K. Watanabe, T. Taniguchi, B. A. Bernevig, and D. K. Efetov, Symmetry broken Chern insulators and magic series of Rashba-like Landau level crossings in magic angle bilayer graphene, Nature Phys. (2021), doi: 10.1038/s41567-021-01186-3.

[16] S. Wu, Z. Zhang, K. Watanabe, T. Taniguchi, and E. Y. Andrei, Chern insulators, Van Hove singularities and topological flat bands in magic-angle twisted bilayer graphene, Nat. Mater. **20**, 488 (2021).

[17] J. M. Park, Y. Cao, K. Watanabe, T. Taniguchi, and P. Jarillo-Herrero, Flavour Hund's coupling, correlated Chern gaps, and diffusivity in moiré flat bands, Nature **592**, 43 (2021).

[18] Y. Xie, B. Lian, B. Jäck, X. Liu, C.-L. Chiu, K. Watanabe, T. Taniguchi, B. A. Bernevig, and A. Yazdani, Spectroscopic signatures of many-body correlations in magic-angle twisted bilayer graphene, Nature (London) **572**, 101 (2019).

[19] Y. Choi, J. Kemmer, Y. Peng, A. Thomson, H. Arora, R. Polski, Y. Zhang, H. Ren, J. Alicea, G. Refael *et al.*, Electronic correlations in twisted bilayer graphene near the magic angle, Nat. Phys. **15**, 1174 (2019).

[20] A. Kerelsky, L. J. McGilly, D. M. Kennes, L. Xian, M. Yankowitz, S. Chen, K. Watanabe, T. Taniguchi, J. Hone, C. Dean *et al.*, Maximized electron interactions at the magic angle in twisted bilayer graphene, Nature (London) **572**, 95 (2019).

[21] Y. Jiang, X. Lai, K. Watanabe, T. Taniguchi, K. Haule, J. Mao, and E. Y. Andrei, Charge order and broken rotational symmetry in magic-angle twisted bilayer graphene, Nature (London) **573**, 91 (2019).

[22] D. Wong, K. P. Nuckolls, M. Oh, B. Lian, Y. Xie, S. Jeon, K. Watanabe, T. Taniguchi, B. A. Bernevig, and A. Yazdani, Cascade of electronic transitions in magic-angle twisted bilayer graphene, Nature (London) **582**, 198 (2020).

[23] U. Zondiner, A. Rozen, D. Rodan-Legrain, Y. Cao, R. Queiroz, T. Taniguchi, K. Watanabe, Y. Oreg, F. von Oppen, A. Stern *et al.*, Cascade of phase transitions and dirac revivals in magic-angle graphene, Nature (London) **582**, 203 (2020).

[24] K. P. Nuckolls, M. Oh, D. Wong, B. Lian, K. Watanabe, T. Taniguchi, B. A. Bernevig, and A. Yazdani, Strongly correlated Chern insulators in magic-angle twisted bilayer graphene, Nature (London) **588**, 610 (2020).

[25] Y. Choi, H. Kim, Y. Peng, A. Thomson, C. Lewandowski, R. Polski, Y. Zhang, H. S. Arora, K. Watanabe, T. Taniguchi, J. Alicea, and S. Nadj-Perge, Tracing out correlated Chern insulators in magic angle twisted bilayer graphene, arXiv:2008.11746 [cond-mat.str-el].

[26] Y. Saito, J. Ge, K. Watanabe, T. Taniguchi, E. Berg, and A. F. Young, Isospin pomeranchuk effect and the entropy of collective excitations in twisted bilayer graphene, Nature **592**, 220 (2021).

[27] A. Rozen, J. M. Park, U. Zondiner, Y. Cao, D. Rodan-Legrain, T. Taniguchi, K. Watanabe, Y. Oreg, A. Stern, E. Berg, P. Jarillo-Herrero, and S. Ilani, Entropic evidence for a Pomeranchuk effect in magic angle graphene, Nature **592**, 214 (2021).

[28] X. Lu, B. Lian, G. Chaudhary, B. A. Piot, G. Romagnoli, K. Watanabe, T. Taniguchi, M. Poggio, A. H. MacDonald, B. A. Bernevig, and D. K. Efetov, Fingerprints of fragile topology in the Hofstadter spectrum of twisted bilayer graphene close to the second magic angle, arXiv:2006.13963 [cond-mat.mes-hall].

[29] G. W. Burg, J. Zhu, T. Taniguchi, K. Watanabe, A. H. MacDonald, and E. Tutuc, Correlated Insulating States in Twisted Double Bilayer Graphene, Phys. Rev. Lett. **123**, 197702 (2019).

[30] C. Shen, Y. Chu, Q. Wu, N. Li, S. Wang, Y. Zhao, J. Tang, J. Liu, J. Tian, K. Watanabe, T. Taniguchi, R. Yang, Z. Y. Meng, D. Shi, O. V. Yazyev, and G. Zhang, Correlated states in twisted double bilayer graphene, Nat. Phys. **16**, 520 (2020).

[31] Y. Cao, D. Rodan-Legrain, O. Rubies-Bigorda, J. M. Park, K. Watanabe, T. Taniguchi, and P. Jarillo-Herrero, Tunable correlated states and spin-polarized phases in twisted bilayer-bilayer graphene, Nature (London) **583**, 215 (2020).

[32] X. Liu, Z. Hao, E. Khalaf, J. Y. Lee, K. Watanabe, T. Taniguchi, A. Vishwanath, and P. Kim, Spin-polarized correlated insulator and superconductor in twisted double bilayer graphene, Nature (London) **583**, 221 (2020).

[33] G. Chen, L. Jiang, S. Wu, B. Lyu, H. Li, B. L. Chittari, K. Watanabe, T. Taniguchi, Z. Shi, J. Jung, Y. Zhang, and F. Wang, Evidence of a gate-tunable Mott insulator in a trilayer graphene moiré superlattice, Nat. Phys. **15**, 237 (2019).

[34] G. Chen, A. L. Sharpe, P. Gallagher, I. T. Rosen, E. J. Fox, L. Jiang, B. Lyu, H. Li, K. Watanabe, T. Taniguchi, J. Jung, Z. Shi, D. Goldhaber-Gordon, Y. Zhang, and F. Wang, Signatures of tunable superconductivity in a trilayer graphene moiré superlattice, Nature (London) **572**, 215 (2019).

[35] G. Chen, A. L. Sharpe, E. J. Fox, Y.-H. Zhang, S. Wang, L. Jiang, B. Lyu, H. Li, K. Watanabe, T. Taniguchi, Z. Shi, T. Senthil, D. Goldhaber-Gordon, Y. Zhang, and F. Wang, Tunable correlated Chern insulator and ferromagnetism in a moiré superlattice, Nature (London) **579**, 56 (2020).

[36] G. W. Burg, B. Lian, T. Taniguchi, K. Watanabe, B. A. Bernevig, and E. Tutuc, Evidence of emergent symmetry and valley Chern number in twisted double-bilayer graphene, arXiv:2006.14000 [cond-mat.mes-hall].

[37] G. Tarnopolsky, A. J. Kruchkov, and A. Vishwanath, Origin of Magic Angles in Twisted Bilayer Graphene, Phys. Rev. Lett. **122**, 106405 (2019).
[38] L. Zou, H. C. Po, A. Vishwanath, and T. Senthil, Band structure of twisted bilayer graphene: Emergent symmetries, commensurate approximants, and Wannier obstructions, Phys. Rev. B **98**, 085435 (2018).
[39] Y. Fu, E. J. König, J. H. Wilson, Y.-Z. Chou, and J. H. Pixley, Magic-angle semimetals, npj Quantum Mater. **5**, 71 (2020).
[40] J. Liu, J. Liu, and X. Dai, Pseudo Landau level representation of twisted bilayer graphene: Band topology and implications on the correlated insulating phase, Phys. Rev. B **99**, 155415 (2019).
[41] D. K. Efimkin and A. H. MacDonald, Helical network model for twisted bilayer graphene, Phys. Rev. B **98**, 035404 (2018).
[42] J. Kang and O. Vafek, Symmetry, Maximally Localized Wannier States, and a Low-Energy Model for Twisted Bilayer Graphene Narrow Bands, Phys. Rev. X **8**, 031088 (2018).
[43] Z. Song, Z. Wang, W. Shi, G. Li, C. Fang, and B. A. Bernevig, All Magic Angles in Twisted Bilayer Graphene are Topological, Phys. Rev. Lett. **123**, 036401 (2019).
[44] H. C. Po, L. Zou, T. Senthil, and A. Vishwanath, Faithful tight-binding models and fragile topology of magic-angle bilayer graphene, Phys. Rev. B **99**, 195455 (2019).
[45] J. Ahn, S. Park, and B.-J. Yang, Failure of Nielsen-Ninomiya Theorem and Fragile Topology in Two-Dimensional Systems With Space-Time Inversion Symmetry: Application to Twisted Bilayer Graphene at Magic Angle, Phys. Rev. X **9**, 021013 (2019).
[46] A. Bouhon, A. M. Black-Schaffer, and R.-J. Slager, Wilson loop approach to fragile topology of split elementary band representations and topological crystalline insulators with time-reversal symmetry, Phys. Rev. B **100**, 195135 (2019).
[47] B. Lian, F. Xie, and B. A. Bernevig, Landau level of fragile topology, Phys. Rev. B **102**, 041402(R) (2020).
[48] K. Hejazi, C. Liu, H. Shapourian, X. Chen, and L. Balents, Multiple topological transitions in twisted bilayer graphene near the first magic angle, Phys. Rev. B **99**, 035111 (2019).
[49] K. Hejazi, C. Liu, and L. Balents, Landau levels in twisted bilayer graphene and semiclassical orbits, Phys. Rev. B **100**, 035115 (2019).
[50] B. Padhi, A. Tiwari, T. Neupert, and S. Ryu, Transport across twist angle domains in moiré graphene, Phys. Rev. Research **2**, 033458 (2020).
[51] C. Xu and L. Balents, Topological Superconductivity in Twisted Multilayer Graphene, Phys. Rev. Lett. **121**, 087001 (2018).
[52] M. Koshino, N. F. Q. Yuan, T. Koretsune, M. Ochi, K. Kuroki, and L. Fu, Maximally Localized Wannier Orbitals and the Extended Hubbard Model for Twisted Bilayer Graphene, Phys. Rev. X **8**, 031087 (2018).
[53] M. Ochi, M. Koshino, and K. Kuroki, Possible correlated insulating states in magic-angle twisted bilayer graphene under strongly competing interactions, Phys. Rev. B **98**, 081102(R) (2018).
[54] X. Y. Xu, K. T. Law, and P. A. Lee, Kekulé valence bond order in an extended Hubbard model on the honeycomb lattice with possible applications to twisted bilayer graphene, Phys. Rev. B **98**, 121406(R) (2018).
[55] F. Guinea and N. R. Walet, Electrostatic effects, band distortions, and superconductivity in twisted graphene bilayers, Proc. Natl. Acad. Sci. USA **115**, 13174 (2018).
[56] J. W. F. Venderbos and R. M. Fernandes, Correlations and electronic order in a two-orbital honeycomb lattice model for twisted bilayer graphene, Phys. Rev. B **98**, 245103 (2018).
[57] Y.-Z. You and A. Vishwanath, Superconductivity from valley fluctuations and approximate SO(4) symmetry in a weak coupling theory of twisted bilayer graphene, npj Quantum Mater. **4**, 16 (2019).
[58] F. Wu and S. Das Sarma, Collective Excitations of Quantum Anomalous Hall Ferromagnets in Twisted Bilayer Graphene, Phys. Rev. Lett. **124**, 046403 (2020).
[59] B. Lian, Z. Wang, and B. A. Bernevig, Twisted Bilayer Graphene: A Phonon-Driven Superconductor, Phys. Rev. Lett. **122**, 257002 (2019).
[60] F. Wu, A. H. MacDonald, and I. Martin, Theory of Phonon-Mediated Superconductivity in Twisted Bilayer Graphene, Phys. Rev. Lett. **121**, 257001 (2018).
[61] H. Isobe, N. F. Q. Yuan, and L. Fu, Unconventional Superconductivity and Density Waves in Twisted Bilayer Graphene, Phys. Rev. X **8**, 041041 (2018).
[62] C.-C. Liu, L.-D. Zhang, W.-Q. Chen, and F. Yang, Chiral spin density wave and $d + id$ superconductivity in the Magic-Angle-Twisted Bilayer Graphene, Phys. Rev. Lett. **121**, 217001 (2018).
[63] N. Bultinck, S. Chatterjee, and M. P. Zaletel, Mechanism for Anomalous Hall Ferromagnetism in Twisted Bilayer Graphene, Phys. Rev. Lett. **124**, 166601 (2020).
[64] Y.-H. Zhang, D. Mao, Y. Cao, P. Jarillo-Herrero, and T. Senthil, Nearly flat Chern bands in moiré superlattices, Phys. Rev. B **99**, 075127 (2019).
[65] J. Liu, Z. Ma, J. Gao, and X. Dai, Quantum Valley Hall Effect, Orbital Magnetism, and Anomalous Hall Effect in Twisted Multilayer Graphene Systems, Phys. Rev. X **9**, 031021 (2019).
[66] X.-C. Wu, C.-M. Jian, and C. Xu, Coupled-wire description of the correlated physics in twisted bilayer graphene, Phys. Rev. B **99**, 161405 (2019).
[67] A. Thomson, S. Chatterjee, S. Sachdev, and M. S. Scheurer, Triangular antiferromagnetism on the honeycomb lattice of twisted bilayer graphene, Phys. Rev. B **98**, 075109 (2018).
[68] J. F. Dodaro, S. A. Kivelson, Y. Schattner, X.-Q. Sun, and C. Wang, Phases of a phenomenological model of twisted bilayer graphene, Phys. Rev. B **98**, 075154 (2018).
[69] J. Gonzalez and T. Stauber, Kohn-Luttinger Superconductivity in Twisted Bilayer Graphene, Phys. Rev. Lett. **122**, 026801 (2019).
[70] N. F. Q. Yuan and L. Fu, Model for the metal-insulator transition in graphene superlattices and beyond, Phys. Rev. B **98**, 045103 (2018).
[71] J. Kang and O. Vafek, Strong Coupling Phases of Partially Filled Twisted Bilayer Graphene Narrow Bands, Phys. Rev. Lett. **122**, 246401 (2019).
[72] N. Bultinck, E. Khalaf, S. Liu, S. Chatterjee, A. Vishwanath, and M. P. Zaletel, Ground State and Hidden Symmetry of Magic-Angle Graphene at Even Integer Filling, Phys. Rev. X **10**, 031034 (2020).
[73] K. Seo, V. N. Kotov, and B. Uchoa, Ferromagnetic Mott State in Twisted Graphene Bilayers at the Magic Angle, Phys. Rev. Lett. **122**, 246402 (2019).

[74] K. Hejazi, X. Chen, and L. Balents, Hybrid Wannier Chern bands in magic angle twisted bilayer graphene and the quantized anomalous Hall effect, Phys. Rev. Research **3**, 013242 (2021).

[75] E. Khalaf, S. Chatterjee, N. Bultinck, M. P. Zaletel, and A. Vishwanath, Charged skyrmions and topological origin of superconductivity in magic angle graphene), arXiv:2004.00638 [cond-mat.str-el].

[76] H. C. Po, L. Zou, A. Vishwanath, and T. Senthil, Origin of Mott Insulating Behavior and Superconductivity in Twisted Bilayer Graphene, Phys. Rev. X **8**, 031089 (2018).

[77] F. Xie, Z. Song, B. Lian, and B. A. Bernevig, Topology-Bounded Superfluid Weight in Twisted Bilayer Graphene, Phys. Rev. Lett. **124**, 167002 (2020).

[78] A. Julku, T. J. Peltonen, L. Liang, T. T. Heikkilä, and P. Törmä, Superfluid weight and Berezinskii-Kosterlitz-Thouless transition temperature of twisted bilayer graphene, Phys. Rev. B **101**, 060505 (2020).

[79] X. Hu, T. Hyart, D. I. Pikulin, and E. Rossi, Geometric and Conventional Contribution to the Superfluid Weight in Twisted Bilayer Graphene, Phys. Rev. Lett. **123**, 237002 (2019).

[80] J. Kang and O. Vafek, Non-Abelian Dirac node braiding and near-degeneracy of correlated phases at odd integer filling in magic-angle twisted bilayer graphene, Phys. Rev. B **102**, 035161 (2020).

[81] T. Soejima, D. E. Parker, N. Bultinck, J. Hauschild, and M. P. Zaletel, Efficient simulation of moire materials using the density matrix renormalization group, Phys. Rev. B **102**, 205111 (2020).

[82] J. H. Pixley and E. Y. Andrei, Ferromagnetism in magic-angle graphene, Science **365**, 543 (2019).

[83] E. J. König, P. Coleman, and A. M. Tsvelik, Spin magnetometry as a probe of stripe superconductivity in twisted bilayer graphene, Phys. Rev. B **102**, 104514 (2020).

[84] M. Christos, S. Sachdev, and M. Scheurer, Superconductivity, correlated insulators, and Wess-Zumino-Witten terms in twisted bilayer graphene, Proc. Nat. Acad. Sci. USA **117**, 29543 (2020).

[85] C. Lewandowski, D. Chowdhury, and J. Ruhman, Pairing in magic-angle twisted bilayer graphene: Role of phonon and plasmon Umklapp, arXiv:2007.15002 [cond-mat.supr-con].

[86] M. Xie and A. H. MacDonald, Nature of the Correlated Insulator States in Twisted Bilayer Graphene, Phys. Rev. Lett. **124**, 097601 (2020).

[87] J. Liu and X. Dai, Theories for the correlated insulating states and quantum anomalous Hall phenomena in twisted bilayer graphene, Phys. Rev. B **103**, 035427 (2021).

[88] T. Cea and F. Guinea, Band structure and insulating states driven by coulomb interaction in twisted bilayer graphene, Phys. Rev. B **102**, 045107 (2020).

[89] Y. Zhang, K. Jiang, Z. Wang, and F. Zhang, Correlated insulating phases of twisted bilayer graphene at commensurate filling fractions: A Hartree-Fock study, Phys. Rev. B **102**, 035136 (2020).

[90] S. Liu, E. Khalaf, J. Y. Lee, and A. Vishwanath, Nematic topological semimetal and insulator in magic angle bilayer graphene at charge neutrality, Phys. Rev. Research **3**, 013033 (2021).

[91] Y. Da Liao, Z. Y. Meng, and X. Y. Xu, Valence Bond Orders at Charge Neutrality in a Possible Two-Orbital Extended Hubbard Model for Twisted Bilayer Graphene, Phys. Rev. Lett. **123**, 157601 (2019).

[92] Y. D. Liao, J. Kang, C. N. Breiø, X. Y. Xu, H.-Q. Wu, B. M. Andersen, R. M. Fernandes, and Z. Y. Meng, Correlation-Induced Insulating Topological Phases at Charge Neutrality in Twisted Bilayer Graphene, Phys. Rev. X **11**, 011014 (2021).

[93] L. Classen, C. Honerkamp, and M. M. Scherer, Competing phases of interacting electrons on triangular lattices in moiré heterostructures, Phys. Rev. B **99**, 195120 (2019).

[94] D. M. Kennes, J. Lischner, and C. Karrasch, Strong correlations and $d + id$ superconductivity in twisted bilayer graphene, Phys. Rev. B **98**, 241407(R) (2018).

[95] P. M. Eugenio and C. B. Dağ, DMRG study of strongly interacting z_2 flatbands: A toy model inspired by twisted bilayer graphene, SciPost Phys. Core **3**, 015 (2020).

[96] Y. Huang, P. Hosur, and H. K. Pal, Deconstructing magic-angle physics in twisted bilayer graphene with a two-leg ladder model, Phys. Rev. B **102**, 155429 (2020).

[97] T. Huang, L. Zhang, and T. Ma, Antiferromagnetically ordered Mott insulator and $d + id$ superconductivity in twisted bilayer graphene: A quantum Monte Carlo study, Sci. Bull. **64**, 310 (2019).

[98] H. Guo, X. Zhu, S. Feng, and R. T. Scalettar, Pairing symmetry of interacting fermions on a twisted bilayer graphene superlattice, Phys. Rev. B **97**, 235453 (2018).

[99] P. J. Ledwith, G. Tarnopolsky, E. Khalaf, and A. Vishwanath, Fractional Chern insulator states in twisted bilayer graphene: An analytical approach, Phys. Rev. Research **2**, 023237 (2020).

[100] C. Repellin, Z. Dong, Y.-H. Zhang, and T. Senthil, Ferromagnetism in Narrow Bands of Moiré Superlattices, Phys. Rev. Lett. **124**, 187601 (2020).

[101] A. Abouelkomsan, Z. Liu, and E. J. Bergholtz, Particle-Hole Duality, Emergent Fermi Liquids, and Fractional Chern Insulators in Moiré Flatbands, Phys. Rev. Lett. **124**, 106803 (2020).

[102] C. Repellin and T. Senthil, Chern bands of twisted bilayer graphene: Fractional Chern insulators and spin phase transition, Phys. Rev. Research **2**, 023238 (2020).

[103] O. Vafek and J. Kang, Towards the Hidden Symmetry in Coulomb Interacting Twisted Bilayer Graphene: Renormalization Group Approach, Phys. Rev. Lett. **125**, 257602 (2020).

[104] R. M. Fernandes and J. W. F. Venderbos, Nematicity with a twist: Rotational symmetry breaking in a moiré superlattice, Sci. Adv. **6**, eaba8834 (2020).

[105] J. H. Wilson, Y. Fu, S. Das Sarma, and J. H. Pixley, Disorder in twisted bilayer graphene, Phys. Rev. Research **2**, 023325 (2020).

[106] J. Wang, Y. Zheng, A. J. Millis, and J. Cano, Chiral approximation to twisted bilayer graphene: Exact intra-valley inversion symmetry, nodal structure and implications for higher magic angles, arXiv:2010.03589 [cond-mat.mes-hall].

[107] B. A. Bernevig, Z. Song, N. Regnault, and B. Lian, Twisted bilayer graphene. I. Matrix elements, approximations, perturbation theory, and a $k \cdot p$ two-band model, Phys. Rev. B **103**, 205411 (2021).

[108] Z.-D. Song, B. Lian, N. Regnault, and B. A. Bernevig, Twisted bilayer graphene. II. Stable symmetry anomaly, Phys. Rev. B **103**, 205412 (2021).

[109] B. Lian, Z.-D. Song, N. Regnault, D. K. Efetov, A. Yazdani, and B. A. Bernevig, Twisted bilayer graphene. IV. Exact insulator ground states and phase diagram, Phys. Rev. B **103**, 205414 (2021).

[110] B. A. Bernevig, B. Lian, A. Cowsik, F. Xie, N. Regnault, and Z.-D. Song, Twisted bilayer graphene. V. Exact analytic many-body excitations in Coulomb Hamiltonians: Charge gap, Goldstone modes, and absence of Cooper pairing, Phys. Rev. B **103**, 205415 (2021).

[111] F. Xie, A. Cowsik, Z.-D. Song, B. Lian, B. A. Bernevig, and N. Regnault, Twisted bilayer graphene. VI. An exact diagonalization study at nonzero integer filling, Phys. Rev. B **103**, 205416 (2021).

[112] K. Uchida, S. Furuya, J.-I. Iwata, and A. Oshiyama, Atomic corrugation and electron localization due to moiré patterns in twisted bilayer graphenes, Phys. Rev. B **90**, 155451 (2014).

[113] M. M. van Wijk, A. Schuring, M. I. Katsnelson, and A. Fasolino, Relaxation of moiré patterns for slightly misaligned identical lattices: Graphene on graphite, 2D Materials **2**, 034010 (2015).

[114] S. Dai, Y. Xiang, and D. J. Srolovitz, Twisted bilayer graphene: Moiré with a twist, Nano Lett. **16**, 5923 (2016).

[115] S. K. Jain, V. Juričić, and G. T. Barkema, Structure of twisted and buckled bilayer graphene, 2D Materials **4**, 015018 (2016).

[116] H. C. Po, H. Watanabe, and A. Vishwanath, Fragile Topology and Wannier Obstructions, Phys. Rev. Lett. **121**, 126402 (2018).

[117] J. Cano, B. Bradlyn, Z. Wang, L. Elcoro, M. G. Vergniory, C. Felser, M. I. Aroyo, and B. A. Bernevig, Topology of Disconnected Elementary band Representations, Phys. Rev. Lett. **120**, 266401 (2018).

[118] C. Mora, N. Regnault, and B. A. Bernevig, Flatbands and Perfect Metal in Trilayer Moiré Graphene, Phys. Rev. Lett. **123**, 026402 (2019).